technische universität
dortmund

mpi

Single molecule imaging of the signaling activity of the epidermal growth factor receptor

Dissertation

zur Erlangung des akademischen Grades eines
Doktors der Naturwissenschaften
(Dr. rer. nat.)

der Fakultät Chemie und Chemische Biologie
der Technischen Universität Dortmund

vorgelegt von

Jenny Denise Ibach

Januar 2014

Diese Arbeit wurde angefertigt am

Max-Planck-Institut
für molekulare Physiologie
in Dortmund

1. Gutachter: Prof. Dr. Philippe I. H. Bastiaens

2. Gutachter: Prof. Dr. Roger S. Goody

EIDESSTATTLICHE VERSICHERUNG

Ich versichere hiermit an Eides statt, dass ich die vorliegende Dissertationsarbeit selbstständig und ohne unzulässige fremde Hilfe erbracht habe. Ich habe keine anderen als die angegebenen Quellen und Hilfsmittel benutzt sowie wörtliche und sinngemäße Zitate kenntlich gemacht. Die Arbeit hat in gleicher oder ähnlicher Form noch keiner Prüfungsbehörde vorgelegen.

Ort, Datum	Unterschrift

SUMMARY

The epidermal growth factor receptor (ErbB1) is a receptor tyrosine kinase involved in various cellular processes, such as growth and differentiation. Its extracellular domains are capable of binding a range of ligands, including the epidermal growth factor (EGF). Parts of these extracellular domains, as well as the transmembrane domain and the juxtamembrane domain are involved in dimerization of the receptor. Upon ligand binding, the intracellular kinase domain forms an asymmetric dimer with the kinase of a second receptor, leading to auto-phosphorylation of several tyrosine and serine residues at the C-terminal tail, where effector proteins bind to propagate the signal.

In this work the transient nature of receptor dimerization and clustering was visualized by tracking a fluorescently labeled receptor in living cells on a single molecule level. At the same time the activity of the receptor was monitored with a probe for phosphorylation. Even after activation, ErbB1 continuously switches between multiple short-lived mobility states, with diffusion coefficients that span two orders of magnitude, indicating that ErbB1 activation is a highly dynamic process. In resting cells the receptor is mainly monomeric arguing against a role of pre-dimerization in the activation of ErbB1. Upon stimulation with EGF, the receptor self-associates and localizes in highly active, immobile clusters that colocalize with clathrin-coated pits. Thus, ErbB1 signaling is stabilized and amplified at the plasma membrane by recruitment of the receptors to clathrin-coated pits prior to endocytosis. However, the receptors are not necessarily trapped, as they maintain their ability to alternate between mobility states. Experiments with a kinase inhibitor and a kinase-dead mutant of ErbB1 showed that although receptors with an inactive kinase are able to convert to the immobile state, kinase activity is necessary for cluster formation. Experiments with a phosphatase inhibitor showed that ligand binding is not necessary for clustering of active ErbB1.

In cells expressing the receptor at a low level, much of the ErbB1 activity is spatially confined to clathrin-coated pits on the plasma membrane, in contrast to the uniform activity observed in over-expressing cells. This clustering into highly active areas represents a potential mechanism for robust signaling from the plasma membrane at low expression levels of the receptor.

ZUSAMMENFASSUNG

Der EGF-Rezeptor (engl. epidermal growth factor), auch ErbB1 genannt, gehört zu den Rezeptor-Tyrosinkinasen und ist an verschiedenen zellulären Prozessen, wie der Proliferation und der Differenzierung, beteiligt ist. Die extrazellulären Domänen des Rezeptors können verschiedene Liganden binden, unter anderem EGF. Teile dieser extrazellulären Domänen, sowie die Transmembrandomäne und die Juxtamembran-Domäne spielen eine Rolle bei der Dimerisierung des Rezeptors. Nach Bindung eines Liganden bildet die intrazelluläre Kinasedomäne ein asymmetrisches Dimer mit der Kinase eines zweiten Rezeptors, wodurch die Autophosphorylierung verschiedener Serine und Tyrosine am C-terminalen Ende des Rezeptors stattfindet. Dort binden Effektorproteine, welche das Signal in die Zelle weiterleiten.

In dieser Arbeit konnte der kurzlebige Charakter der Rezeptor-Dimerisierung und der Cluster-Bildung durch die Verfolgung fluoreszenzmarkierter Rezeptoren in lebenden Zellen auf Einzelmolekül-Ebene visualisiert werden. Gleichzeitig wurde die Aktivität des Rezeptors durch eine Sonde für den Phosphorylierungszustand verfolgt. Auch nach Aktivierung wechselt ErbB1 permanent zwischen mehreren kurzlebigen Mobilitätszuständen, deren Diffusionskoeffizienten einen Bereich von zwei Größenordnungen umfassen. Dies verdeutlicht, dass die Aktivierung von ErbB1 ein hochdynamischer Prozess ist. In unstimulierten Zellen liegt der Rezeptor hauptsächlich monomer vor, was gegen eine entscheidende Rolle der Vordimerisierung bei der Aktivierung von ErbB1 spricht. Nach Stimulierung mit EGF assoziieren die Rezeptoren und lokalisieren in hochaktiven, immobilen Clustern, welche mit Clathrin-umhüllten Einstülpungen kolokalisieren. Demnach wird das Signal durch die Rekrutierung der Rezeptoren zu Clathrin-umhüllten Einstülpungen vor der Endozytose an der Membran stabilisiert und amplifiziert. Allerdings sind die Rezeptoren dort nicht unbedingt gefangen, da sie immer noch zwischen den Mobilitätszuständen wechseln können. Experimente mit einem Kinaseinhibitor und einer Kinase-inaktiven Mutante des Rezeptors zeigten, dass diese zwar den immobilen Zustand erreichen, aber dass für die Cluster-Bildung auch die Kinaseaktivität benötigt wird. Zudem zeigten Experimente mit einem Phosphataseinhibitor, dass die Bindung eines Liganden für die Cluster-Bildung aktiver ErbB1 Rezeptoren nicht notwendig ist.

In Zellen mit geringem Expressionslevel von ErbB1, ist die meiste Aktivität des Rezeptors räumlich beschränkt in Clathrin-umhüllten Einstülpungen zu finden, wohingegen eine gleichmäßige Verteilung der Aktivität bei Überexpression beobachtet wird. Die Anhäufung in hochaktiven Membranbereichen beschreibt einen möglichen Mechanismus, um bei geringem Expressions-level des Rezeptors eine stabile Signalweiterleitung zu gewährleisten.

TABLE OF CONTENTS

1. INTRODUCTION

1.1. Receptor tyrosine kinases

Receptor tyrosine kinases (RTKs) are cell surface receptors that play an important role in a broad range of processes in mammalian cells, such as proliferation, differentiation, migration and control of the cell cycle[1,2]. In the human genome 58 RTKs are known, which are divided into 20 subfamilies[3] (Figure 1).

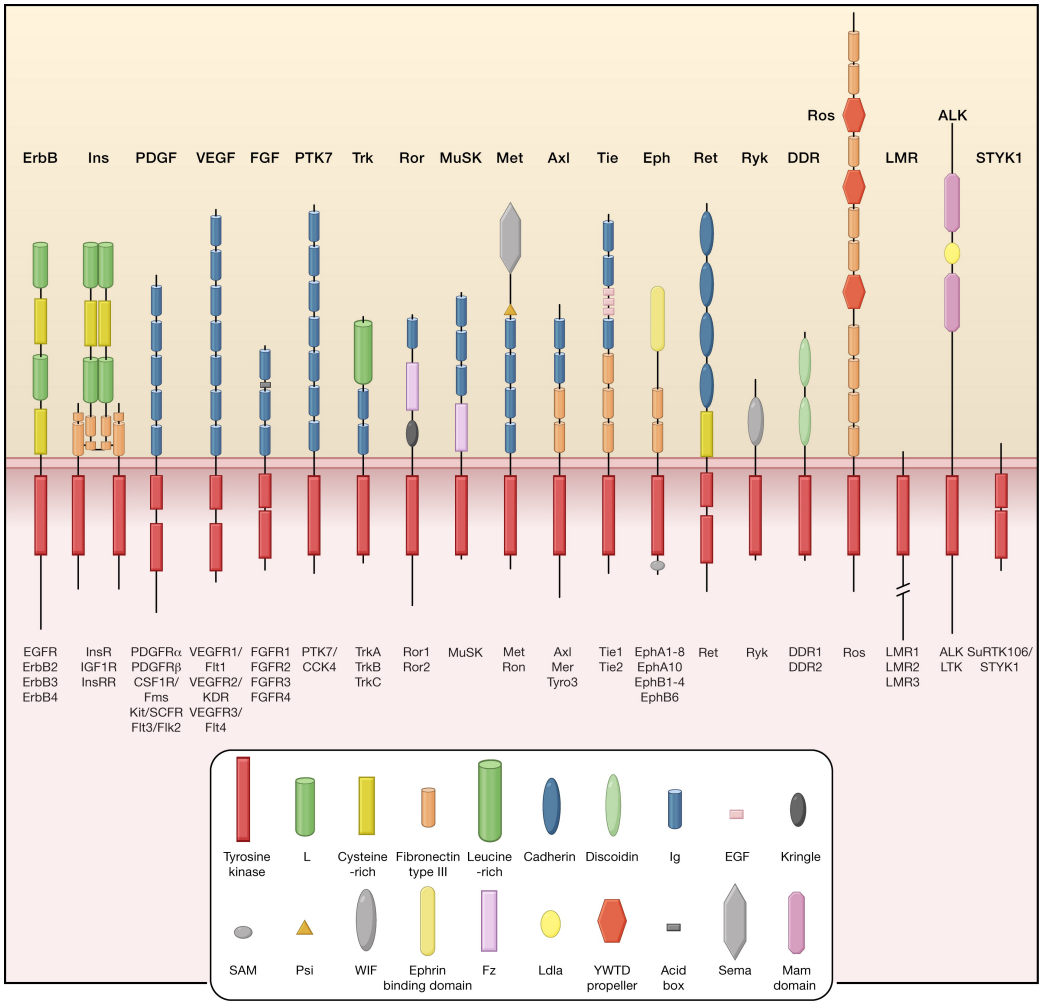

Figure 1: Overview of receptor tyrosine kinase families. The 20 subfamilies of human RTKs are schematically shown with the respective family members listed below the receptor. The intracellular kinase domains are visualized as red rectangles. The variable composition in the extracellular regions are depicted by structural domains grouped by their functions, as indicated in the key (Figure adapted from Lemmon and Schlessinger 2010[3]).

The structure of RTKs as well as their activation mechanisms and the key components of the corresponding signaling pathways are highly conserved. They all share the same basic molecular structure, consisting of intracellular domains linked to the extracellular domains via a transmembrane helix. In the extracellular region the ligand binding domains (LBD) and various regulatory domains, for instance for dimerization, are found. The intracellular part contains mainly the catalytic domain, the tyrosine kinase. Binding of a ligand to the extracellular LBD leads to autophosphorylation of tyrosine residues in the cytoplasmic region. In its active state the receptor recruits various effector proteins to induce different signal transduction pathways.

1.1.1. Epidermal growth factor receptors

An important subfamily of the RTKs is the epidermal growth factor receptor or ErbB receptor family, which are expressed in epithelial, neuronal and mesenchymal tissues. They play a critical role in cell proliferation, differentiation and migration during embryogenesis and carcinogenesis[3–5]. The ErbB receptor family consists of four members, the epidermal growth factor receptor (EGFR/HER1/ErbB1), ErbB2 (HER2/Neu), ErbB3 (HER3) and ErbB4 (HER4).

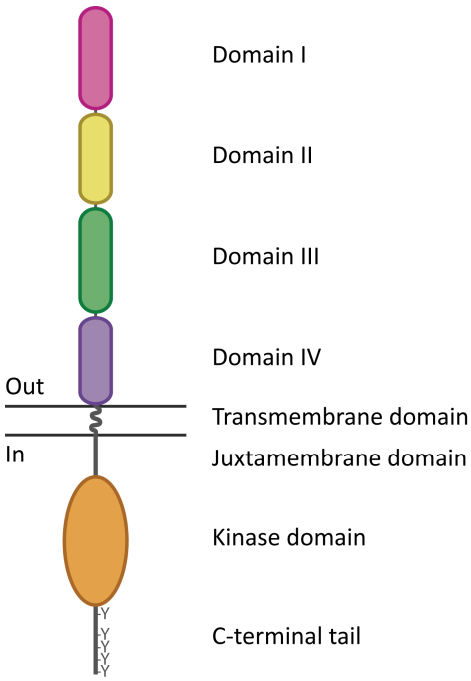

Figure 2: Schematic representation of the structure of the ErbB family members. The N-terminal extracellular domain consists of four subdomains (I – IV), involved in ligand binding and dimerization. The transmembrane domain makes a single pass through the membrane, followed by the juxtamembrane domain, the kinase domain and the C-terminal tail which contains tyrosines available for phosphorylation.

All four members of the ErbB receptor family share the same molecular structure: an extracellular domain with four subdomains including a ligand binding domain, a single transmembrane helix and an intracellular juxtamembrane domain, followed by a kinase domain and a C-terminal tail (Figure 2).

To activate the relevant signaling pathways the members of this receptor family undergo homo- or hetero- dimerization. ErbB1 and ErbB4 are able to become active after homo-dimerization upon ligand binding, whereas ErbB2 and ErbB3 depend on hetero-dimerization with other family members. ErbB2 likely lacks the ability to bind a ligand, since no ligand is known, and its activation occurs by dimerization with other ligand-bound members of the receptor family[6], mainly ErbB1[7,8]. In contrast, ErbB3 has an inactive kinase domain and is unable to generate signals by homo-dimerization[9], but it can still bind a ligand and form active hetero-dimers with other family members. ErbB1, ErbB3 and ErbB4 can bind several ligands (Figure 3). The epidermal growth factor (EGF) is the main ligand for ErbB1, but other ligands are also known to bind ErbB1 such as the transforming growth factor alpha (TGF-α), epiregulin, the heparin-binding epidermal growth factor-like factor (HB-EGF), betacellulin and amphiregulin[10]. Betacellulin, HB-EGF and epiregulin also bind to ErbB4, whereas neuregulins (NRGs, also called heregulins) are ligands for both ErbB4 and ErbB3[11].

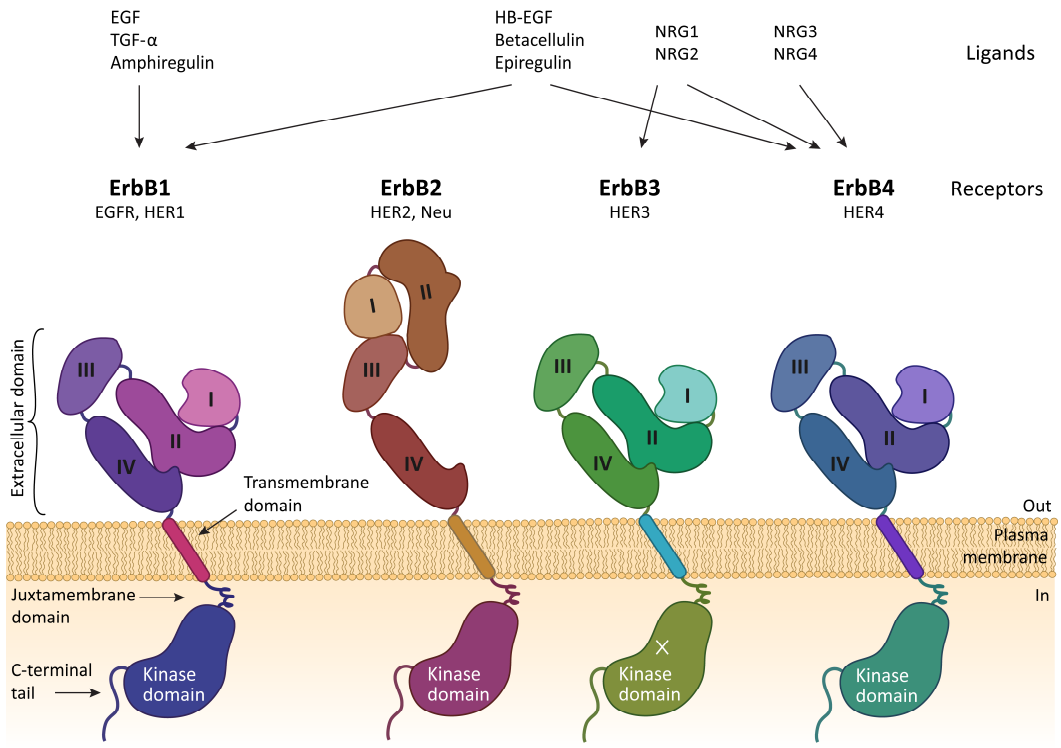

Figure 3: Members of the ErbB receptor family and their ligands. The family members ErbB1, ErbB2, ErbB3 and ErbB4 share the same structure and can bind several ligands except for ErbB2, for which no ligand is known. ErbB3 has an inactive tyrosine kinase domain.

1.2. The epidermal growth factor receptor

The epidermal growth factor receptor (EGFR, in the following referred to as ErbB1) is the most thoroughly investigated member of the ErbB receptor family, since its aberrant expression and receptor mutations have been linked to different types of cancers[12]. Therefore, it is of great importance to understand the cellular mechanisms that regulate ErbB1 activation, and how an extracellular signal is propagated and translated into a specific cellular response.

The extracellular EGF-binding domain of ErbB1 consists of four subdomains I-IV, where I and III play a role in EGF binding and subdomains II and IV have regulatory functions (Figure 4). Without ligand, ErbB1 adopts a tethered conformation where the subdomains II and IV interact[13], inhibiting dimerization of the receptor. In addition to the tethered conformation the extracellular domains can also be found in an extended conformation, where the binding affinity of EGF is increased and the dimerization arm of subdomain II is exposed[13]. When EGF is bound, this extended conformation of ErbB1 is stabilized[14,15].

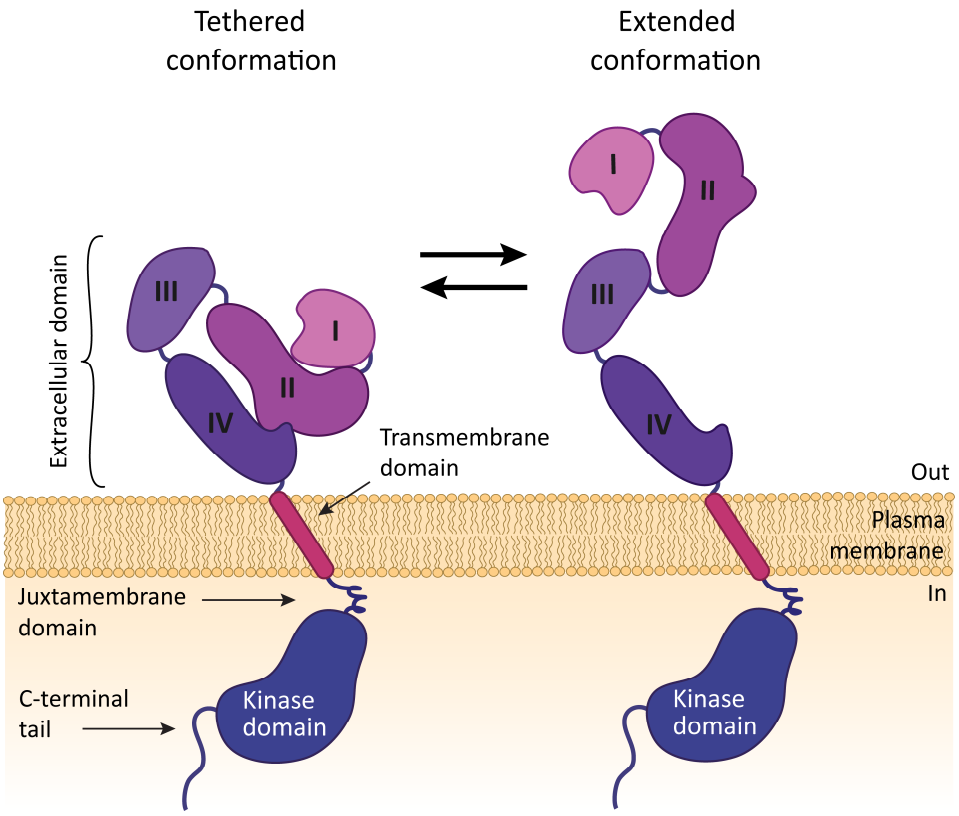

Figure 4: Structure and conformations of ErbB1. ErbB1 switches between a tethered and an extended conformation. The extended conformation has a higher affinity to bind EGF.

Binding of a ligand leads to phosphorylation of several tyrosine and serine residues at the C-terminal tail of ErbB1. These phosphorylated tyrosines and serines act as recruitment sites for

downstream effector proteins containing phosphotyrosine binding (PTB) domains or Src homology 2 (SH2) domains. Upon binding of effector proteins several signaling pathways like the MEK/Erk, the phosphatidylinositol 3-kinase/AKT (PI3K/AKT) and the phospho-lipase C γ (PLCγ) signal transduction pathways as well as signal transducers and activators of transcription (STAT) are activated, leading to different cell responses (Figure 5).

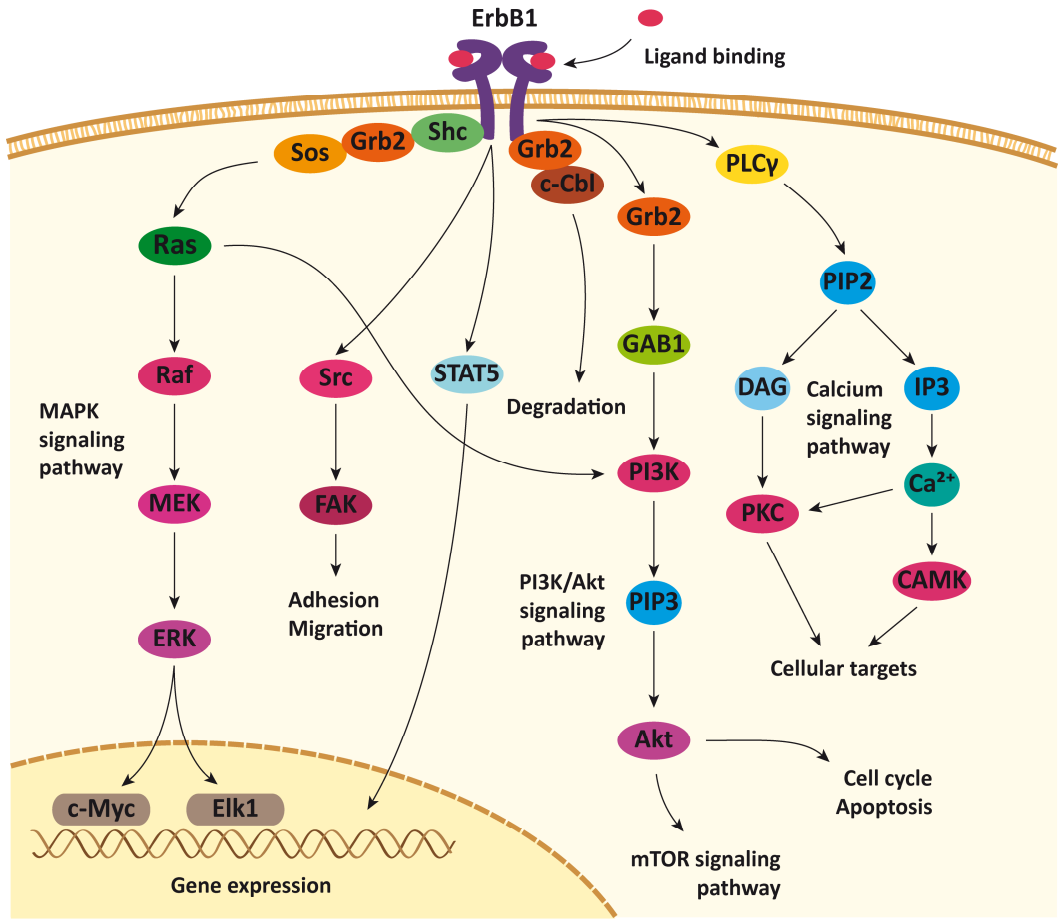

Figure 5: ErbB1 signaling pathways. Through recruitment of several adaptor proteins to phosphorylated tyrosines or serines at the C-terminal tail of ErbB1, different signaling pathways like the MAPK signaling pathway or the PI3K/Akt signaling pathway are activated.

The growth-factor-receptor bound-2 (Grb2) and the Src-homology-2-containing (Shc) adaptor proteins link ErbB1 to the signaling molecule SOS (Ras GTP exchange factor)[16–18], leading to activation of the mitogen-activated protein kinase (MAPK) cascade culminating in the activation of a number of transcriptional regulators by ERK1/2 to induce cell growth and proliferation. Phospholipase C γ (PLCγ) binds to phosphorylated ErbB1 via its SH2 domain, thereby activating the PLC/PKC pathway[19]. The PI3K/Akt signaling pathway is mainly activated by direct binding of PI3K to active ErbB3 in a hetero-dimer, or indirectly via recruitment to ErbB1 by Grb2 and Gab1[3,20]. PI3K initiates a positive feedback loop including Akt activation, promoting cell proliferation and survival. Binding of the ubiquitin ligase c-Cbl via its PTB

domain or by interaction with Grb2 designates the receptor for endocytosis and degradation by attachment of ubiquitin[21]. This negative regulation mechanism is important to control receptor activity and to terminate signaling after stimulation (see also chapter 1.2.2).

1.2.1. Activation of ErbB1

Ligand binding and dimer formation are essential for signal transduction of ErbB1[3]. The so-called 'signaling dimer' consists of two ligand-bound ErbB1 receptors, a complex also known as the active or asymmetric dimer, referring to the conformation of the kinase domains. The extracellular domains in the signaling dimer associate in a way such that the transmembrane domains interact at their N-terminal parts, allowing the juxtamembrane domains to associate and form an asymmetric dimer[22–24]. In this conformation one receptor is acting as an "activator" and the other as a "receiver" kinase, where the latter is phosphorylated by the former[25]. The activator kinase stabilizes the receiver kinase in the "αC-in active" conformation, in which the αC-helix is in a position that the catalytically important KE salt bridge between Lys721 and Glu738 is preserved[25] (Figure 6 A). In the "αC-out inactive" conformation the αC-helix disrupts the KE salt bridge[24] (Figure 6 C). Between both conformations the kinase domain was shown to be intrinsically disordered at the region of the αC-helix, which is thought to play an important role for the regulation of receptor activation[26] (Figure 6 B).

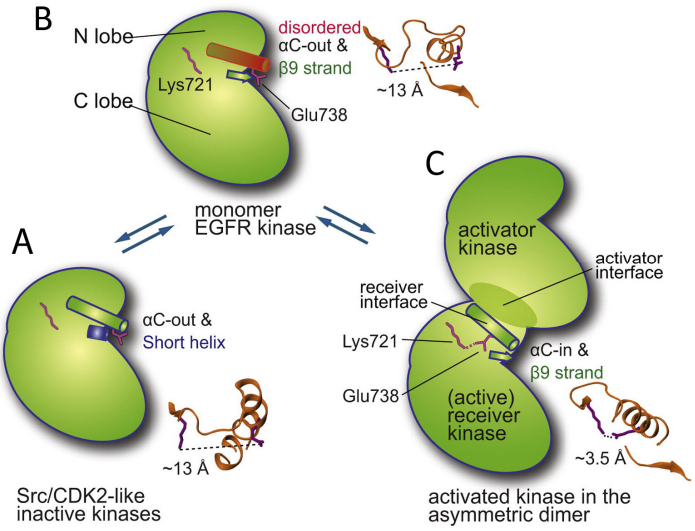

Figure 6: Schematic view of the three conformational states of the kinase domain of ErbB1. A: "αC-out inactive" conformation of the kinase, where the αC-helix disrupts the KE salt bridge. **B**: Kinase conformation, which is intrinsically disordered at the region of the αC-helix, where the KE salt bridge is broken. **C**: "αC-in active" conformation of the receiver kinase in an asymmetric dimer with intact KE salt. (Figure adapted from Shan *et al.*[26])

However, it is still under discussion how the signaling dimer is formed and how the signal transduction is regulated[3,22,27,28]. Early models for signaling dimer formation proposed that EGF binding to receptor monomers is required to promote active dimer formation between two EGF-bound receptor monomers[29] (Figure 7 A). Later it was shown that besides ligand-induced dimerization, ErbB1 dimers can also form independently of ligand binding[30–35] (Figure 7 B). These so-called predimers or inactive dimers show no kinase activity, because they do not adopt the asymmetric configuration that is required for kinase activation. In this conformation a C-terminal dimerization of the transmembrane helices is favored, which prevents the juxtamembrane domains from associating and forming the asymmetric kinase domain dimer[22-24].

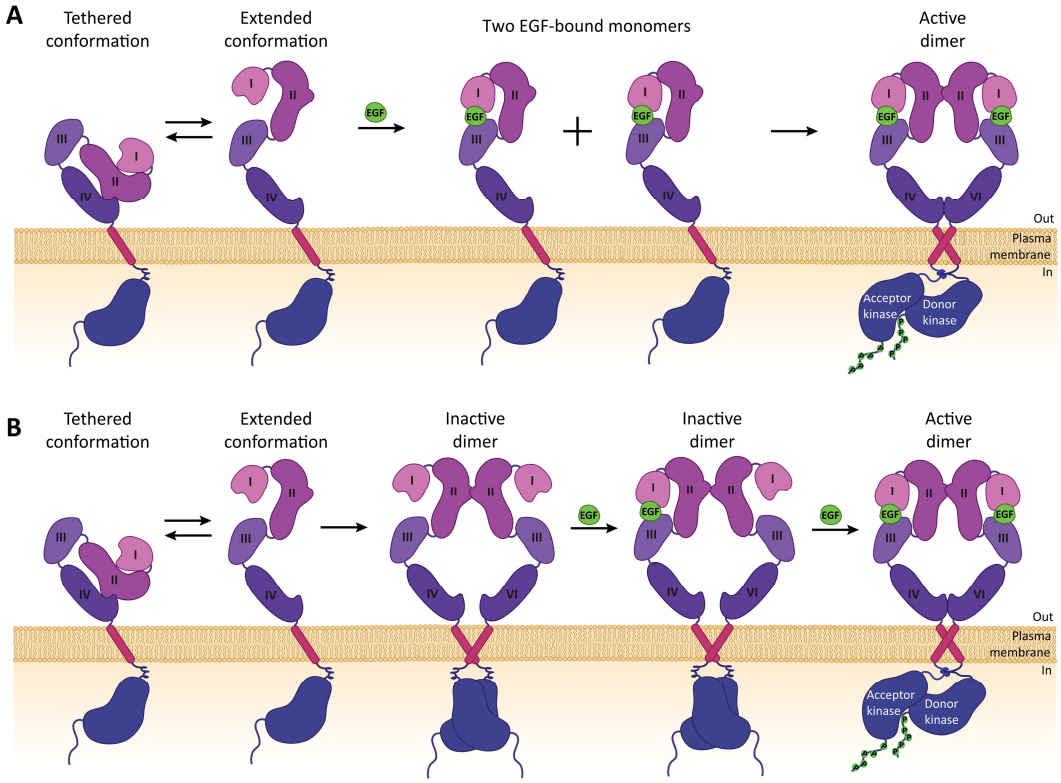

Figure 7: Two alternative models for formation of signaling ErbB1 dimers. A: One ErbB1 in extended conformation binds EGF, then dimerizes with a second ErbB1 bond to one EGF to form the signaling dimer. **B**: Two ErbB1 receptors in extended conformation form an predimer without ligand. EGF binds with higher affinity to this predimer but the dimer is still inactive. With binding of second EGF the asymetric kinase dimer can form, building the signaling dimer.

Teramura *et al.* showed that EGF binds with two orders of magnitude higher affinity to unoccupied predimers compared to monomers, and that binding of a second EGF to predimers, with one EGF already bound, is again one order of magnitude higher[36]. In this model for active dimer formation the monomers in extended conformations tend to form predimers (Figure 7 B). They suggested that the binding of EGF to an unoccupied predimer

induces an allosteric conformational change in the other receptor, which increases the EGF association rate to its binding site.

So far, the experimental evidence for predimerization and its significance for receptor activation have been conflicting[31,37–40]. Single molecule studies in living cells contradict each other on that point: one reports shows that predimerized unliganded receptors are primed for EGF binding[41], whereas a second study could not detect dimer formation of two unliganded receptors but detected stable dimer formation of two ligand bound receptors[42]. Number and brightness analysis in living cells showed that predimers only form in cells expressing receptors at high levels, suggesting that a different density of receptors on the surface of the cell might be a reason for the observed differences[43].

In addition to ligand-induced activation of ErbB1, ligand-independent activation has been observed in cells expressing the receptor at high levels (over 1 million receptors per cell)[23,43–45]. Normally there are several mechanisms to regulate ligand-independent activation, such as phosphatases that convert receptors in their dephosphorylated, inactive state[45]. Recent simulations showed that high overexpression of ErbB1 accompanied by the relative deficiency of anionic lipids in the plasma membrane could weaken the coupling between the intra- and extracellular domains so that the active kinase dimer conformation can form independently from the conformation of the extracellular domains[22,23]. This could lead to a drastic change in the balance of the system, which cannot be compensated by phosphatases.

Besides dimer formation, oligomerization of ErbB1 has been reported in several studies[43,46–50], but its significance for receptor activation and signal transduction is still disputed. Clayton *et al.* reported the formation of clusters with 15-30 unliganded receptors in human A431 cells that express ErbB1 at high levels[46]. Oligomer formation in A431 cells was confirmed by several other methods, including number and brightness analysis[43], FRET-FLIM combined with flow cytometry[48] and surface plasmon coupling microscopy[49]. Abulrob *et al.* observed ErbB1 clusters of an average diameter of 150 ± 80 nm in fixed HeLa cells (10 min EGF stimulation) using near-field scanning optical fluorescence microscopy[50]. Together, these studies yield an incoherent and confusing picture of ErbB1 clustering, possibly due to the large variations in experimental methods employed, and the experimental conditions that have been applied[43].

1.2.2. Endocytosis, intracellular trafficking and recycling

Signals from outside the cell need to be processed robustly, making it necessary to regulate the activity of membrane proteins. One of the major regulating mechanisms for ErbB1 is endocytotic trafficking[51]. By endocytosis, followed by recycling or degradation, ErbB1 activity can be spatially and temporally regulated to determine cell fate decisions (Figure 8).

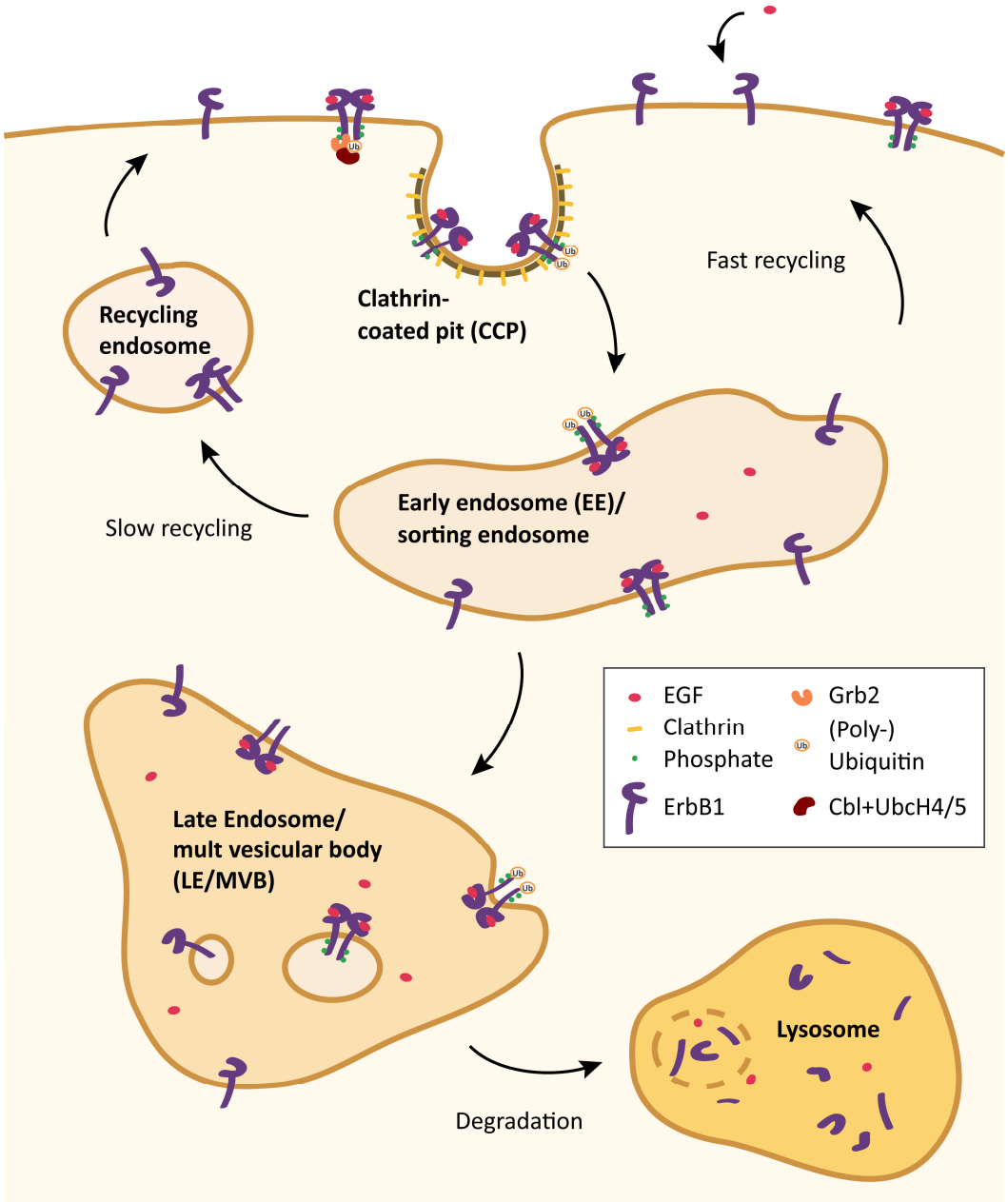

Figure 8: Model for recycling and clathrin mediated endocytosis (CME) of ErbB1. After binding of EGF to ErbB1 the receptor is phosphorylated. A complex of Grb2 and Cbl recognizes phosphotyrosines on the receptor and further recruits E2 enzymes (UbcH4/5) which ubiquitinate the receptor. Epsins bind to ubiquitins and recruit the receptor to clathrin-coated pits (CCP). The receptor can then be either recycled quickly from the early endosomes (EE) back to the membrane or remain in EE which mature to multi vesicular bodies (MVB) and late endosomes (LE). Poly-ubiquitination of the receptors is the signal for degradation in lysosomes.

The majority of receptors is internalized via clathrin-mediated endocytosis (CME, Figure 8). A complex of Grb2 and Cbl proteins (E3 ubiquitin ligases) is recruited to phosphorylated receptors, followed by the binding of E2 ubiquitin conjugating enzymes (UbcH4/5) to the RING domain of Cbl proteins for receptor polyubiquitination. The ubiquitinated receptors are recognized by the ubiquitin binding domains (UBD) of epsins (Eps15 and EPS15R) which recruit the receptor to clathrin-coated pits[52]. Although Cbl can also bind directly to phosphorylated ErbB1, it was shown this is not essential for receptor endocytosis[53].

Clathrin-independent pathways for endocytosis are involved when ErbB1 is highly overexpressed like in A431 cells[54,55] or when high concentrations of EGF are used[56,57]. These pathways are mainly observed together with membrane ruffling and pinocytosis and are significantly slower than CME.

EGF receptors are continuously internalized from the plasma membrane to endosomes and at the same time recycled from endosomes to the plasma membrane. Without stimulation by a specific ligand the rate of recycling (rate constant $k_r \geq 0.2\ min^{-1}$) is much higher than the rate of endocytosis (rate constant $k_e \sim 0.02 - 0.05\ min^{-1}$)[58], leading to a high level of receptors at the plasma membrane. When the receptor becomes phosphorylated upon ligand binding, its internalization rate increases, and it accumulates in early endosomes 2-5 minutes after the start of endocytosis[59]. These early endosomes (EE) are highly dynamic and fuse rapidly to the larger sorting or intermediate endosomes. ErbB1 will then either be sorted to lysosomes for degradation or to recycling endosomes. From early and sorting endosomes, receptors can either be recycled directly to the membrane at a high rate ($t_{1/2}$ of 2-6 min) or be transported back to the membrane via early recycling endosomes (ERC) at a much slower rate ($t_{1/2}$ of 15 - 30 min). The decision for degradation or recycling depends on the ligand bound to ErbB1. While EGF bound receptors are degraded and recycled in equal amounts, the recycling rate of TGF-α bound ErbB1 receptors increases significantly[60,61]. This difference is caused by the sensitivity of TGF-α binding for the low pH ($6.4 - 6.8$) in early endosomes[60,62], while EGF binding is not influenced at this pH. At an acidic pH the dissociation constant K_D between TGF-α and ErbB1 is low either due to a reduced affinity or to a high off rate. In contrast, EGF remains bound to ErbB1. This is essential for polyubiquitination of the receptor, which is the signal for sorting into late endosomes for lysosomal degradation. By manipulating the degradation and recycling rates of ErbB1, the specific responses to different stimuli can be regulated accurately. However, the exact recycling processes contributing to the regulation of ErbB1 activity and its signaling are still poorly understood.

1.2.3. ErbB1 mutations

Mutated forms of ErbB1 or disturbed regulation of its expression or activation occur in several cancer species. Here two point mutations that are relevant for the work described in this thesis are discussed.

The L834R somatic point mutation (also named L858R when including the 24 aa signaling sequence) accounts for around 40 % of all mutations found in ErbB1 in non-small-cell lung cancer (NSCLC)[63,64]. This mutation is located in the activation loop of the kinase domain, where it is close to the A-loop stabilizing DFG (Asp-Phe-Gly) motif. Lung cancers with this mutation are reported to respond to the competitive tyrosine kinase inhibitors (TKI) gefitinib (Iressa) and erlotinib (Tarceva)[65–68], which bind to the ATP binding site of the kinase. The binding affinity of gefitinib to the L834R mutant (K_D = 2.6 nM) is about 20-fold stronger than to the wild type ErbB1 (K_D = 53.5 nM)[69]. It was shown that the L834R mutant exhibits higher activation levels even without EGF stimulation[26,70,71]. Some studies showed considerably increased phosphorylation levels of Y992, Y1068 and especially Y845 while others observed no change in the relative levels of phosphorylation for different tyrosine residues but increased phosphorylation at all positions[71]. It has been suggested that the higher phosphorylation levels without EGF binding result from a strongly increased dimerization affinity of the L834R mutant[26,72]. Crystal structures indicate that the L834R mutation locks the kinase in a constitutively active state[69]. Shan *et al.* concluded from simulations that the "αC-in active" conformation is favored over the disordered state by the mutation such that the kinase domain is primed for dimerization[26]. They also propose that Y845 phosphorylation could play an important role for increased activation, and that it could be a trigger for lateral signal propagation that was reported earlier to be important for ErbB1 signal amplification[44,73].

The ErbB1 mutant K721A was introduced in 1987 by Honegger *et al.* to examine the possible tyrosine kinase function of ErbB1[74,75]. The lysine at position 721 is part of the ATP-binding site of the tyrosine kinase of ErbB1. The mutation of L721 to alanine leads to inactivity of the kinase domain, thereby preventing autophosphorylation of tyrosines.

1.3. Fluorescence microscopy

Fluorescence microscopy is a variant of light microscopy based on the characteristic of fluorescent particles to be excited by light and emit the absorbed energy as photons at red-shifted wavelengths. Today fluorescent microscopy is one of the most commonly used microscopy techniques. Fluorescence microscopy provides several advantages over other techniques like electron microscopy, such as specific labeling of cellular components and the possibility to observe processes in living cells.

1.3.1. Total internal reflection fluorescence (TIRF) microscopy

For single molecule microscopy of molecules in the membrane of the cells it is important to enhance the signal to noise ratio (SNR) and minimize the fluorescent background from the cytosol of a cell. By use of total internal reflection fluorescent (TIRF) microscopy the background from the cytosol can be significantly reduced. For TIRF illumination an evanescent field is produced by an incident light beam which is totally reflected at the interface between two media with different refractive indices *n*, usually the glass bottom of a dish (*n* = 1.52) and the aqueous solution (*n* = 1.33) surrounding the cells (Figure 9). The resulting evanescent wave decreases exponentially, thereby achieving a penetration depth of 100 – 200 nm[76]. As the background from the cytosol is drastically reduced, TIRF microscopy is a good choice for single particle measurements at the basal plasma membrane of adhered cells.

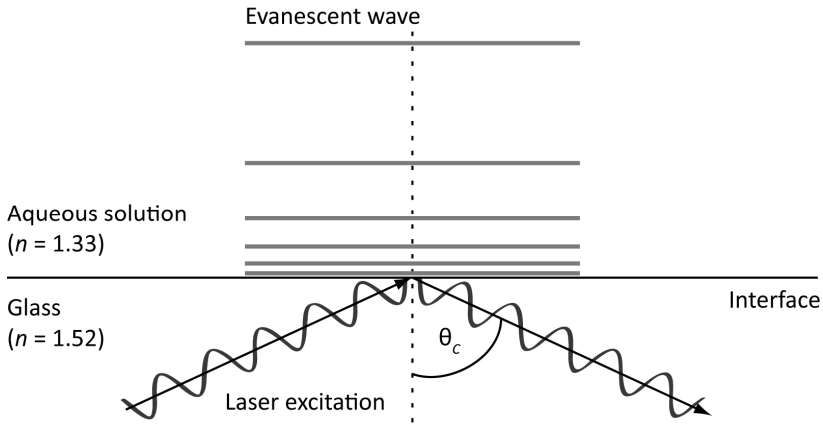

Figure 9: Principle of total internal reflection fluorescence (TIRF) microscopy. Light from a laser excitation source passes through the glass (refractive index *n* = 1.52) and is reflected at the glass-buffer (aqueous solution *n* = 1.33) interface. Light incident with an angle greater than the critical angle θ_C is totally reflected generating an evanescent wave that travels approximately 100 - 200 nm into the cell. Fluorophores in the cell near the glass interface are excited by the evanescent wave and emit fluorescence, while those further away from the interface are not excited.

1.3.2. Single molecule fluorescent microscopy

Conventional fluorescence microscopy is limited by the diffraction limit of light[77]. Typically a maximal spatial resolution of 200-300 nm in lateral direction and 500-700 nm along the optical axis can be achieved. The challenge for the development of single molecule fluorescence microscopy methods is to resolve molecules with a precision that exceeds the diffraction limit. In the early 1990s the first single fluorophore detection experiments at room temperature were published[78–81] that were able to overcome the diffraction barrier. Since then new possibilities for the development of techniques with unprecedented precision and resolution have been opened[82–84].

1.3.3. Single particle tracking

Single molecule imaging evolved as one of the main techniques to visualize and analyze sub-cellular structures, protein networks and functions. Protein interactions and activation occur on short time scales of a few milliseconds up to seconds, thus high spatial and temporal resolutions are essential to resolve signaling processes. Single particle tracking (SPT) follows the movements of single emitting particles at a relative low density in living cells. In contrast to bulk measurements like fluorescence recovery after photobleaching (FRAP)[85], fluorescence correlation spectroscopy (FCS)[86] or image correlation based techniques (e.g. ICS, ICCS[87]), SPT allows the observation of single events with high spatial and temporal resolution, revealing the full distribution of the measured quantity rather than an average value (as in FRAP and FCS based techniques). Another significant advantage of single particle tracking experiments at low protein density is that protein behavior might be more physiological than in cells overexpressing the targeted protein, which is usually needed to gain a reasonable signal-to-noise ratio in ensemble measurements. When imaging the dynamics of plasma membrane proteins, SPT is often combined with TIRF microscopy to reduce cytosolic background signals.

The localization of single molecules can be accomplished by fitting a Gaussian function to the intensity distribution of an emitting molecule described by the point spread function (PSF)[88]. Tracking algorithms localize the particles in each frame of an image series and temporally link them to form trajectories. Problems that often hinder robust tracking and track assembly are high particle density, particle motion heterogeneity, temporary particle disappearance and particle merging or splitting[89]. Some of these issues can be overcome by decreasing the particle density, but this is not always feasible or desirable. Therefore Jackaman *et al.*[90]

developed an algorithm that copes with most of these problems using a mathematical framework, the linear assignment problem (LAP)[91,92].

During the last decades single particle tracking methods were extensively implemented in the field of microscopy. Single molecule tracking can be used to investigate a wide range of molecules like lipids, membrane receptors and ligands. In 1981 Barak and Webb published the first single molecule tracking experiment on cell membranes[93]. They tracked a fluorescent low-density lipoprotein (LDL) derivate complexed to its receptor and could determine its diffusion coefficient. In 2000 Schütz *et al.* were the first to show the compartmentalization of lipids in the plasma membrane of living cells[94]. In 2002 Fujiwara *et al.* showed compartmentalization of the plasma membrane of rat kidney fibroblasts (NRK) by studying the movement of unsaturated phospholipids (DOPE) at the single molecule level with a temporal resolution of 25 µs[95]. Murase *et al.* used Cy3-labeled unsaturated phospholipids to further characterize plasma membrane compartments in various cell types[96]. They concluded that compartmentalization of the plasma membrane is universal and might play various biologically important roles in a variety of membrane functions. In accordance to that Lommerse *et al.* could show partitioning of H-Ras in different types of microdomains by tracking H-Ras labeled with EYFP[97]. In other studies quantum dots (QD) were used to label proteins of interest. For example, the dimerization of ErbB1 was visualized by using Qdot-labeled EGF and nanobodies[41,42,98].

1.3.4. Labeling methods

The choice of the fluorophore used in SPT is critical. For example quantum dots and gold nanoparticles have a high photo-stability and thereby enable long observation times, but for some biological applications the use of genetically encoded fluorescent proteins like GFP, tags or antibodies labeled with a bright dye might be more suitable. Thus, the choice of a labeling strategy strongly depends on the target protein and the imaging method.

There are several methods to label a protein of interest for single molecule fluorescence microscopy. A common approach is to link a fluorescent protein genetically to the DNA sequence of the targeted protein. The green fluorescent protein GFP was discovered 1961 by Osamu Shimomura in *Aequorea victoria*[99]. Douglas Prasher was the first to isolate and sequence the cDNA of GFP with a primary sequence of 238 amino acids (27 kDa) and to use it to tag other proteins[100,101]. GFP has two absorption maxima, at 395 nm and at 475 nm, the maximum of the emission spectrum lies at 509 nm. Meanwhile several variations of GFP have

been engineered with enhanced or different properties, e.g. color, stability and brightness (EGFP, CFP, BFP, YFP). Many fluorescent proteins from other species were also discovered, like the red fluorescent protein mCherry, which was derived from a protein isolated from *Discosoma* sp.[102].

Some applications need fluorophores with higher extinction coefficients, higher quantum yields or better photostability than fluorescent proteins. Dyes with high quantum yield include cyanide dyes like Cy3 and Cy5 or Alexa (Life Technologies, Grand Island, NE, USA) and Atto (Atto-Tec, Siegen, Germany) dyes. They are small in size and are commercially available in a wide range of colors. Quantum dots are semiconductor nanocrystals with a very low bleaching rate but they are relatively large and the labeling ratio is difficult to control as they generally have multiple binding sites.

There are several possibilities to introduce organic dyes or QDs to a protein of interest. For a broad range of biochemical approaches antibodies are used. Antibodies are generated to bind specifically to an antigene to identify and label proteins. The main disadvantages of antibodies are their size of 150 - 160 kDa and that they have two binding sites. Due to their size, a targeted protein could be influenced in its binding behavior and dynamic properties. Especially when measuring on a single molecule level, these attributes can be problematic. The two binding sites on one antibody molecule can lead to crosslinking of the targeted proteins, thereby perturbing their behavior.

To overcome the drawbacks of conventional antibodies Roovers *et al.* engineered nanobodies against ErbB1. Nanobodies are derived from antibodies from species of the *camelidae* family consisting only of heavy chains[103], from which they used only a single immunoglobulin (Ig) variable region, which leads to the drastically reduced size of a nanobody of 15 kDa. Additionally, nanobodies have only one binding site, making them an ideal tool for labeling single molecules. Analogous to genetically encoded tags, the protein of interest can be labeled with a range of fluorophores that are coupled to the nanobody. The only constraint is that a specific nanobody has to be developed for the protein of interest. So far the available range of specific nanobodies is relatively small but due to the big advantages over classical antibodies the number will certainly grow in the coming years.

Other methods use genetically encoded tags to introduce a specific site into a protein to which fluorescent dyes or quantum dots (QD) can be coupled[104]. Examples for such tags are SNAP/CLIP[105], FLASH[106] or Halo[107]. The advantage of these tags is that the same construct can be used to label the protein of interest with a variety of fluorophores. For example cell

impermeable dyes can be used to label only proteins on the cell surface, which is beneficial for imaging membrane receptors like ErbB1.

In this work, the SNAP-tag was used to label ErbB1 at the extracellular N-terminus. The SNAP-tag is a mutant of the O^6-alkylguanine-DNA alkyltransferase (AGT) of 20 kDa, which is a DNA repair protein that irreversibly transfers an alkyl residue from the O^6 position of guanine to one of the cysteins of AGT[105]. The SNAP-tag was mutated so that it has an increased affinity against O^6 benzylguanine (BG) as a substrate, on which several residues, such as functional groups or fluorescent dyes can be coupled. The SNAP-tag can be fused genetically to the target protein, to which the residue from a BG derivative will be covalently bound after the reaction (Figure 10).

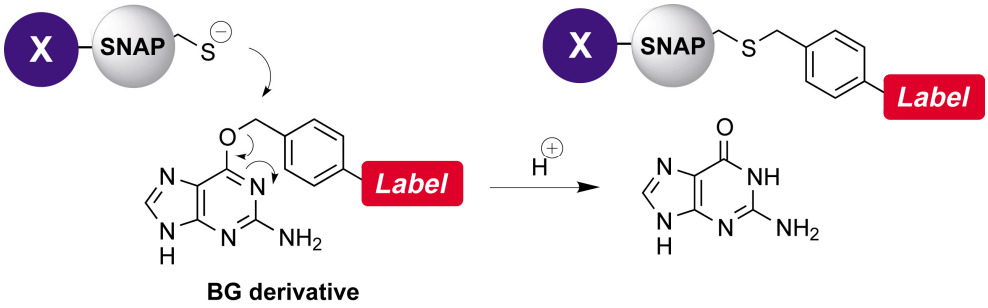

Figure 10: SNAP-tag labeling reaction. The SNAP-tag on a target protein (X) reacts with a benzylguanine derivative and transfers the label from the BG derivative to a cycsteine on the SNAP-tag (Figure adapted from Keppler *at al.* 2003[105]).

2. AIM OF THE THESIS

Although ErbB1 is one of the most studied members of the receptor tyrosine kinase family, the model for ErbB1 activation is still vividly discussed in the literature.

Binding of an external ligand to ErbB1 leads to the phosphorylation of several tyrosines and serines at its C-terminal tail, which are then recognized by effector proteins that transmit the signal into the cell. Dimerization is a key step in the activation process[108] and was shown to be highly dynamic by FRET studies[44] and more recently by single molecule studies[41,42]. As a result, the receptor is susceptible to activation in the absence of a ligand[23,43,44] and active regulation mechanisms for the receptor activity have to exist at plasma membrane level[45]. Receptor clustering was suggested as one possible mechanism to amplify the signal upon ligand binding, but the reported results were often contradictory[43,73,109–111]. These discrepancies are likely a result of the variety of employed methods and experimental conditions that were employed[43]. However, the relation between receptor activity and self-association has not been investigated directly in living cells, due to the lack of adequate methods, especially at low expression levels.

In this work, single particle tracking of the ErbB1 receptor, in combination with a probe for phosphorylation to visualize its activity, is used to answer the following questions:

1. How does ErbB1 dimerization and clustering relate to its signaling activity?
2. How is a stable signal generated from the plasma membrane?

These questions are investigated in cells with low ErbB1 densities at the plasma membrane, to avoid possible artifacts due to over-expression of the receptor.

3. MATERIALS AND METHODS

3.1. Materials

3.1.1. Equipment

Table 1: Equipment used for experiments.

Instrument	Name	Company
Argon laser, 476 nm Krypton laser, 568 nm	Innova Sabre: Argon DBW20/4, Krypton DBW	Coherent Inc., Dieburg, Germany
Blotting chambers	XCell Secure Lock	Invitrogen, Life Technologies GmbH, Darmstadt, Germany
Cell counter	Vi-CELL	Beckman Coulter, Krefeld, Germany
Chambered Cover Glass	Nunc Lab-Tek Chambered Cover Glass	Thermo Fisher Scientific, Waltham, USA
Clean bench	Cellgard Class II Biological Safety Cabinet	Nuaire, Integra Biosciences GmbH, Fernwald, Germany
Dichroic mirror DM570	DM 570 from U-MNIGA3	Olympus GmbH, Hamburg, Germany
Diode laser 640 nm	Toptica iBeam smart-640-S	Topica Photonics, München
DPSS laser	532 nm DPSS laser	UltraLasers, Toronto, Canada
Electrophoresis chambers	Electrophoresis chambers MINI and MIDI	Roth, Karlsruhe, Germany
Electroporator	Gene-pulser and Pulse controller	Bio-Rad, München, Germany
EM-CCD camera	iXon+, DU-897	Andor, Belfast, Northern Ireland
ESI-MS	Finnigan LCQ Advantage MAX	Thermo Fisher Scientific, Waltham, USA
Emission filter green	500-550	AHF, Tübingen, Germany
Emission filter red	BP 575-625 from U-MNIGA3	Olympus GmbH, Hamburg, Germany
Fluorescence microscope	Olympus IX81	Olympus GmbH, Hamburg, Germany
Gel imager	GelDoc XR	Bio-Rad, München, Germany
Helium neon (HeNe) laser	HeNe laser	Newport, Irvine, USA

Instrument	Name	Company
Image splitter	Optosplit II	Cairn Research, Faversham, UK
Incubator Shaker	Innova 4000 Incubator Shaker	New Brunswick Scientific, Nütringen, Germany
Infrared Imaging System	Odyssey	LI-COR Biosciences GmbH, Bad Homburg, Germany
Inverted confocal microscope	Leica TCS SP5	Leica Microsystems GmbH, Wetzlar, Germany
Objective heater system	Objective Heater System	Bioptechs, Butler, USA
Oil immersion objective for TIRF, 60x	PLAPON 60xO/TIRFM-SP, NA = 1.45	Olympus GmbH, Hamburg, Germany
PCR-Cycler	Mastercycler® pro vapo.protect™, Mastercycler® EP gradient	Eppendorf, Hamburg, Germany
Pipettes	Reference and Research plus	Eppendorf, Hamburg, Germany
Power supplies for electrophoresis and blotting	Power Pac 300, HC and Universal	Bio-Rad, München, Germany
Reverse phase (RP) HPLC	Beckman System Gold HPLC	Beckman Coulter, Krefeld, Germany
Spectrophotometer	Spectrophotometer DU 800	Beckman Coulter, Krefeld, Germany
Spectrophotometer	NanoDrop Spectrophotometer ND 1000	PEQLAB Biotechnologie GmbH, Erlangen, Germany
Tabletop centrifuge	Centrifuge 5424	Eppendorf, Hamburg, Germany
Thermo shaker	ThermoShaker TS1	Biometra, Göttingen, Germany
Vacuum Centrifuge	Concentrator plus	Eppendorf, Hamburg, Germany
Vortex	Vortex Genie1 Touch Mixer	Scientific Industries, Karlsruhe, Germany
Water bath	Isotemp 205 Water bath	Fisher Scientific, Schwerte, Germany

3.1.2. Chemicals, Enzymes

All basic chemicals were purchased from Serva (Heidelberg, Germany), Sigma-Aldrich (Taufkirchen, Germany) or Roth (Karlsruhe, Germany) and used as recieved.

Table 2: Chemicals and enzymes used for experiments.

Name	Company
AccuPrime *Pfx* DNA polymerase, AccuPrime Reaktion Mix, 10x	Invitrogen, Life Technologies GmbH, Darmstadt, Germany
Albumin Bovine Fraction V, pH 7.0 (BSA)	Serva, Heidelberg, Germany
Anti-rabbit/goat/mouse-IRDye800/IRDye700,	New England Biolabs, Frankfurt am Main, Germany
Anti-EGFR (#2232)	Cell Signaling Technology, Inc., Danvers, USA
Anti-phosphotyrosines (pY72)	Invivo Biotech Services, Hennigsdorf, Germany
Blocking buffer (Odyssey) for western blots	LI-COR Biosciences GmbH, Bad Homburg, Germany
Bradford reagent	Sigma-Aldrich, Taufkirchen, Germany
Cell Lysis buffer, 10x	Cell Signaling Technology, Inc., Danvers, USA
Dynasore	Calbiochem, Merck KGaA, Darmstadt, Germany
DMEM, FCS, L-Glutamine, Trypsin, NEAA, DPBS	PAN Biotech, Aidenbach, Germany
DPBS, Calcium, Magnesium (DPBS+)	Gibco, Life Technologies GmbH, Darmstadt, Germany
EGF, human	Sigma-Aldrich, Taufkirchen, Germany
EGF-Alexa488, EGF-Alexa647	Michael Sonntag, AG Brunsveld, TU Eindhoven, Netherlands
Erlotinib	Cayman Chemical, Ann Arbor, USA
Glycine, Poly-L-Lysine	Sigma-Aldrich, Taufkirchen, Germany
IgG donkey anti-mouse Alexa647 or Alexa488	Invitrogen, Life Technologies GmbH, Darmstadt, Germany
Immobilon-FL PVDF	Millipore, Merck KGaA, Darmstadt, Germany
Licor ladder (Odyssey)	LI-COR Biosciences GmbH, Bad Homburg, Germany
Mono-reactive Cy3 NHS ester	Amersham, GE Healthcare
(Sodium-)Orthovanadate, H_2O_2	Sigma-Aldrich, Taufkirchen, Germany
Paq5000 DNA polymerase, Paq buffer, 10 x	Agilent, Böblingen, Germany
Penicillin/Streptomycin	PAN Biotech, Aidenbach, Germany
Phosphatase Inhibitor 2 + 3	Sigma-Aldrich, Taufkirchen, Germany
Precision Plus ladder	Bio-Rad, München, Germany
Primers, HPSF purification	Eurofins MWG Operon, Ebersberg, Germany

Name	Company
Protease Inhibitor Cocktail tablet, Complete, Mini, EDTA-free	Roche, Mannheim, Germany
RedSafe, DNA Stain	Chembio Ltd, Hertfordshire, UK
Restriction enzymes	New England Biolabs, Frankfurt am Main, Germany
T4-DNA-Ligase	Invitrogen, Life Technologies GmbH, Darmstadt, Germany
TetraSpecks	Life Technologies GmbH, Darmstadt, Germany
Tween-20	Sigma-Aldrich, Taufkirchen, Germany

3.1.3. Kits

Table 3: Used Kits.

Application	Name	Company
Clean-up of Sequencing Reactions	NucleoSEQ	MACHEREY-NAGEL, Düren, Germany
Gel extraction	QIAquick Gel Extraction Kit	QIAGEN, Hilden, Germany
Plasmid preparation, mini	QIAprep Spin Miniprep Kit	QIAGEN, Hilden, Germany
	High Pure Plasmid Isolation Kit	Roche Applied Science, Mannheim, Germany
Plasmid preparation, midi, endotoxin-free	NucleoBond® Xtra Midi EF	MACHEREY-NAGEL, Düren, Germany
Transfection	Effectene® Transfection Reagent	QIAGEN, Hilden, Germany

3.1.4. Buffers and solutions

TAE buffer 1x

40 mM Tris-acetate
1 mM EDTA
pH 8.3

TBS-T

25 mM Tris
137 mM NaCl
2.7 mM KCl
0.05 % TWEEN-20

Lysis buffer (10 ml)

1 ml Cell Lysis buffer 10x
9 ml ddH_2O
100 µl Phosphatase Inhibitor Cocktail 2
100 µl Phosphatase Inhibitor Cocktail 3
1 tablet Protease Inhibitor cocktail, complete, Mini, EDTA-free

Phosphate buffered saline (PBS) 1x

137 mM NaCl
2.7 mM KCl
10 mM Na_2HPO_4 x 12 H_2O
2 mM KH_2PO_4
pH 7.4

Paraformaldehyde

4 % (w/v) Paraformaldehyde
10 mM NaOH
in 1x PBS
pH 7.4

SDS sample buffer, 5x

60 mM Tris-HCl
14.4 mM 2-Mercaptoethanol
25 % Glycerol
2 % SDS
0.1 % Bromphenol blue

SDS running buffer (pH 8.3), 1x

25 mM Tris base
192 mM Glycine
0.1 % SDS
in ddH_20

Transfer buffer, 1x

12 mM Tris base
96 mM Glycine
in 20 % methanol

LB medium

10 g Bact. Tryp
5 g Yeast extract
10 g NaCl
ad 1 L H_2O
pH 7.4

LB agar

LB medium + 1.5 % Bacto Agar

SOB medium

20 g Trypton
5 g Yeast extract
0.58 g NaCl
0.19 g KCl
2.03 g $MgCl_2$ x 6 H_2O
2.46 g $MgSO_4$ x 7 H_2O
ad 1 L H_2O

SOC medium

SOB medium + 2 % (v/v) glucose

DMEM (PAN Biotech)

DMEM with 4.5 g/l glucose
without L-glutamine
with sodium pyruvate
with phenol red
with 3,7 g/l $NaHCO_3$

Imaging medium (PAN Biotech)

DMEM with 4.5 g/l glucose
with stab. glutamine
with sodium pyruvate
with 25 mM Hepes
without Phenol red
with 0,5 g/l $NaHCO_3$

3.1.5. Software

Table 4: Used Software.

Name	Source
Matlab	Version R2013A, MathWorks, Ismaning, Germany
ImageJ	Rasband, W.S., ImageJ, U. S. National Institutes of Health, Bethesda, Maryland, USA, http://imagej.nih.gov/ij/, 1997-2012
Fiji	Schindelin *et al.* Nature Methods (2012)[112]
IGOR Pro	WaveMetrics, Portland, USA
vbSPT	Persson *et al.* Nature Methods (2013)[113]

3.2. Molecular biology

3.2.1. Plasmids

Table 5: Plasmids used for cloning and transfections.

Name	Description	Origin
pSNAP-tag(m)®	SNAP tag encoding plasmid	New England Biolabs, Frankfurt am Main, Germany
pEGFP-N1	EGFP encoding plasmid	Clontech Laboratories, Inc., Mountain View, USA
pmCherry-N1	mCherry encoding plasmid	Clontech Laboratories, Inc. Mountain View, USA
EGFP-PTB	Encoding PTB domain from Shc with N-terminal EGFP	Martin Offterdinger
EGFP-hLCA	Encoding human clathrin light chain A with N-terminal	Martin Offterdinger
EGFP-ErbB1	Encoding ErbB1 with N-terminal EGFP after signaling sequence	Martin Offterdinger
ErbB1-EGFP	Encoding ErbB1 with C-terminal EGFP	Wouters *et al.* 1999[114]
ErbB1-mCherry	Encoding ErbB1 with C-terminal mCherry	Cloned from ErbB1-EGFP
SNAP-ErbB1	Encoding ErbB1 with N-terminal SNAP-tag after signaling sequence	Cloned from EGFP-ErbB1
SNAP-ErbB1 L834R	Encoding SNAP-ErbB1 with point mutation L834R	Cloned from SNAP-ErbB1
SNAP-ErbB1 K721A	Encoding SNAP-ErbB1 with point mutation K721A	Cloned from SNAP-ErbB1

3.2.1.1. Cloning of constructs

For the construction of SNAP-ErbB1 the DNA sequences for SNAP were amplified by PCR from pSNAP-tag(m) with primers SNAP_AgeI_F and SNAP_XhoI_R (Table 11) and afterwards digested with AgeI and XhoI. EGFP-ErbB1 (Table 5) was also digested with AgeI and XhoI to cut out the EGFP sequence and replace with the SNAP sequence.

Point mutations K721A and L834R were inserted into SNAP-ErbB1 plasmids by mutation PCR (see chapter 3.2.4.2) using primers listed in Table 12.

The PTB sequence was amplified by PCR from PTB-Citrine with the primers PTB_EcoRI_for and PTB_SalI_rev (Table 11), digested with EcoRI and SalI and ligated into the mCherry-N1 vector. Correctness of constructed plasmids was verified by DNA sequencing (chapter 3.2.4.4).

3.2.2. Plasmid preparation

Plasmid DNA was purified from 3 ml or 200 ml *E. coli* overnight cultures in LB medium with the Plasmid Mini / Midi Kit (QIAGEN) or the High Pure Plasmid Isolation Kit (Roche).

3.2.3. Agarose gel electrophoresis

The separation of DNA fragments due to their length was performed by agarose gel electrophoresis. In this method an electric field is applied so that at neutral pH the negatively charged DNA fragments migrate in the direction of the positive charged anode due to the DNA's negatively charged phosphates on their backbone. With agarose as a matrix the migration speed of the DNA fragments only depends on their molecular weight due to same mass to charge ratio per DNA fragment. All gels were prepared with 1 – 2 % agarose in TAE buffer. To stain the DNA the DNA binding dye RedSafe™ was added to the agarose gel, so that the DNA bands could be visualized under UV light. 1 kb DNA ladder (Fermentas) was loaded on the gel in parallel to estimate the length of the fragments. If necessary fragments of expected length were sliced out of the gel and extracted with the QIAquick Gel Extraction Kit.

3.2.4. Polymerase chain reaction

The polymerase chain reaction (PCR) is a standard method to amplify DNA. For the reaction a small amount of matrix DNA is mixed with two single stranded DNA primers, the four desoxy nucleotides dATP, dCTP, dGTP, dTTP and a thermo stable DNA polymerase like *Taq, Pfx* or *Pfu*.

In three steps the double stranded DNA is first denatured to single strand DNA, followed by hybridization with the primers, which are then elongated by the polymerase from 5' to 3'. These steps are repeated several times leading to an exponential amplification of DNA.

3.2.4.1. Amplification PCR

A typical PCR, where an insert for cloning, like PTB or SNAP, was amplified, is listed in Table 6 and Table 7.

Table 6: Typical composition of an amplification PCR.

reagent	amount
Matrix DNA	30 - 50 ng
Primer 1	300 nM
Primer 2	300 nM
AccuPrime reaction mix	1x
AccuPrime *Pfx* DNA polymerase	1 U
	filled up with ddH_2O to 50 µl

Table 7: Cycling parameters for an amplification PCR.

temperature	time	
Denaturation (95°C)	2 min	
Denaturation (95°C)	15 s	25x
Annealing (55°C)	30 s	
Elongation (68°C)	1 min/kb	
Final elongation (68°C)	10 min	
8°C	∞	

3.2.4.2. Mutation PCR

Point mutations were introduced into the coding DNA of a protein by mutation PCR. Two complementary primers containing the mutation flanked by 15 - 17 bp at each side complementary to the target sequence were used together with a plasmid containing the target DNA sequence in a PCR (Table 6 for reaction, Table 8 for cycling parameters). After the PCR the plasmid DNA was digested with *DpnI* for 1 h at 37°C. 1 - 2 µl of the reaction were used to transform *E. coli* to religate and amplify the mutated plasmid.

Table 8: Cycling parameters for a mutagenese PCR.

temperature	time	
Denaturation (95°C)	2 min	
Denaturation (95°C)	30 s	16x
Annealing (55°C)	60 s	
Elongation (68°C)	1 min/kb	
Final elongation (68°C)	7 min	
8°C	∞	

3.2.4.3. Colony PCR

During particular cloning procedures it was useful to select promising clones by colony PCR. For this method a small amount of an *E. coli* colony from an agar plate is used in a PCR (Table 9, Table 10). With a pipette tip that was dipped in the colony a few cells were transferred into the PCR reaction tube. Specific primers were chosen to amplify a region of the plasmid where the cloning success could be evaluated, for example a forward primer binding to the multiple cloning site (MCS) together with a reverse primer binding to the terminator sequence.

Table 9: Typical composition of a colony PCR.

reagent	amount
Primer 1	250 nM
Primer 2	250 nM
dNTPs	Each 250 µM
Paq buffer	1x
Paq5000 DNA polymerase	1 U
filled up with ddH_2O to 25 µl	

Table 10: Cycling parameters for a colony PCR.

temperature	time	
Denaturation (95°C)	10 min	
Denaturation (95°C)	30 s	30x
Annealing (55°C)	30 s	
Elongation (72°C)	1 min/kb	
Final elongation (72°C)	10 min	
8°C	∞	

3.2.4.4. Sequencing

To verify the accuracy of DNA after cloning, DNA sequences were sequenced by the Sanger method[115]. In this method chain terminating didesoxynucleotides (ddNTPs) labeled with one color for each nucleotide are added to a normal PCR mixture consisting of matrix DNA, desoxynucleotides (dNTPs) and polymerase but only one primer. After denaturation of the matrix DNA and annealing of the primer the polymerase elongates the strand until one didesoxynucleotide is incorporated and the lacking 3'-OH group precludes further elongation. After repeated cycles of this PCR reaction several newly synthesized DNA sequences of different lengths are generated. By capillary agarose electrophoresis the sequences are separated by their length and by detecting the color of the terminating didesoxynucleotide the DNA sequence can be concluded.

Using this method it is usually possible to sequence up to 1000 bases starting from the primer, so that it is necessary to repeat this reaction multiple times with different primers for longer sequences like the ErbB receptors. 4 - 5 reactions with primers binding to different parts of the receptor sequence were prepared.

3.2.4.5. Cloning primers

Table 11: Primer sequences used for cloning.

Name	Sequence (5' → 3')
SNAP_AgeI_F	GCG ACC GGT AAT GGA CAA AGA CTG CGA AAT G
SNAP_XhoI_R	CTC CTC GAG CAC CCA GCC CAG GCA
PTB_EcoRI_for	CGC GAA TTC ATG GGC CAG CTT GGG
PTB_SalI_rev	CGC GTC GAC GTC CTG AGG TAT TGT TTG AAG C

3.2.4.6. Mutation primers

Table 12: Primer sequences used for mutation.

Mutation	Primer	Sequence (5' → 3')
ErbB1 L834R (dimerization enhanced)	ErbB1_L858R_F	CAC AGA TTT TGG GCG GGC CAA ACT GCT GG
	ErbB1_L858R_R	CCA GCA GTT TGG CCC GCC CAA AAT CTG TG
ErbB1 K721A (kinase-dead)	ErbB1_K721A_F	GTT AAA ATT CCC GTC GCT ATC GCG GAA TTA AGA GAA GCA ACA TC
	ErbB1_K721A_R	GAT GTT GCT TCT CTT AAT TCC GCG ATA GCG ACG GGA ATT TTA AC

3.2.5. Ligation

Ligation of DNA fragments and plasmids, both treated with the same restriction enzymes, was carried out using the T4-DNA Ligase. A typical ligation reaction with cohesive ends after restriction contained 30 fmol insert, 10 fmol vector and 0.4 U T4 DNA Ligase in 20 µl. After 1 h incubation at room temperature 2 - 5 µl of the ligation reaction were used for transformation. For religation of a digested plasmid with blunt ends, 50 fmol plasmid were incubated with 1 U T4 DNA Ligase overnight at 14°C.

3.2.6. Transformation

For chemical transformation of *E. coli* XL10 Gold 1 µl purified plasmid DNA or 2 - 5 µl ligation reaction were added to 100 µl chemically competent cells. Cells were kept on ice for 30 min, heat shocked for 45 s in a water bath at 42°C and then kept on ice for another 2 min. 400 µl SOC medium were added, cells were plated on LB agar plates containing antibiotics (50 µg/ml kanamycin or 100 µg/ml ampicillin) and incubated overnight at 37°C.

3.3. Protein analysis

3.3.1. Bradford assay

The Bradford assay is a photometric method to quantify protein concentrations in solution[116]. When the applied dye, Coomassie Brilliant Blue G-250, binds to proteins in acidic solution, its absorbance maximum is shifting from 465 to 595 nm. This shift can be measured photometrically and along with a calibration measurement the absorbance can be correlated to the protein concentration.

For calibration a dilution series was prepared from a 1 mg/ml BSA stock solution and 4 dilution steps to obtain standard samples with 16, 8, 4, 2 and 1 µg/ml. Samples were prepared by adding 1 µl of the cell lysates (or lysis buffer as blank) to 500 µl ddH_2O. To all samples 500 µl Bradford reagent were added, mixed well and incubated 5 min at RT. The absorption values were measured in plastic cuvettes in a spectrophotometer at 595 nm. A linear calibration curve was calculated via the BSA sample measurements and the concentrations of the cell lysate samples were calculated by the resulting equation.

3.3.2. SDS polyacrylamide gel electrophoresis (SDS-PAGE)

Table 13: Recipe for 4 SDS stacking gels.

Amount	Reagent
1 ml	50 Acrylamide-Bis (29:1)
4.2 ml	0.375 M Tris-HCl, pH 6.8
6.3 ml	ddH_2O
125 µl	10 % SDS
1 ml	APS (50 mg/ml)
5 µl	TEMED

Table 14: Recipe for 3 small 6 % SDS seperating gels.

Amount	Reagent
3 ml	50 % Acrylamide-Bis (29:1)
9.4 ml	1 M Tris-HCl, pH 8.8
7.8 ml	ddH_2O
250 µl	10 % SDS
4 ml	50 % Sucrose
625 µl	APS (50 mg/ml)
6.25 µl	TEMED

Proteins can be separated by their size in an electric field by SDS-PAGE. Sodium dodecyl sulfate (SDS) is an anionic detergent, which binds to proteins. This leads to an equal mass to charge ratio and the linearization of the proteins. Thus the negatively charged proteins can be separated through a gel based on an acrylamide matrix only by their size when migrating towards the positively charged anode in an electric field. After electrophoresis gels can be either used for western blotting or stained directly with Coomassie Brilliant Blue R-250.

20 µg of protein samples were mixed with 5x sample buffer and incubated 10 min at 95°C. 6 % acrylamide gels were prepared according to Laemmli[117] (Table 13 and Table 14) and loaded with the protein samples, as well as with the Precision Plus Dual Color ladder (Bio-Rad) in parallel. A constant current of 60 mA was applied for 90 min.

3.3.3. Western Blotting

In a western blot proteins, e.g. in cell lysates, are first separated by size in an SDS-PAGE and then transferred to the surface of a membrane on which proteins can be specifically stained with primary antibodies. Using secondary antibodies with fluorescent dyes to tag the primary antibodies gives the opportunity to stain for different proteins or tags at the same time and read out with a fluorescence scanner. After an SDS-PAGE (see 2.3.1.) proteins were transferred to an Immobilon-FL PVDF membrane with constant 180 mA in 70 min. In Western blots for EGFR activation antibodies against total EGFR and phosphorylated tyrosines (PY72) were used. As secondary antibodies donkey anti-rabbit/goat/mouse-IRDye800/IRDye700 were used with a 1:5000 dilution. The blot was scanned on a Licor machine with the ability to scan 2 colors in parallel.

Densitometric analysis of western blot bands

The intensity of individual protein signals in Coomassie stained SDS-gels or with some regards in immunostained western blots can be used for a quantitative analysis. Therefor the program Adobe Photoshop CS3 was used to cut out the interesting bands with the correspondent background from high-resolution tiff-file images. The resulting tiff-file image with the signal and correspondent background cutouts was analyzed with the program Scion Image (Scion Corporation) to obtain the intensities of each cutout. After subtracting the background intensities from the signal intensities the relative ratios of phosphorylated to total receptor were calculated.

3.4. Cell biology

3.4.1. Cell culture

The human breast cancer cell line MCF-7 (Michigan Cancer Foundation - 7) isolated in 1970 from a 69-year-old Caucasian woman was used for all experiments as it has a low endogenous level of ErbB1 but expresses medium levels or ErbB2 and ErbB3[118]. All cells were cultured in DMEM with phenol red, 10 % (v/v) FCS, 1 % L-glutamine and 1 % non-essential amino acids (NEAA) at 37°C with 5 % CO_2. Cells were split two to three times a week with a ratio of 1:5 to 1:10.

For single particle tracking experiments cells were seeded in eight-well Lab-Tek chambers at a density of 3×10^4 cells per well 24 h before transfection and two days before the measurement. For experiments followed by western blot analysis, 5×10^5 cells were seeded in 35 mm Mattek dishes and transfected 6 h after seeding.

3.4.2. Transfection

Cells were transfected with Effectene® Transfection Reagent, which is a non-liposomal lipid formulation, according to manufacturer's protocol with an Effectene:DNA ratio of 1:10. For most of the experiments cells were transfected 24 h before the experiment. When cotransfecting two plasmids the total amount of DNA was kept constant. When cotransfecting an ErbB receptor construct together with a PTB domain or clathrin construct, the ratio of receptor-DNA:PTB-/clathrin-DNA was 2:1.

3.4.3. SNAP-labeling

For SNAP-labeling cells were washed with imaging medium containing 0.5 % BSA and then incubated for 5 min with 500 nM SNAP substrate in imaging medium containing 0.5 % BSA at 37°C. Cells were washed 3 times with imaging medium containing 0.5 % BSA (2x quick, 1x 10 min at 37°C) and 2 times with DPBS, then imaged in DPBS with calcium and magnesium.

Benzylguanine-Cy3 was synthesized in a standard chemical coupling reaction with BG-NH_2 and Cy3 NHS ester. The purity of the product was analyzed by reverse phase (RP) HPLC Beckmann System Gold (modules 126, 168, 508 with a dual-pump and high-pressure mixing system) using a C18 column (Bischoff, 250 × 4.6 mm, 5 µm) at 214 nm and 550 nm. The correct molecular

mass of the product was determined by electrospray ionization mass spectrometry (ESI-MS). A 1 mM stock solution of benzylguanine-Cy3 in DMSO was kept at -20°C.

3.4.4. Cell lysis

Cell lysates for western blot assays were prepared from 35 mm cell culture dishes. The day of transfection 3 - 5 x 10^5 cells were seeded and transfected after 6 - 8 h. 24 h after transfection cells were starved overnight in serum free DMEM with 1 % L-glutamine and 1 % NEAA at 37°C with 5 % CO_2. The next day cells were stimulated with 16 nM EGF (or labeled EGF) in imaging medium for defined periods (e.g. 0, 2, 5, 10 min) at 37°C. After stimulation cells were placed on ice and washed once with ice cold PBS. PBS was drained, 50 µl lysis buffer added and cells were scraped. After 10 min incubation on ice cell suspensions were transferred in pre cooled tubes and centrifuged 15 min at 13,000 rpm and 4°C. The supernatants were transferred in fresh tubes and protein concentration was determined by Bradford assay (chapter 3.3.1). Lysates were stored at -20°C until further use in western blot analysis (chapter 3.3.3).

3.5. Microscopy

3.5.1. Single particle tracking

3.5.1.1. Setup

Single molecule tracking data were acquired with an Olympus IX81 microscope equipped with a TIRF illuminator and a 60x oil immersion objective suitable for TIRF imaging. Laser illumination was provided by an argon-ion laser emitting at 476 nm, and a krypton-ion laser emitting at 568 nm, coupled into the TIRF illuminator via an optical fiber. The emission light was separated by an image splitter equipped with a dichroic mirror DM570 and emission filters 500 - 550 and 575 - 625 (Figure 11). The sample was imaged on a back-illuminated electron-multiplying CCD (EM-CCD) camera with 512 x 512 pixels. For dual-color imaging the excitation was alternated between the 476 nm and 568 nm sources, using custom build electronics to trigger the shutters in synchronization with the EM-CCD camera. The image was magnified by the image splitter to an effective pixel size of 107 nm. An objective heater was used to keep the sample at 37°C.

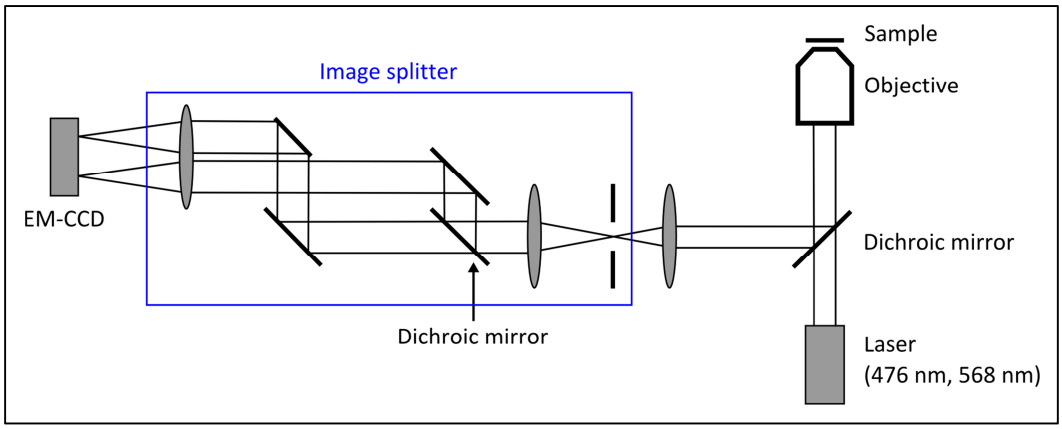

Figure 11: Experimental setup for dual-color fluorescence single particle tracking. The dichroic mirror in the image splitter separates the emission light at 570 nm resulting in two images of the sample on the EM-CCD camera.

3.5.1.2. Measurements

For experiments with EGF stimulation cells were starved overnight in DMEM with phenol red, 1 % L-glutamine and 1 % non-essential amino acids at 37°C with 5 % CO_2. After SNAP-labeling, directly before the measurements, the medium was removed, cells were washed twice with DPBS+ and imaged in 190 µl DPBS+. Stimulation with 16 nM EGF (100 ng/ml) or EGF-Alexa488 (113 ng/ml) was performed by adding 10 µl of a 20x EGF solution to the cells and mixing by pipetting 3 times up and down. For single particle tracking measurements a sequence of 300 - 2000 images was taken with alternating excitation, with a frequency of 30 frames/s, resulting in 15 frames/s for each channel, and an exposure time of 31.6 ms. One cell was imaged before addition of EGF, and another cell for every time point after addition of EGF (2, 5 and 10 min).

Drug treatments

For experiments with dynasore, cells were washed twice with DPBS+ immediately prior to imaging as described above, but then 190 µl of an 80 µM dynasore solution in PBS were added to the cells. Cells were incubated for 30 minutes in the drug solution before stimulation with 16 nM EGF and imaging.

A 25 mM pervanadate solution was prepared directly before the experiment by mixing orthovanadate with 30 % hydrogen peroxide at a molar ratio of 2.5:1. Until use it was kept on ice. 1 mM pervanadate incubations were performed by adding 8 µl of the freshly prepared stock solution to 192 µl DPBS+ on the cells.

For kinase inhibition after SNAP labeling cells were incubated with 10 µM erlotinib in imaging medium for 1 h. Before the measurement cells were washed twice with DPBS+ and imaged in 190 µl DPBS+ including 10 µM erlotinib. EGF stimulation was carried out as described above.

3.5.1.3. Calibration

TetraSpecks (100 nm diameter) diluted 1:10 from stock were imaged in an 8-well- chamber with the same settings as the tracking measurement. Channels were separated and the transformation matrix was calculated with Matlab script cp2form 'projective'. The transformation matrix was used to align the channels during analysis.

3.5.1.4. Image processing

Before the particles in each particular image where localized and connected to trajectories, dual-color tif-stacks (512 x 512 pixels) where split in two (each 512 x 256 pixels) and one channel was shifted according to the transformation matrix calculated as described in chapter 3.5.1.3 using custom written Matlab scripts.

3.5.2. Confocal microscopy

3.5.2.1. Setup and measurements

Confocal microscopy measurements were performed on a Leica SP5 inverted confocal microscope equipped with a 63x oil objective (HCX PL APO lambda blue 1.4NA) and an incubation chamber at 37°C and 5 % CO_2. The scanner unit of the microscope was coupled to an argon laser, a DPSS laser (UltraLasers, Toronto, Canada) and a helium neon (HeNe) laser (Newport, Irvine, USA). The wavelength for excitation was selected by acousto-optical tunable filters (AOTF) and scanned over the sample with a frequency of 400 Hz with 4 lines averaged. Emission signals were also selected using AOTFs with sequential imaging of different fluorophore channels. The emission signal was passed through a pinhole to block out-of-focus light. The signals were detected by photomultiplier tubes (PMTs) with sensitivity adjusted to 1250 V. The channels for multi-color imaging were set as follows:

ch00 (EGFP/Alexa488) excitation with 476 nm (argon laser at 27 %), emission 500 – 550 nm
ch01 (bleedthrough) excitation with 476 nm (argon laser at 27 %), emission 575 – 625 nm
ch02 (Cy3/mCherry) excitation with 561 nm (DPSS laser at 34 - 40 %), emission 575 – 625 nm
ch03 (Alexa647) excitation with 633 nm (HeNe laser at 31 %), emission 680 – 750 nm.

Cells were imaged in imaging medium and stimulated with 16 nM EGF (100 ng/ml), EGF-Alexa488 (113 ng/ml) or EGF-Alexa647 (118 ng/ml).

3.6. Data analysis

3.6.1. Single molecule tracking data analysis and classification

To separate the two channels of each image series and align to them using the parameters calculated from calibration measurements (Chapter 3.5.1.3) a custom written MATLAB script was used. With the ImageJ image-processing package cells of interest were manually selected by drawing masks.

Single particle tracks were obtained using the u-Track package[90], and tracks within the masked areas were further analyzed with the vbSPT package[113] to classify each localization in each track according to a 3-state model. For further analysis by custom written MATLAB scripts the obtained classified tracks were stored in an intermediate file. In further analysis only tracks with a length of at least 10 localizations were selected. The diffusion coefficients calculated by vbSPT but were not used, because the analysis does not consider the localization error, which can lead to significant errors. The occupations were recalculated from the classified tracks using only tracks with at least 10 localizations, the same applies to further analysis based on the classified tracks. Tracks were segmented by state and mean-squared-displacement analysis was performed as described by Michalet *et al.*[119]. Diffusion coefficients were derived from fits to the first 5 points of the MSD curves.

3.6.2. Single molecule colocalization analysis

A colocalization event was defined when two particles from the two channels moved together for 5 consecutive frames. Two particles were determined to move together, if the second was found within the area that the first could explore during one frame acquisition. For this the distance one particle may travel within one frame acquisition has to be calculated. The mean-squared-distance over one acquisition frame is given by[119]:

$$MSD = \left(4\sigma^2 - \frac{4}{3} D\Delta t \right) + 4D\Delta t$$

Where σ is the standard deviation of the localization error, *D* is the diffusion coefficient, and Δ*t* is the time lag between two frame acquisitions. It was assumed that the probability of finding the particle at a given distance could be approximated by a normal distribution with a variance equal to this MSD value. The distance threshold was calculated by the probability that the distance would be less than 95 %. For each state a specific threshold was calculated, using the

diffusion coefficients found in unstimulated cells. Using an estimated localization error of 30 nm for the used system[120], the following values for the thresholds were found: T_{free} = 248 nm, $T_{confined}$ = 172 nm, and $T_{immobile}$ = 122 nm. By counting the number of particles that colocalize to tracks in a given state or track class absolute binding was quantified. The probabilities for the detection of a colocalization event were calculated by normalizing the number of colocalization events by the number of particles in each state.

For dual-color tracking of SNAP-ErbB1 labeled with BG-Cy3 and BG-Alexa488, the tracking and vbSPT analysis was applied to the Cy3 data, and the Alexa488-labeled particles were colocalized as described above.

Clathrin colocalization analysis

A new approach was developed to quantify colocalizations between single particles and the fluorescence image of EGFP-clathrin. Starting from the equation of Manders[121], the intensities of the red channel *R* were colocalized with the green channel *G*:

$$M_1 = \frac{\sum_i R_{i,coloc}}{\sum_i R_i},$$

where $R_{i,coloc} = G_i$ if $G_i > 0$. M_1 is a measure for the amount of fluorescence of the colocalizing objects relative to its total fluorescence. In this case the number of particles where the clathrin signal *C* is greater than zero would be counted. Thus, the equation above was used to define a measure of colocalization between a set of particles and an image, setting R_i equal to the number of particles in pixel *i,*:

$$P = \frac{\sum_i R_{i,coloc}}{\sum_i R_i} = \frac{N_{coloc}}{N},$$

where N_{coloc} is the number of particles located in the pixels *i* where $C_i > 0$, and *N* is the total number of particles. However, a large number of particles will be assigned incorrectly to the colocalizing fraction, because the clathrin signal is strongly blurred by the finite resolution of the microscope. Thus, the requirement $C_i > 0$ was replaced by a weighting factor that assigns a higher probability of colocalization to high intensities in the clathrin signal:

$$P = \frac{\sum_{i \in S} R_i C_i}{N},$$

where *S* is the set of pixels that contain localizations. However, this measure is depending on the absolute intensities C_i. For randomly distributed particles, this equation can be interpreted as randomly drawing *N* pixels, adding their intensities and dividing by *N*. In this case, $P = \langle C \rangle$ for sufficiently large values of *N*, with $\langle C \rangle$ representing the average intensity of the image *C*. Therefore the colocalization measure was redefined, such that for randomly distributed particles $P = 0$:

$$P = \frac{\sum_{i \in S} R_i C_i}{N \langle C \rangle} - 1 .$$

4. RESULTS

4.1. Validation of the SNAP-ErbB1 construct

The fusion of a protein with a tag is useful to investigate its function, but it can lead to unwanted alterations. For example, such a fusion might modify ligand binding, interactions with other proteins or activity. Hence, it is important to verify the functionality of a modified protein prior to further experiments. In this case, the phosphorylation of the SNAP-ErbB1 construct upon EGF stimulation was verified by western blot analysis and confocal microscopy.

4.1.1. Western blot analysis of ErbB1 expression and phosphorylation levels

In order to determine the functionality of SNAP-tagged ErbB1, specifically its expression levels and its phosphorylation upon EGF stimulation, western blot analysis was conducted. ErbB1-EGFP, which was successfully used in earlier studies for fluorescence microscopy experiments[44,114] was used as a reference for the expression and phosphorylation levels of the SNAP-tagged ErbB1. Lysates from MCF-7 cells expressing SNAP-ErbB1, ErbB1-EGFP or untransfected cells were analyzed by western blots. Before stimulation with 16 nM EGF (equivalent to 100 ng/ml) one set of cells expressing SNAP-ErbB1 was labeled with BG-Cy3 while the other set was left unlabeled. The amount of expressed ErbB1 receptor and its phosphorylation level were visualized using antibodies against total EGFR and against phosphorylated tyrosines (Figure 12).

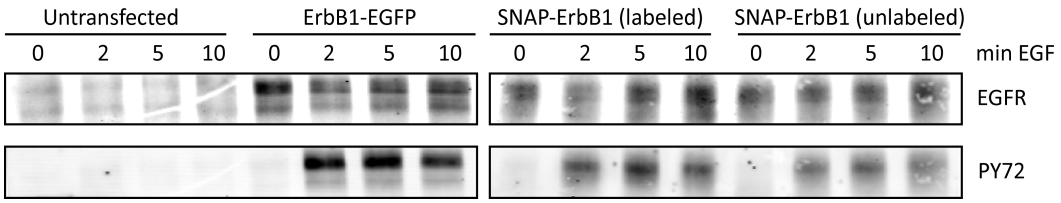

Figure 12: Western blots of lysates from MCF-7 cells transfected with SNAP-ErbB1 or ErbB1-EGFP stimulated with EGF. MCF-7 cells transfected with SNAP-ErbB1 or ErbB1-EGFP, and untranfected cells were stimulated with 16 nM EGF for the indicated times. Before stimulation one set of cells expressing SNAP-ErbB1 was labeled with BG-Cy3 while the other set was left unlabeled. Western blots were stained against total ErbB1 (EGFR) and phosphorylated tyrosines (PY72).

The expression levels of SNAP-ErbB1 were about 70 % of the expression of ErbB1-EGFP. Densitometric analysis of the western blots revealed that stimulation with EGF led to receptor phosphorylation with a maximum after 2 minutes (Figure 13). SNAP-tagged ErbB1 receptors showed the same phosphorylation profile upon EGF stimulation as EGFP-tagged ErbB1 receptors, while in untransfected cells no receptor phosphorylation was detected. The phosphorylation level of Cy3-labeled SNAP-ErbB1 receptors was slightly lower compared to unlabeled SNAP-ErbB1 receptors. Taking into account that densitometric analyses of western blots tend to show large variations, the results of the western blot analysis showed that the activity of SNAP-ErbB1 was comparable to that of ErbB1-EGFP.

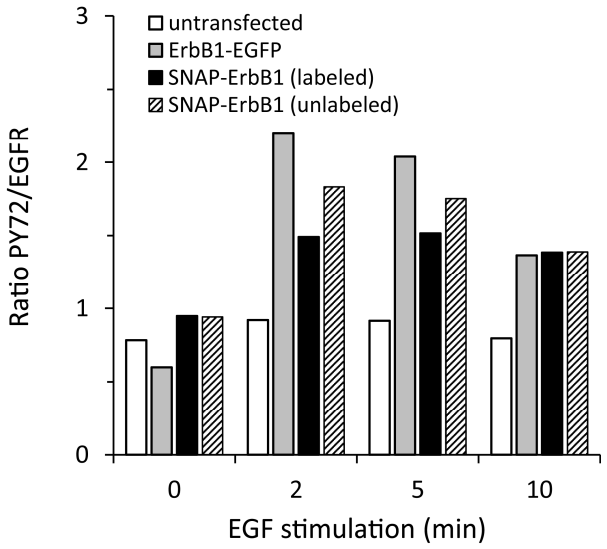

Figure 13: Densitometric analysis of western blots of MCF-7 cells transfected with ErbB1 receptor stimulated with 16 nM EGF. Plotted are the ratios of the intensities of PY72-stained bands to total EGFR-stained bands against EGF stimulation.

4.1.2. ErbB1 activation visualized by confocal microscopy

In addition to western blot analysis the activity of the SNAP-ErbB1 construct was verified in living cells by confocal fluorescence microscopy. MCF-7 cells coexpressing the ErbB1 receptor and the PTB domain from human Shc were imaged by confocal microscopy during stimulation with EGF. PTB domains bind to phosphorylated ErbB1 receptors, hence upon EGF stimulation recruitment of PTB domains to the membrane was expected. Cells coexpressing EGFP-PTB together with SNAP-ErbB1 or ErbB1-mCherry were stimulated with EGF and the PTB domain recruitment to the membrane was compared. SNAP-ErbB1 was labeled with BG-Cy3 or BG-Cy5, and EGF was either unlabeled, or labeled with Alexa647 or Alexa488. Cells were serum starved overnight and stimulated with 16 nM labeled or unlabeled EGF. One image was taken before addition of EGF (0 min), followed by images taken every 30 seconds for 10 minutes (Figure 14).

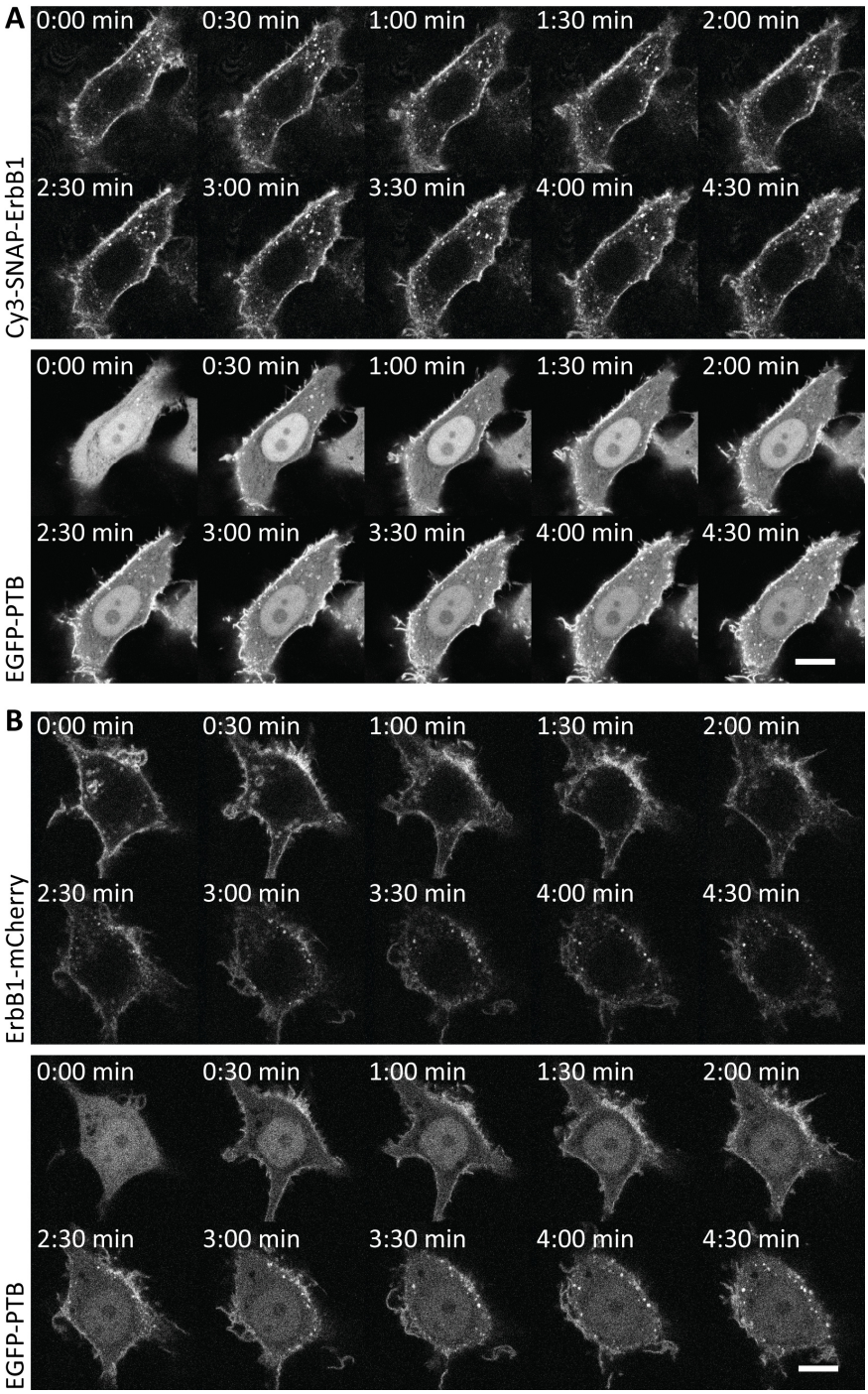

Figure 14: SNAP-ErbB1 or ErbB1-mCherry coexpressed with EGFP-PTB stimulated with EGF. MCF-7 cells coexpressing EGFP-PTB with SNAP-ErbB1, labeled with BG-Cy3 (A), or ErbB1-mCherry (B) stimulated with 16 nM EGF. Scale bars are 10 µm.

Both with SNAP-ErbB1 (Figure 14 A) and with the ErbB1-mCherry control (Figure 14 B), PTB domains were initially located in the cytosol and the receptor was found at the plasma membrane. The recruitment of PTB domains to the plasma membrane was observed already in the second image, recorded 30 seconds after EGF addition (Figure 14). After 1 – 3 minutes of EGF stimulation, internalization of receptors and bound PTB domains became visible. Stimulation with Alexa647-labeled EGF showed that EGF binding occurred immediately and

that the receptors were saturated already 30 seconds after stimulation (Figure 15, Figure 16). In parallel with ErbB1 and PTB domain internalization, EGF internalization was observed after 1 - 3 minutes of stimulation with EGF.

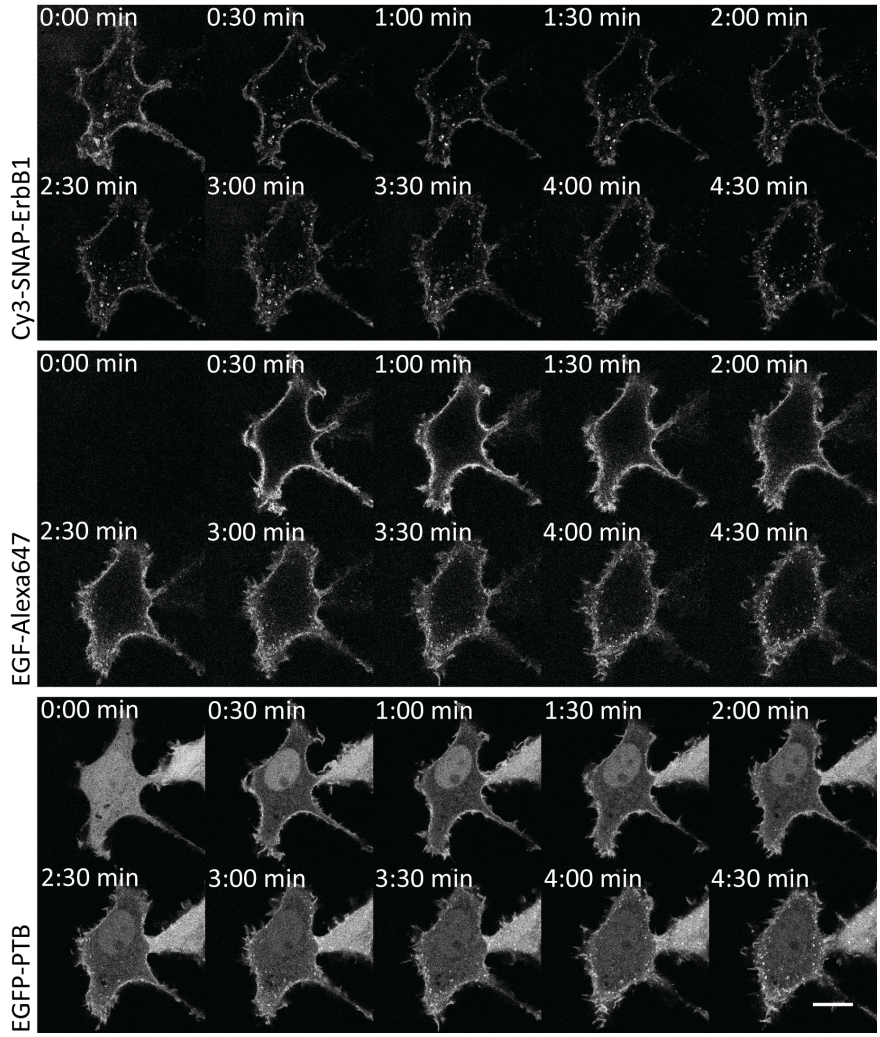

Figure 15: SNAP-ErbB1 coexpressed with EGFP-PTB domain stimulated with EGF-Alexa647. MCF-7 cell coexpressing EGFP-PTB with SNAP-ErbB1, labeled with BG-Cy3, stimulated with 16 nM EGF-Alexa647. Scale bar is 10 µm.

These confocal measurements show that the N-terminally SNAP-tagged ErbB1 receptor is activated by EGF in a fashion comparable to C-terminal mCherry-tagged ErbB1 receptor. In addition, EGF-Alexa647 and EGF-Alexa488 bind and activate ErbB1 receptors efficiently (Figure 15).

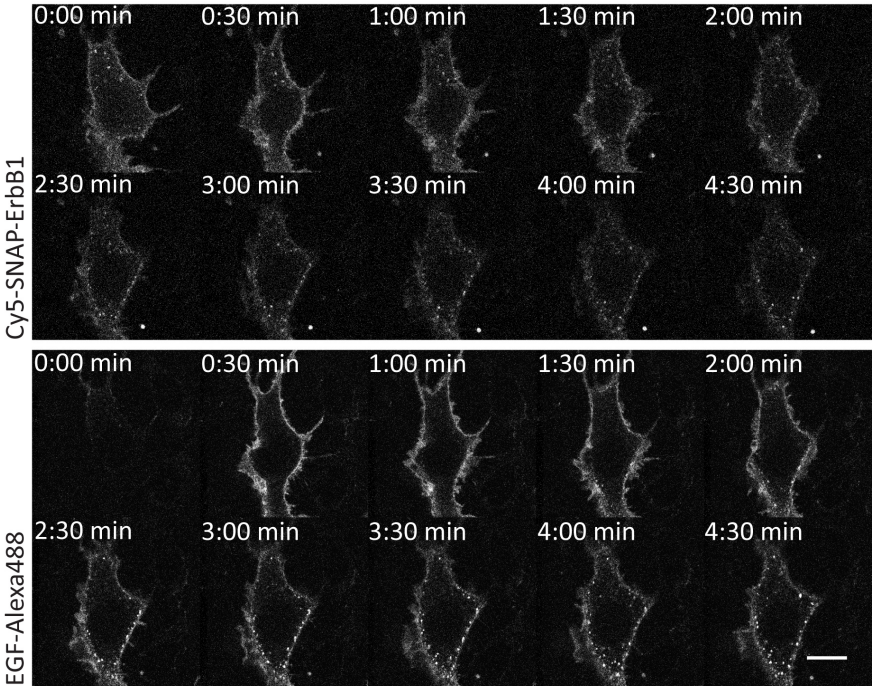

Figure 16: MCF-7 cell expressing SNAP-ErbB1 stimulated with EGF-Alexa488. MCF-7 cell expressing SNAP-ErbB1, labeled with BG-Cy5, stimulated with 16 nM EGF-Alexa488. Scale bar is 10 µm.

4.2. Single particle tracking of ErbB1

Single particle tracking experiments were performed with TIRF microscopy which mostly detects fluorescence from the basal plasma membrane of a cell. The ErbB1 receptor was labeled via a SNAP-tag, which allows flexibility in the choice of the fluorophore. Another advantage of the SNAP-tag is that only receptors at the plasma membrane are labeled when using cell impermeable BG-derivatives, thus reducing background fluorescence from receptors not localized at the plasma membrane. The use of a highly sensitive EM-CCD camera allows the localization and tracking of individual particles using the u-track software package developed by Jaqaman *et al.*[90] (Figure 17).

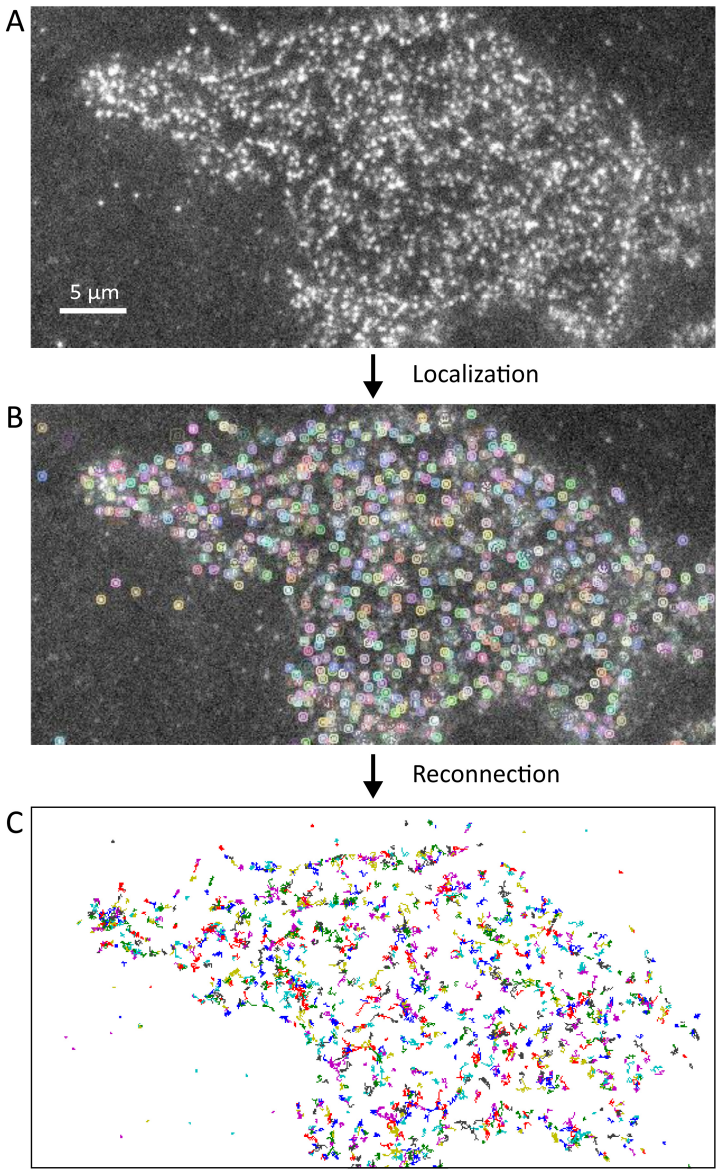

Figure 17: Procedure for single molecule tracking analysis of TIRF images of a cell expressing SNAP-ErbB1, labeled with BG-Alexa488. A: One frame of a live cell single particle tracking series. **B**: Localizations of single particles in one frame marked with circles. **C**: Trajectories reconnected from single particle localizations from a time series of 300 frames recorded at a rate of 25 frames per second.

Data were generally recorded in a dual-color setup at a rate of 30 frames per second using alternating excitation, resulting in an effective rate of 15 frames per second for the individual channels. The typical duration of a tracking series was 10 seconds. As bleaching of the tracked fluorophore within this acquisition time could lead to artifacts in the analysis, the bleaching kinetics for two different fluorophores were determined to select the appropriate fluorophore. The two SNAP substrates BG-Cy3 and BG-Alexa488 were adhered to the glass surface of a LabTek chamber and imaged under the same conditions used in tracking experiments. The average bleaching time of BG-Cy3 ($\tau \approx 30$ s) was three times longer than the acquisition time, while the mean bleaching time of BG-Alexa488 ($\tau \approx 13$ s) was only slightly longer than the acquisition time (Figure 18). Therefore, BG-Cy3 was used to label SNAP-ErbB1 for tracking in live cell experiments. In dual-color experiments, tracking analysis was generally applied only to the Cy3 signal, while the Alexa488 fluorescence was used for colocalization.

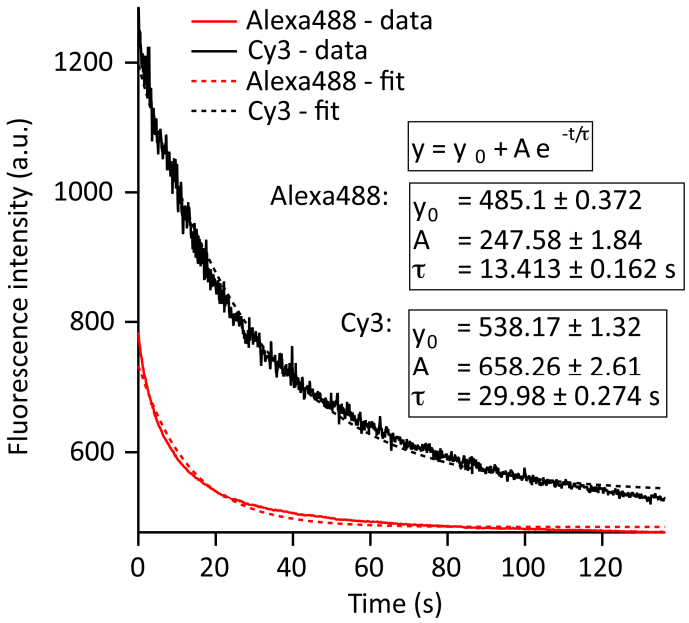

Figure 18: Bleaching kinetics of BG-Cy3 and BG-Alexa488. BG-Cy3 and BG-Alexa488 adhering to the glass were imaged under tracking conditions. The average bleaching time of BG-Cy3 ($\tau \approx 30$ s) is roughly three times longer than the acquisition time of 10 s. BG-Alexa488 has an average bleaching time that is in the order of the acquisition time ($\tau \approx 13$ s).

For the localization of single molecules, the density of particles of interest needs to be sufficiently low. Therefore, MCF-7 cells with an appropriate expression level were selected for tracking experiments. To get a measure of the number of receptors expressed in these cells, the average fluorescence intensities of the selected cells were compared to the average intensities of the whole transfected cell population (Figure 19). Assuming that the average expression level of SNAP-ErbB1 was about 70 % (estimated from the western blots in chapter

4.1.1, Figure 12) of the published EGFP-ErbB1 construct, which was 5.0×10^5 receptors per cell[44], the selected cells expressed about 9×10^4 receptors.

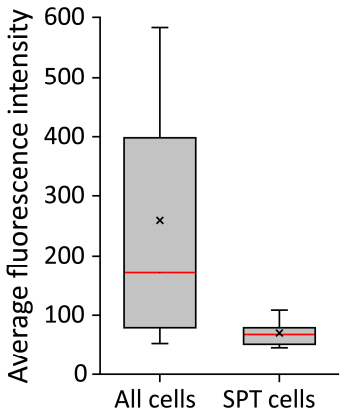

Figure 19: Relative expression of SNAP-ErbB1 in MCF-7 cells selected for single particle tracking, compared to a random population of cells imaged by TIRF. The bottom and the top of the box represent the 25th and 75th percentiles, the bottom and top whiskers represent the 10th and 90th percentiles. The red line represents the median value and the cross represents the mean value. The total number of cells was 80, from which 25 were selected as candidates for tracking analysis (SPT cells).

With these experiments the expression level of SNAP-tagged ErbB1 in cells used for single particle tracking experiments was confirmed to be low compared to expression levels used in studies with other fluorescent microscopy techniques. Cy3 was shown to be a suitable dye to be used in single particle tracking experiments, as the average bleaching time was three times longer than the typical duration of a tracking series.

Data obtained from single particle tracking experiments can be analyzed by several analysis methods. Here, the variational Bayes single particle tracking (vbSPT) algorithm[113], which classifies track fragments by their diffusive behavior, was used. The vbSPT algorithm assumes that the particles make memoryless jumps between different states of diffusion, determines the diffusion properties of each state, and calculates for each track the most likely sequence of states[113]. These classified track segments were then further analyzed for their co-localization with the signal in the second channel, to quantify the binding of other molecules, such as other ErbB1 molecules, EGFP-PTB, EGF-Alexa488, or EGFP-clathrin.

4.3. Characterization of the mobility states of ErbB1

In order to characterize the dynamics of the ErbB1 receptor in the plasma membrane, the receptor movements in the membrane of a cell during EGF stimulation were recorded (Figure 20 A, B).

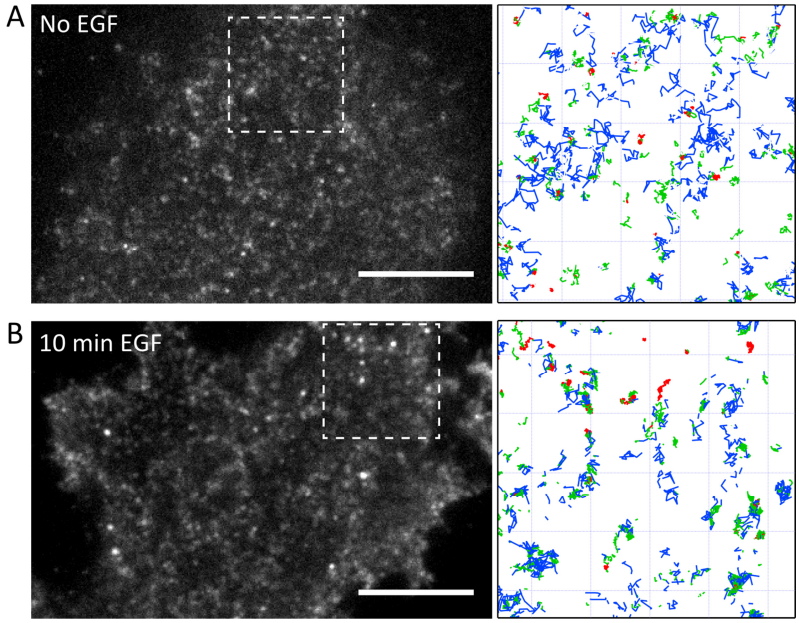

Figure 20: Single molecule tracking of ErbB1 receptors in MCF-7 cells. Single slices from a time series of MCF-7 cells expressing SNAP-ErbB1 labeled with BG-Cy3. **A**: Cell without EGF stimulation. **B**: Cell after 10 min of EGF stimulation. Right panels: Single molecule tracks of Cy3-SNAP-ErbB1 in the indicated regions of the left panels. The color-coding follows the classification of the specific states by the vbSPT algorithm in free (blue), confined (green) and immobile (red) states. Scale bars are 10 µm.

The resulting tracks were analyzed by the vbSPT algorithm, assuming a three-state model (Figure 21). The diffusion coefficients calculated by the vbSPT algorithm were not used directly, because vbSPT does not incorporate corrections for the localization error, which can lead to significant errors. Instead, further analysis was performed by custom written MATLAB scripts using the classified tracks from the vbSPT analysis with at least 10 localizations.

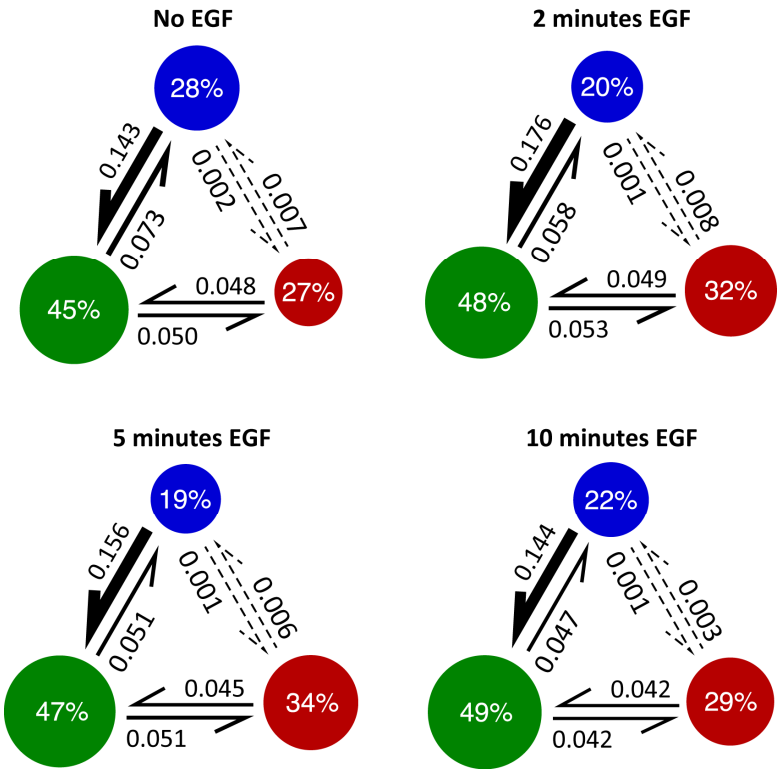

Figure 21: Variational Bayes single particle tracking (vbSPT) analysis of Cy3-SNAP-ErbB1 after stimulation with 16 nM EGF in MCF-7 cells. Circles represent the different states, with their area proportional to the occupation (the percentage of particle localizations) of that state. Arrows between circles represent transitions and are annotated by the corresponding transition probability. Dotted arrows indicate transition probabilities < 0.01.

Mean-squared-displacement (MSD) analysis was performed with the classified track segments to calculate the diffusion coefficients for each state (Figure 22). The linear curves formed by the blue symbols are typical for Brownian motion, indicating free diffusion on this time-scale. The green symbols show a flattening of the curve due to confinement of the particles within a limited area. The red symbols show only minor displacement on this time-scale, indicating that the particles are immobile. According to their diffusive behavior, the states were designated as “free” (blue), “confined” (green) and “immobile” (red). The diffusion coefficients for each state were calculated with linear fits to the first 5 points of each MSD curve for each time point. The states differed in their diffusion coefficients by two orders of magnitudes with minimal dependency on EGF stimulation (Figure 23 A).

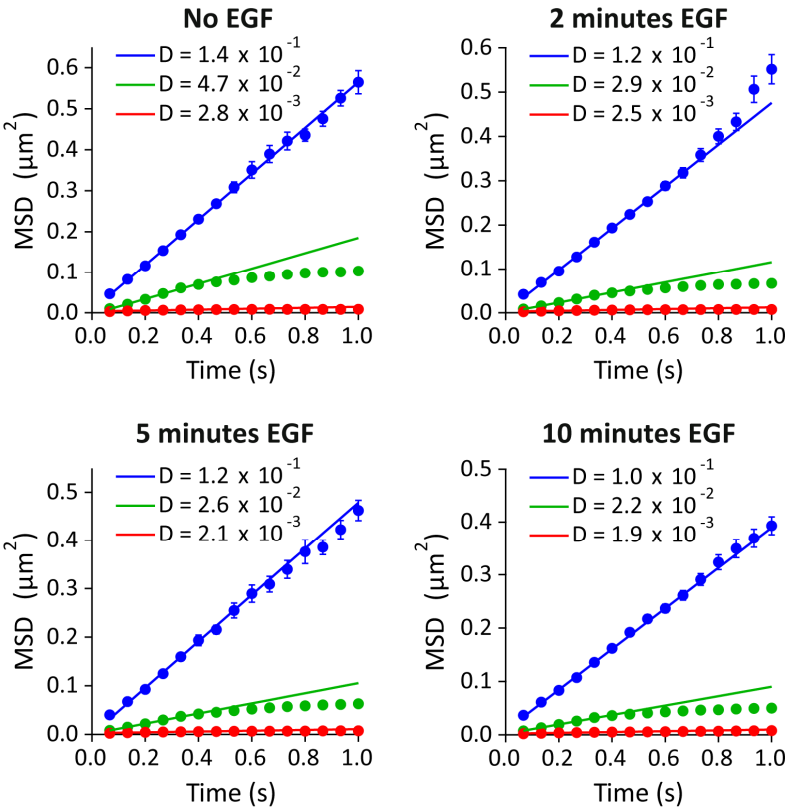

Figure 22: MSD analysis of the diffusion of Cy3-SNAP-ErbB1 upon stimulation with EGF, after classification of the data by mobility state. Straight lines: linear fits to the first 5 points of each curve. Legend: diffusion coefficients (D, $\mu m^2 s^{-1}$) derived from these fits. Error bars denote SEM, n = 43 cells per time point.

The populations of ErbB1 receptors in the different states changed upon EGF stimulation (Figure 23 B). In unstimulated cells 50 % of particles were in the confined state, while 26 % were freely diffusing and 24 % were in the immobile state. After addition of EGF the population of the immobile state increased up to 31 % after 5 minutes, then decreased again, while the amount of molecules in the free state decreased to 17 % after 5 minutes and increased again at 10 minutes with EGF. The occupancy of the confined state remained within a few percent over 50 % for all measured time points (Figure 23 B).

The calculated transition probabilities revealed that particles mainly switched between free and confined states or between confined and immobile states (Figure 21). The transition probability from the free to the immobile state increased notably after 2 minutes of EGF stimulation, while the probability for the transition from confined to immobile state increased only marginally (Figure 24). Both before and after stimulation, the probability of direct transitions between the free and immobile state was very low. Thus, conversion from the free to the immobile state happened via an intermediate confined state that by itself did not change much in population after ligand stimulation (Figure 23 B).

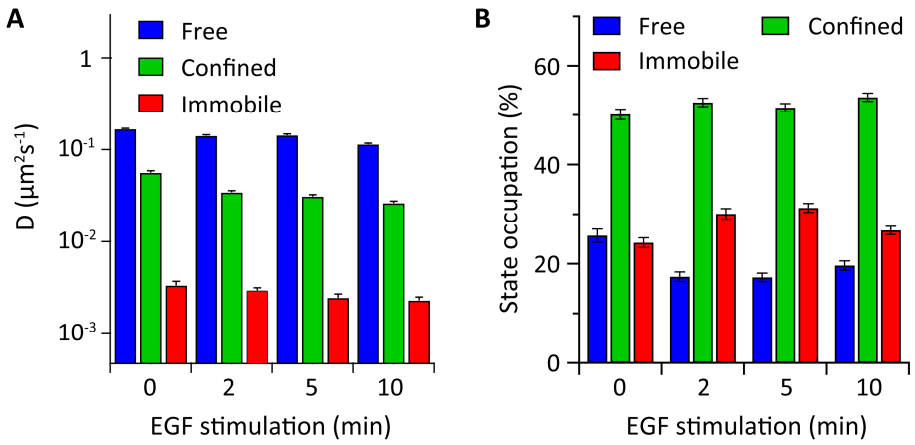

Figure 23: Diffusion coefficients and state occupations derived from single particle tracking analysis. A: Diffusion coefficients as a function of EGF stimulation, calculated as in Figure 22. **B**: State occupancy of ErbB1 mobility states over EGF stimulation. *n* = 43 cells per time point.

Besides the calculation of the state occupancies, the tracking analysis also allows the determination of the lifetime of each state, providing further insights into the dynamics of the system. The mean lifetime of each state was relatively short (0.4 – 1.2 s, Figure 25), with a significant longer lifetime of the immobile state, that increased after stimulation with EGF.

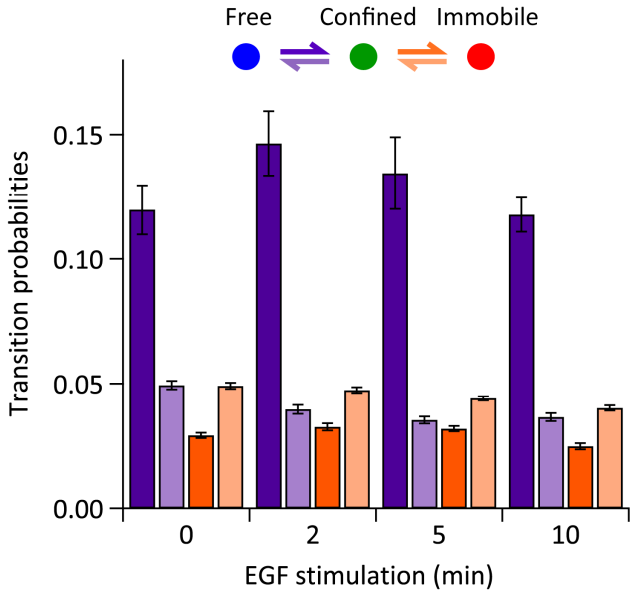

Figure 24: Transition probabilities between mobility states of ErbB1 found by vbSPT as a function of EGF stimulation. Probabilities for ErbB1 receptors to switch between mobility states during tracking. Circles represent states: free (blue), confined (green) and immobile (red). The transitions between free and immobile state were < 0.01 and are not plotted here. *n* = 43 cells per time point.

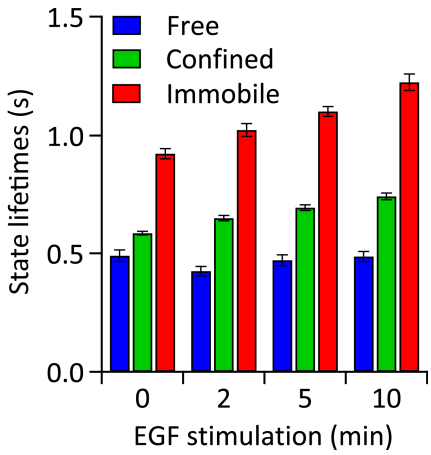

Figure 25: State lifetimes of ErbB1 diffusion with EGF stimulation. Lifetimes of the immobile, confined and free states of ErbB1 receptor diffusion plotted against EGF stimulation. *n* = 43 cells per time point.

Taken together the single particle tracking data show that ErbB1 maintained its dynamic nature after ligand stimulation, switching between multiple mobility states. However, due to an increased net rate of conversion from the free to the confined state, the balance was shifted towards an increased population of the immobile state with an increased lifetime after EGF stimulation.

4.4. Characterization of the activity of ErbB1

4.4.1. Identification of active receptors by the recruitment of PTB domains

After their identification, the three mobility states of ErbB1 were further investigated. The signaling fraction of ErbB1 receptors is characterized by phosphorylated tyrosine residues to which further proteins are recruited. Therefore, phosphorylated receptors can be identified by colocalization of the EGFP-labeled phosphotyrosine-binding (PTB) domain from human Shc with the ErbB1 receptors. The PTB domains are recruited to the plasma membrane when ErbB1 is activated as was shown by confocal microscopy in chapter 4.1.2. Thus, PTB-binding can be interpreted as a measure for ErbB1 activity.

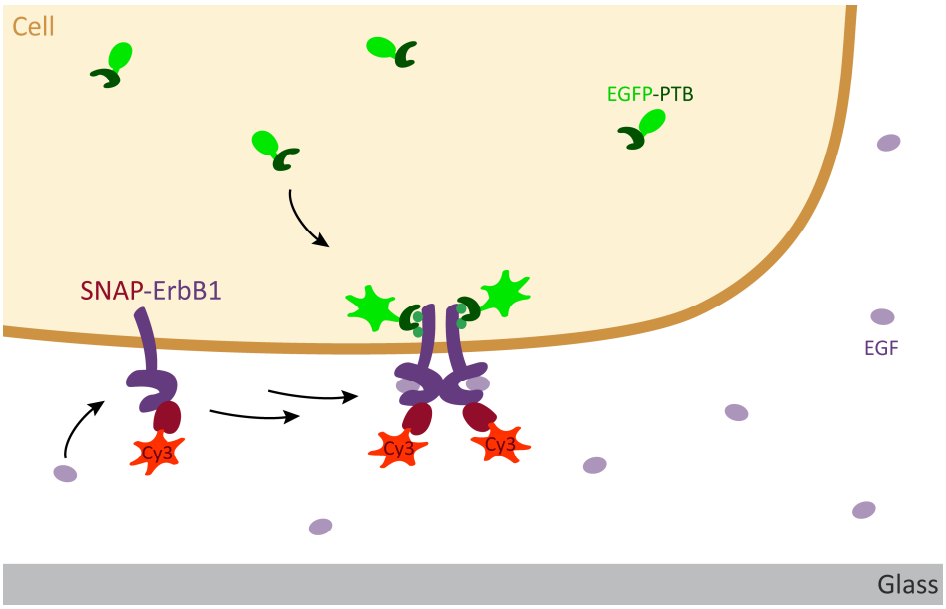

Figure 26: Principle of measuring ErbB1 activity at a single molecule level. ErbB1 is expressed in MCF-7 cells with an N-terminal SNAP-tag labeled with BG-Cy3. At the same time, a phosphotyrosine-binding domain tagged with EGFP (EGFP-PTB) is expressed in the cytosol. Using TIRF microscopy, individual receptors are tracked. In resting cells, EGFP-PTB fluorescence is visible as a constant background due to its relatively fast diffusion. Upon stimulation with EGF, EGFP-PTB molecules bind to phosphorylated tyrosine residues at the C-terminal tail of ErbB1 and are observed in the TIRF field as single molecules, identifying active receptors.

Due to the evanescent wave excitation in the used experimental setup, only EGFP-PTB domains near the basal membrane were excited. As a consequence of the relatively long acquisition time of 31 ms per frame the fast diffusing cytosolic EGFP-PTB domains were only visible as a constant blurred background. Upon EGF stimulation the PTB domains were bound to phosphorylated ErbB1 receptors and could be detected as single molecules (Figure 26). With an image splitter installed in the emission path of the microscope, Cy3-labeled SNAP-

ErbB1 receptors and EGFP-labeled PTB domains could be observed at the plasma membrane on a single molecule level.

In unstimulated cells cytosolic PTB domains labeled with EGFP were visible as a diffuse background over the whole cell (Figure 27 A). However, after 10 minutes of EGF stimulation, recruitment of PTB domains to the membrane was clearly visible as bright spots at the membrane (Figure 27 B). After overlaying the images taken in the channels for Cy3-labeled SNAP-ErbB1 and EGFP-PTB, it was evident that the PTB domains colocalized strongly with clusters of immobile ErbB1, while without EGF no colocalization was observed (Figure 27 C, D).

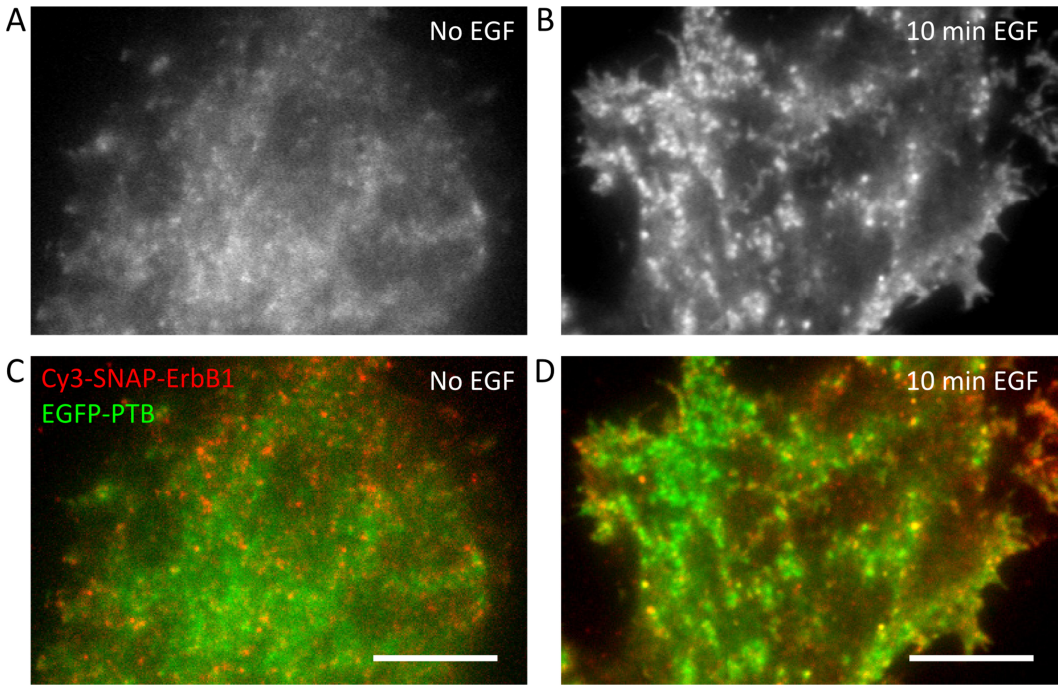

Figure 27: Recruitment of PTB domains to active ErbB1 receptors. Single slices from a dual-color time series in MCF-7 cells expressing SNAP-ErbB1 labeled with BG-Cy3 and EGFP-PTB. **A**: Fluorescence of EGFP-PTB without EGF. **B**: Fluorescence of EGFP-PTB after 10 minutes of stimulation with EGF. **C**: Overlay of the fluorescence intensities from EGFP-PTB (green) and Cy3-labeled SNAP-ErbB1 (red) without EGF. **D**: Overlay of the fluorescence intensities from EGFP-PTB (green) and Cy3-labeled SNAP-ErbB1 (red) after 10 minutes of stimulation with EGF. Scale bars are 10 µm.

The recruitment of EGFP-PTB to active ErbB1 receptors on the basal membrane was observed by TIRF imaging in cells expressing SNAP-ErbB1, labeled with BG-Cy3, or ErbB1-mCherry at high or low levels (Figure 28). In cells with low expression level of ErbB1, which for Cy3-SNAP-ErbB1 was comparable to the intensities generally used for single molecule imaging, a punctuated recruitment of PTB domains was observed (Figure 28 B, D). In contrast, in cells expressing either SNAP-ErbB1 or ErbB1-mCherry at high levels, EGFP-PTB was recruited uniformly to the plasma membrane (Figure 28 A, C).

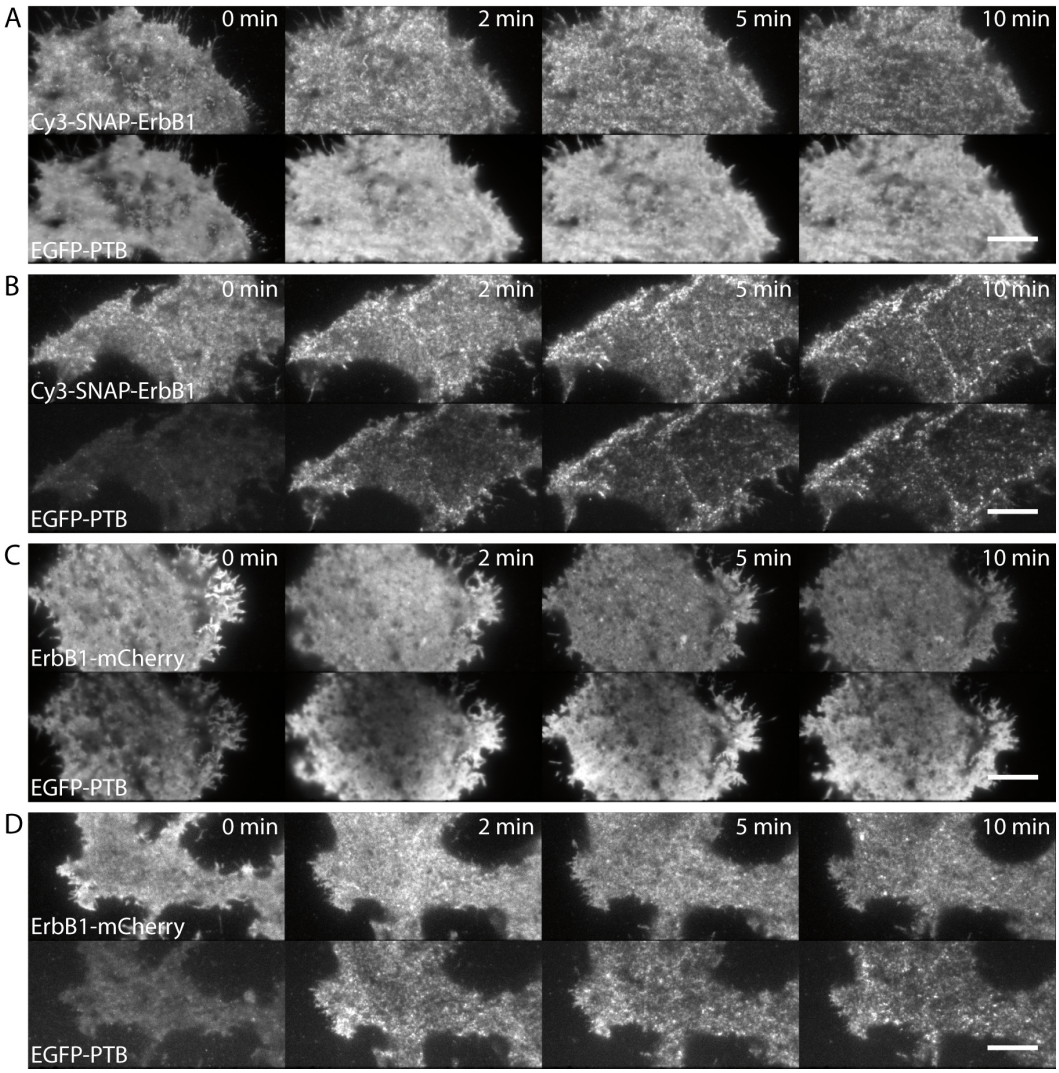

Figure 28: PTB domain recruitment to ErbB1 upon EGF stimulation in TIRF imaging. MCF-7 cells coexpressing higher (A) or lower (B) levels of SNAP-ErbB1, labeled with BG-Cy3, and higher (C) or lower (D) levels of ErbB1-mCherry together with EGFP-PTB, stimulated with 16 nM EGF, imaged at the indicated time points. The mean fluorescence intensity of Cy3-SNAP-ErbB1 was 2.2 times higher in A compared to B, the latter being comparable to intensities generally used for single molecule imaging. For ErbB1-mCherry the mean fluorescence intesitiy in C was 6.3 times higher compared to D. Scale bars are 10 µm.

Tracking experiments with Cy3-labeled SNAP-ErbB1 receptors in MCF-7 cells coexpressing EGFP-labeled PTB domains were analyzed to reveal the activity of the receptors in each state. A plot of the number of colocalization events per state showed that receptors in the free state were virtually inactive, whereas receptors in both the confined and immobile states showed increased phosphorylation when stimulated with EGF (Figure 29 A). To quantify the activity of individual receptors in a given state, the probability of colocalization was estimated from the data taking the amount of receptors per state into account (Figure 29 B, Figure 23 B). This quantification indicated that receptors in the immobile state were phosphorylated with a significantly higher probability compared to receptors in the confined state.

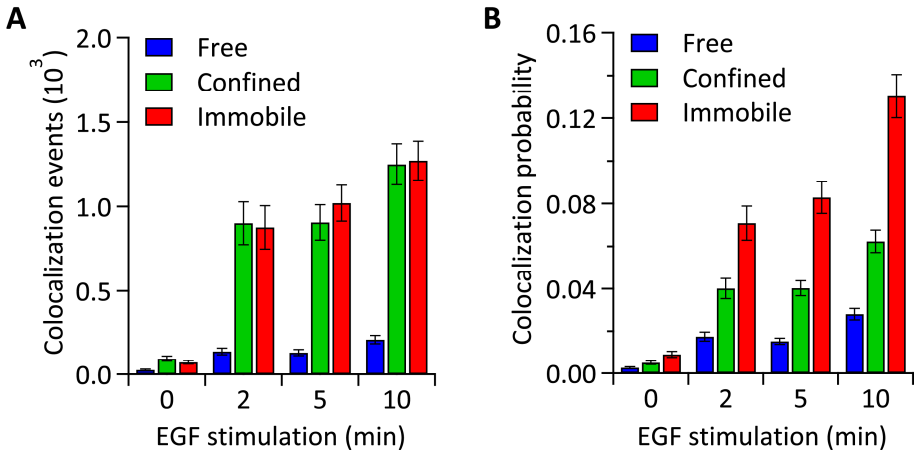

Figure 29: Quantification of the colocalization of EGFP-PTB molecules with SNAP-ErbB1 molecules as a function of EGF stimulation. A: Number of colocalization events per state, as determined by vbSPT analysis (see Figure 20). **B:** Probability of colocalization of PTB with ErbB1 per state. *n* = 43 cells per time point.

In order to find out if the activation of ErbB1 receptors, characterized by PTB domain binding, influenced their diffusive behavior, the state lifetimes of the particles that colocalized with PTB were calculated. Indeed the duration of active ErbB1 receptors in the immobile state was significantly increased (Figure 30).

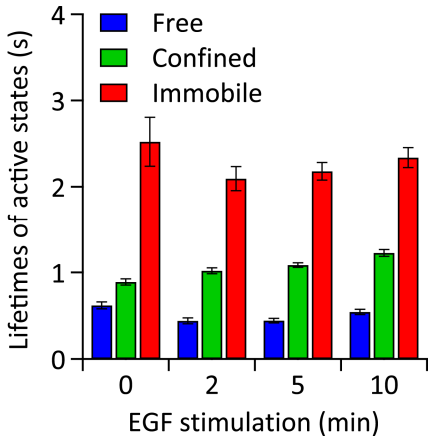

Figure 30: Lifetimes of mobility states after selecting for active ErbB1 receptors that colocalized with PTB domains. Lifetimes of active receptors in each state. *n* = 43 cells per time point.

The higher activity of receptors in the immobile state could be due to receptor aggregation, accompanied by a higher EGF binding probability and auto-phosphorylation. To verify if the receptors aggregated, fluorescence intensity histograms of the receptors were plotted for each state (Figure 31). Indeed, the intensity of receptors in the immobile state increased compared to the confined or free states, in particular when selecting the particles that colocalized with PTB domains. Also for the free and confined states a slight increase in particle intensity was observed when colocalized with PTB, possibly indicating that active receptors in these states were more likely to be dimeric, while the much higher increase in intensity of

active receptors in the immobile state points to the presence of higher order aggregates. Note that the degree of receptor oligomerization is likely underestimated, taking into account a population of dark receptors, composed of endogenous, unlabeled and bleached receptors.

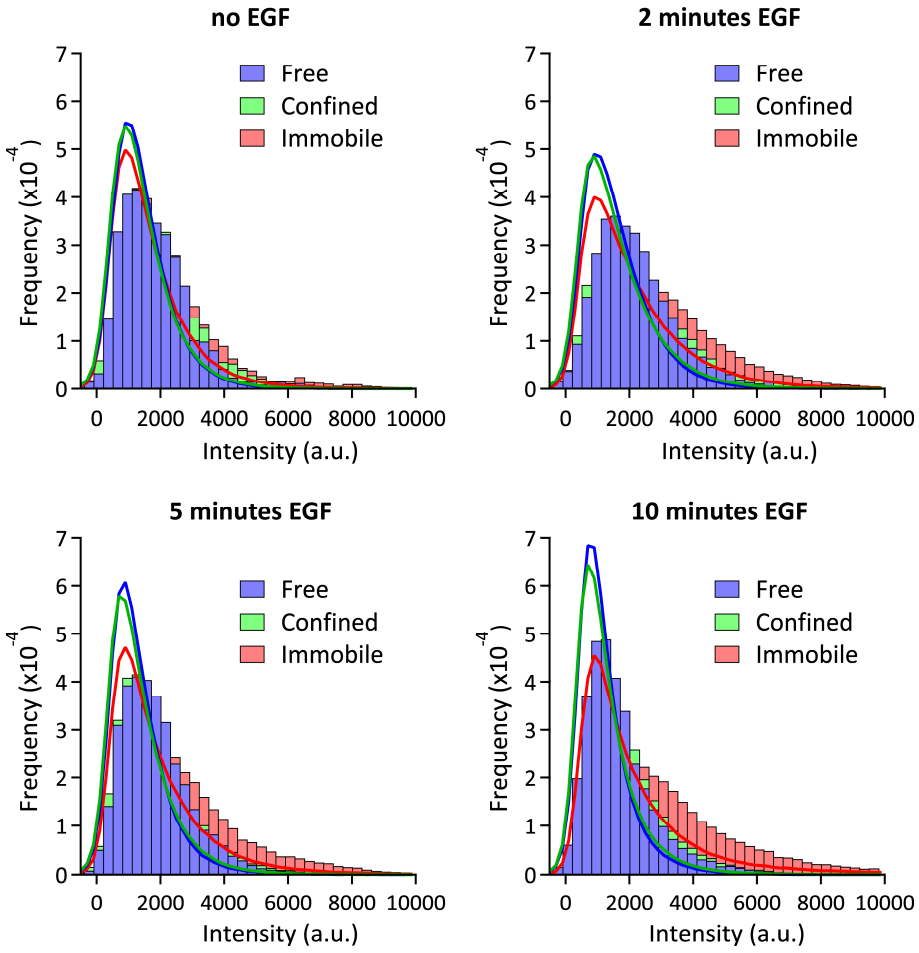

Figure 31: Intensity histograms of Cy3-labeled ErbB1 receptors colocalizing with EGFP-PTB per mobility state. Intensity histograms of the fluorescence of tracked Cy3-SNAP-ErbB1 particles before and after 2, 5 and 10 minutes of EGF stimulation, for all particles (lines) and for the particles that colocalized with EGFP-PTB domains (bars).

The colocalization experiments of ErbB1 receptors with PTB domains showed that upon EGF stimulation mainly receptors in the immobile and confined state were phosphorylated, and that the lifetime of the immobile state was significantly increased. Furthermore, the analysis of the intensity histograms indicated that active receptors in the immobile state form clusters upon EGF stimulation.

4.4.2. Dual-color single particle tracking of ErbB1

For ErbB1 receptor activation it is known that the formation of signaling dimers is essential[31,108]. Therefore, it is of interest to correlate the mobility states of ErbB1 to its level of aggregation.

To evaluate the extent of self-association of ErbB1 after stimulation with EGF, single particle tracking experiments were performed with MCF-7 cells expressing SNAP-tagged ErbB1 labeled with equal amounts of BG-Alexa488 and BG-Cy3. The TIRF images already showed that colocalization between receptors without EGF stimulation was low, while 10 minutes after EGF addition clear colocalizations between receptors were observed (Figure 32).

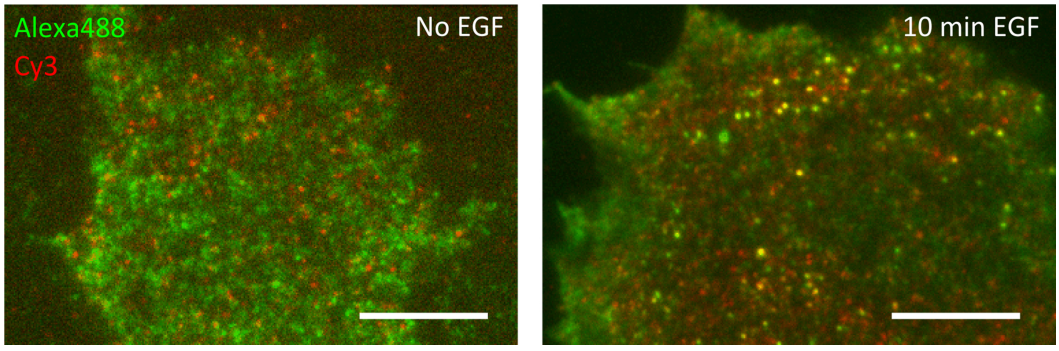

Figure 32: Dual-color single molecule tracking of ErbB1 receptors. Single slices from a dual-color time series in MCF-7 cells expressing SNAP-ErbB1 labeled with BG-Cy3 (red) and BG-Alexa488 (green) without EGF and after 10 minutes of EGF stimulation. Scale bars are 10 µm.

Tracking analysis was applied to the Cy3-labeled SNAP-ErbB1 receptors and the results were correlated to the localizations of Alexa488-labeled receptors in order to gain information about the mobility states of colocalized receptors as well as their level of aggregation. Plotting the number of colocalization events of Alexa488-labeled with Cy3-labeled SNAP-ErbB1 per state showed that receptors in the free state were mainly monomeric, whereas receptors in the confined and immobile state showed clear self-association after stimulation with EGF (Figure 33 A). After 5 minutes the probability of colocalization for receptors in the immobile states was significantly larger than for receptors in the confined state (Figure 33 B). These results clearly show that ErbB1 receptors form at least dimers or higher order clusters after EGF stimulation.

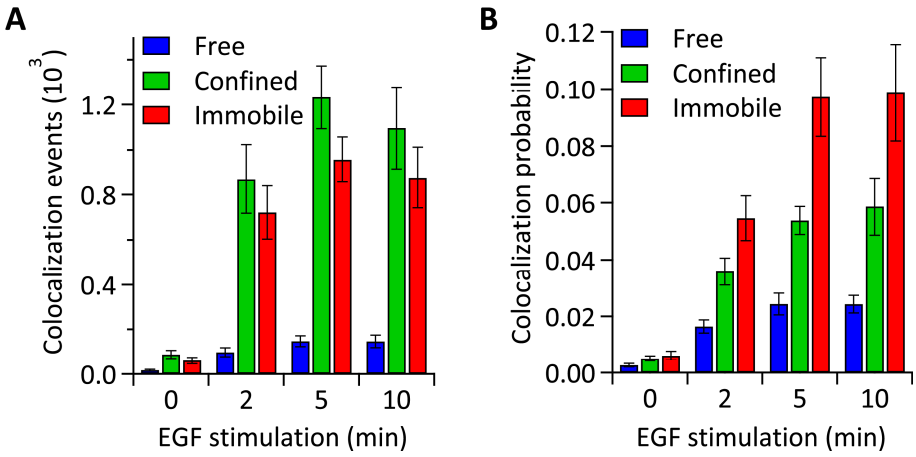

Figure 33: Quantification of colocalization of dual-color labeled ErbB1 receptors as a function of EGF stimulation. A: Number of colocalization events of Alexa488-labeled receptors with Cy3-labeled ErbB1 receptors per state. **B**: Probability of colocalization of an Alexa488-labeled receptor with a Cy3-labeled ErbB1 receptor per state. *n* = 43 cells per time point.

To establish if the increase of colocalization was caused by an increased number of dimers in the immobile population or due to receptor clustering, the fluorescence intensities of the Cy3-labeled receptors that colocalized after 10 minutes of EGF stimulation were quantified and compared to the intensities of all particles per state (Figure 34). In the immobile state, a population of bright particles was observed, compared to the intensity distributions of the free and confined states. Thus, in the immobile state, particles were present that consisted of aggregates of more than two receptors.

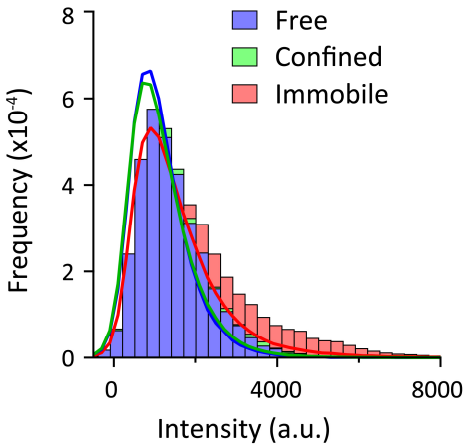

Figure 34: Intensity histograms of colocalized ErbB1 receptors. Intensity histograms of Cy3-labeled ErbB1 receptors per mobility state for all particles (lines) and for the particles that colocalized with Alexa488-labeled ErbB1 receptors (bars) after 10 minutes of EGF stimulation. *n* = 43 cells per time point.

Taking the probabilities of self-association into account, which were much higher for the confined than for the free state, it can be concluded that particles in the free state were mainly monomeric. In the confined state dimers could be found, whereas in the immobile state the receptor also formed higher order aggregates.

4.4.3. Single molecule visualization of EGF binding to ErbB1

Besides the activity status of ErbB1, the identification of the populations that bind EGF can provide further insight into the course of events in ErbB1 signaling. By colocalizing Cy3-labeled SNAP-ErbB1 receptors with Alexa488-labeled EGF, ligand binding dynamics were visualized. Tracking analysis of the Cy3-labeled receptor and concomitant colocalization analysis with EGF-Alexa488 was performed. The colocalization events and probabilities for each mobility state of ErbB1 are shown in Figure 35.

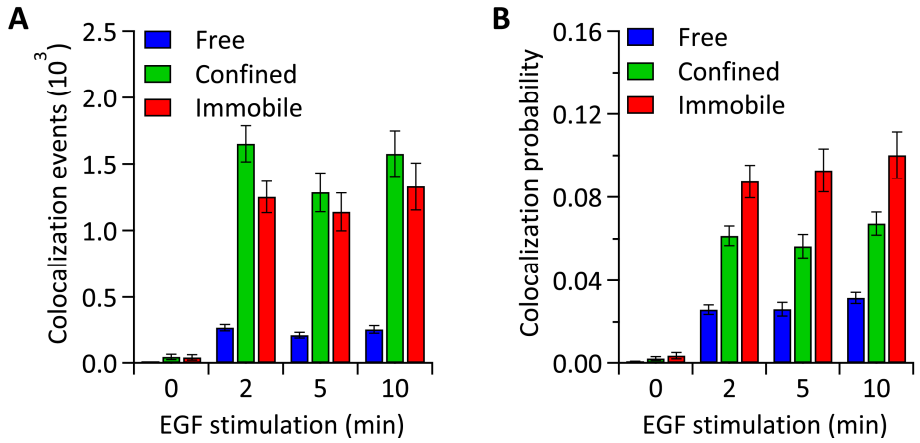

Figure 35: Analysis of EGF-Alexa488 binding to Cy3-labeled SNAP-ErbB1 receptors in MCF-7 cells. Quantification of the colocalization of EGF-Alexa488 to Cy3-SNAP-ErbB1 receptors as a function of stimulation time: **A:** Number of colocalization events of EGF with ErbB1 per state. **B:** Probability of colocalization of EGF with ErbB1 per state. *n* = 36 cells per time point.

Colocalization analysis of Cy3-SNAP-ErbB1 with Alexa488-EGF revealed that EGF was mainly bound to ErbB1 receptors in the confined and immobile state in equal absolute amounts (Figure 35 A), and that EGF binding was already saturated after 2 minutes. The probability for binding of an EGF molecule to receptors in the immobile state was higher than for the confined state (Figure 35 B), due to the lower occupancy of the immobile state (Figure 23 B). This could be explained if the receptors in the immobile state formed clusters occupied with several EGF molecules.

The results from EGF binding (Figure 35) and self-association (Figure 33) experiments both support the concept of ligand binding as the main driving force for dimerization and clustering of the receptor. However, receptors in the immobile state exhibited a higher activity compared to the confined state than would be expected from the EGF binding probabilities (compare Figure 35 B with Figure 29 B). A plot of the ratio of the probabilities of PTB- and EGF-colocalization in the immobile and confined states confirmed that the phosphorylation of

immobile receptors did not increase linearly with the amount of bound EGF (Figure 36), indicating that the signaling activity is amplified in the immobile ErbB1 clusters.

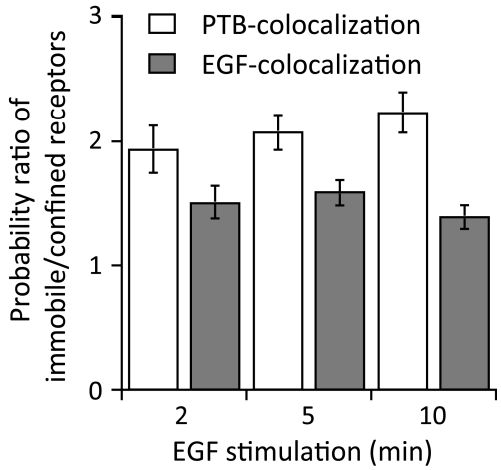

Figure 36: Ratio of the colocalization probabilities for immobile to confined receptors for PTB and EGF. The ratios between the colocalization probabilities of immobile and confined receptors for EGFP-PTB colocalizations and for EGF-Alexa488 colocalizations plotted against EGF stimulation.

4.4.4. Phosphatase inhibition by pervanadate

Pervanadate is an inhibitor of a wide range of tyrosine phosphatases in the cell. The inhibitor prevents the receptors from being dephosphorylated after activation. Without ligand stimulation, phosphorylated receptors will accumulate due to the basal kinase activity of the receptor. Phosphatase inhibition should reveal if ligand-independent activation of the ErbB1 receptor occurs in all mobility states and give a hint how the receptor signaling is regulated.

MCF-7 cells coexpressing EGFP-PTB with SNAP-ErbB1, labeled with BG-Cy3, were serum starved overnight and incubated with 1 mM pervanadate for 10 – 30 minutes. After incubation with pervanadate an increased number of PTB domains was recruited to the membrane (Figure 37).

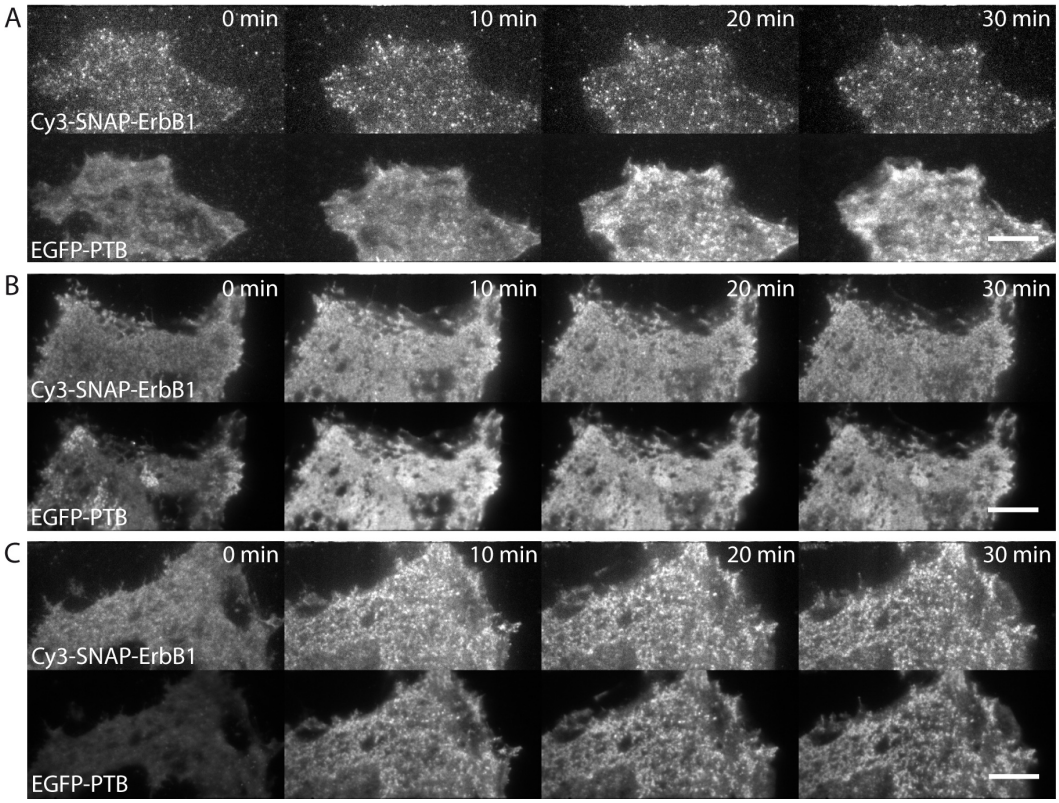

Figure 37: PTB domain recruitment to phosphorylated ErbB1 receptors at the plasma membrane during incubation with pervanadate or EGF. MCF-7 cells expressing SNAP-ErbB1, labeled with BG-Cy3, and EGFP-PTB. **A**: Cell with low ErbB1 expression level incubated with 1 mM pervanadate. **B**: Cell with high ErbB1 expression level incubated with 1 mM pervanadate. **C**: Cell with high ErbB1 expression level stimulated with 16 nM EGF. Scale bars are 10 µm.

In cells with a low receptor expression the recruitment of PTB domains reached its maximum after 20 - 30 minutes of incubation with pervanadate (Figure 37 A), while in cells with a high expression of receptors maximal PTB recruitment was observed after 10 minutes with pervanadate (Figure 37 B) or EGF (Figure 37 C). Thus, the basal level of receptor activity is

dependent on receptor density. In cells with a high receptor density, ErbB1 exhibited a high level of ligand-independent activation. In cells with low receptor density, autophosphorylation of the receptors was much lower. These results show that phosphatases play an important role in the regulation of ErbB1 receptor signaling, but also that the system is very sensitive to receptor density at the plasma membrane.

In single particle tracking experiments with pervanadate incubation instead of EGF stimulation the colocalization of PTB domains with ErbB1 receptors per state was quantified. For these experiments only cells with a low expression level of ErbB1 were selected and analyzed for PTB domain colocalization upon treatment with 1 mM pervanadate (Figure 38). The recruitment of PTB domains to ErbB1 receptors upon pervanadate treatment was much slower compared to stimulation with EGF (compare to Figure 29). Colocalization events with PTB domains were mainly observed for receptors in the confined or immobile state and increased for all states until 20 minutes of pervanadate treatment.

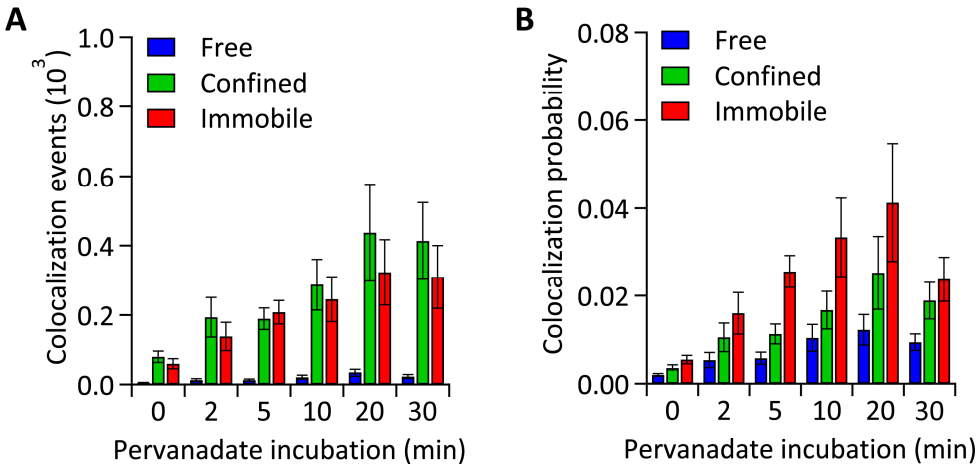

Figure 38: Analysis of EGFP-PTB colocalization with Cy3-labeled SNAP-ErbB1 receptors in MCF-7 cells upon pervanadate treatment. Quantification of the colocalization of EGFP-PTB to Cy3-SNAP-ErbB1 receptors upon treatment with 1 mM pervanadate: **A:** Number of colocalization events of PTB with ErbB1 per state. **B:** Probability of colocalization of PTB with ErbB1 per state. *n* = 10 cells per time point.

A plot of the histograms of the fluorescence intensities of Cy3-SNAP-ErbB1 after 10 minutes of incubation with pervanadate showed an increase of the intensities of immobile receptors colocalizing with PTB domains (Figure 39). Although clustering was less than observed upon EGF stimulation, the results indicate that ligand binding is not required for cluster formation.

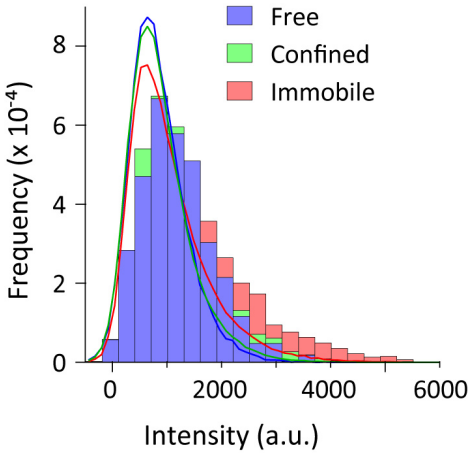

Figure 39: Intensity histograms of Cy3-labeled ErbB1 receptors incubated with pervanadate colocalizing with EGFP-PTB per mobility state. Intensity histograms of the fluorescence of tracked Cy3-SNAP-ErbB1 particles after incubation with 1 mM pervanadate for 10 minutes, for all particles (lines) and for the particles that colocalized with EGFP-PTB domains (bars). *n* = 10 cells per time point.

By tracking and colocalization experiments on a single molecule level it was shown that ligand-independent phosphorylation of ErbB1 receptors in cells with low receptor density was low compared to EGF stimulation. In cells with high ErbB1 density, ligand-independent receptor phosphorylation, observed upon phosphatase inhibition by pervanadate, was high and occurred much faster, in accordance with previous studies using pervanadate to induce ligand-independent receptor phosphorylation[45,122,123].

4.4.5. Kinase inhibition by erlotinib

Erlotinib is a competitive kinase inhibitor, which competes with ATP for the ATP binding site of ErbB1 and thereby traps the receptor in its extended conformation[69,124]. Thus, it would be interesting to see if the active conformation, even when the kinase is inhibited, promotes cluster formation. Single particle tracking experiments were performed as previously with Cy3-SNAP-ErbB1 and EGFP-PTB, but before the experiment cells were pre-incubated for 1 hour with 10 µM erlotinib. The analysis of the occupations of the three states showed that the inhibited receptor is driven into the confined and immobile states (Figure 40).

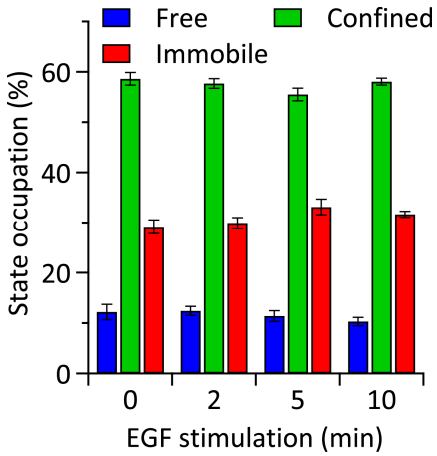

Figure 40: State occupations for ErbB1 inhibited with 10 µM erlotinib and stimulated with EGF. Occupations of mobility states for Cy3-SNAP-ErbB1 in MCF-7 cells preincubated for 1 h with 10 µM erlotinib and stimulated with 16 nM EGF. *n* = 14 cells per time point.

Without stimulation the population of free receptors was reduced to 10 % while the populations of confined and immobile receptors were increased to 60 % and 30 %, respectively (Figure 40). Upon EGF stimulation the state occupations of inhibited receptors did not change significantly.

Colocalization analysis of the tracked ErbB1 receptors with EGFP-tagged PTB domains showed that erlotinib efficiently inhibited phosphorylation of the receptor upon stimulation with EGF as expected (Figure 41).

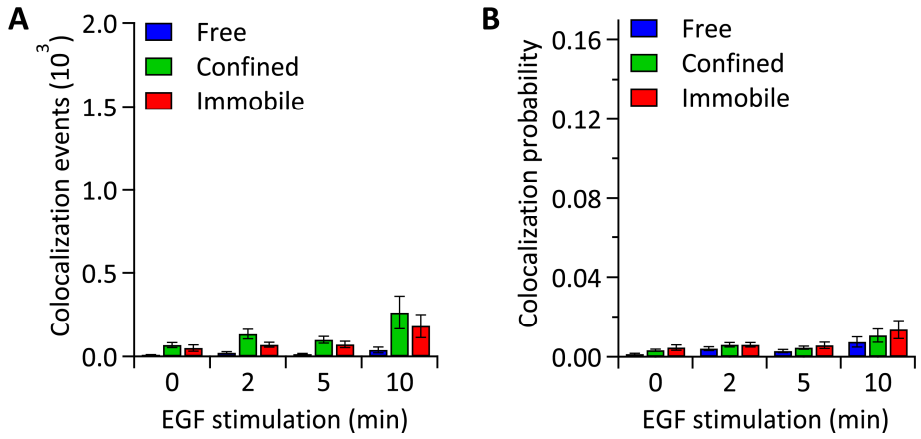

Figure 41: Colocalization analysis of EGFP-PTB domains with SNAP-ErbB1 after inhibition with 10 µM erlotinib and stimulation with EGF. MCF-7 cells were cotransfected with EGFP-PTB and SNAP-ErbB1, incubated for 1 h with 10 µM erlotinib and stimulated with 16 nM EGF. **A**: Colocalization events of PTB domains with ErbB1 per state. **B:** Colocalization probability for PTB domains with ErbB1 per state. *n* = 14 cells per time point.

The fluorescence intensity histograms for each state revealed that the aggregation state of the inhibited receptors was generally similar in all states (Figure 42, lines). The increased intensity observed for receptors that colocalized with PTB (Figure 42, bars) derives from the small population of receptors that were not inhibited by erlotinib.

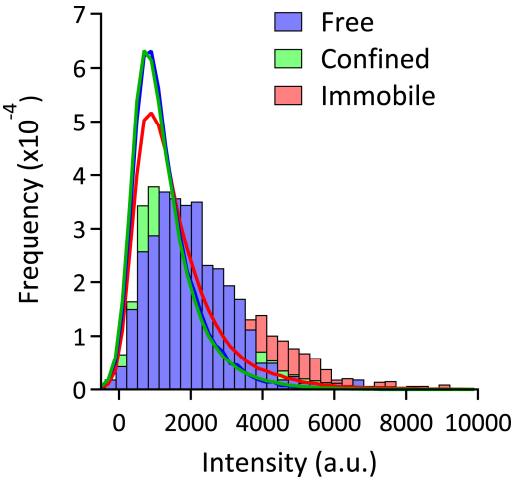

Figure 42: Intensity histograms of Cy3-labeled ErbB1 receptors per mobility state after inhibition with 10 µM erlotinib and stimulation with EGF. Intensity histograms of the fluorescence of tracked Cy3-SNAP-ErbB1 particles after 10 minutes of stimulation with EGF, for all particles (lines) and for the particles that colocalized with EGFP-PTB domains (bars). *n* = 14 cells per time point.

From these single particle tracking experiments it can be concluded that receptors are driven to more confined and immobile states when they are trapped in the extended conformation by erlotinib, but that kinase activity is required for cluster formation.

4.5. Localization of ErbB1 in the plasma membrane

4.5.1. Colocalization with clathrin

As shown by PTB domain colocalization, after 2 – 5 minutes of stimulation half of the signaling activity was associated with immobile receptors (Figure 29), which represent only a relatively small population (Figure 23 B). An overlay of the classified tracks with the PTB colocalization events after 10 minutes of EGF stimulation showed that the activity of ErbB1 was mostly focused in small spots where the receptors were in the immobile state (Figure 43).

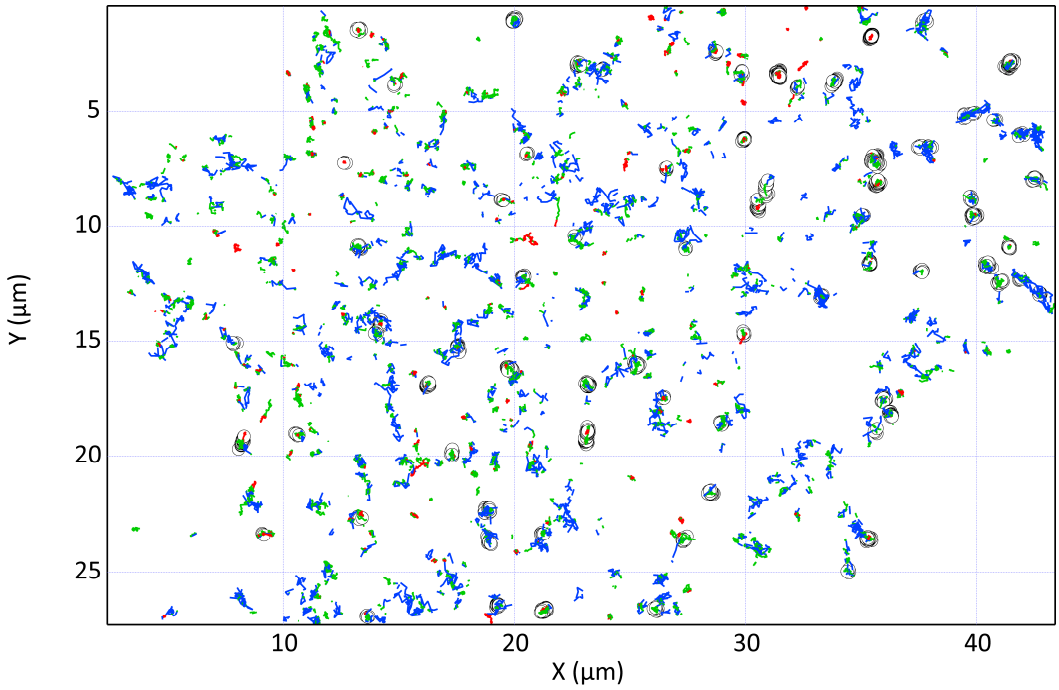

Figure 43: Single particle tracks of Cy3-SNAP-ErbB1 after 10 minutes of stimulation with EGF in a single MCF-7 cell. The tracks are colored according to the mobility states: free (blue), confined (green) and immobile (red). The circles represent colocalization events with EGFP-PTB.

Given that after ligand binding and phosphorylation, active ErbB1 receptors are internalized mainly via clathrin-mediated endocytosis, the colocalization of immobile receptors with clathrin-coated pits was investigated. An overlay of the localizations of immobile receptors with a TIRF image of EGFP-tagged human clathrin light chain A (EGFP-hLCA) for an MCF-7 cell stimulated for 10 minutes with EGF indeed showed a strong colocalization of immobile receptors with clathrin-coated pits (Figure 44).

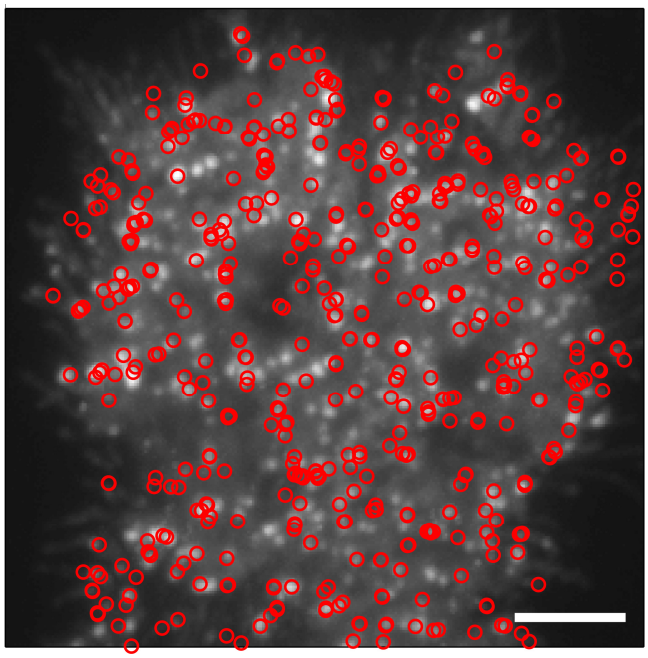

Figure 44: Colocalization of immobile ErbB1 receptors with clathrin-coated pits in an MCF-7 cell after 10 minutes of stimulation with EGF. Overlay of a TIRF image of EGFP-hLCA (grey intensities) with localizations of immobile Cy3-SNAP-ErbB1 receptors (red circles). Scale bar is 5 µm.

Single particle tracking experiments were done in MCF-7 cells coexpressing SNAP-tagged ErbB1, labeled with BG-Cy3, and EGFP-tagged hLCA to localize clathrin-coated pits. Clathrin-coated pits could not be treated as diffraction limited particles, as was the case in previous dual-color experiments, and therefore a new method was developed to quantify the colocalization of single particles with an image of fluorescent structures (see chapter 3.6.2).

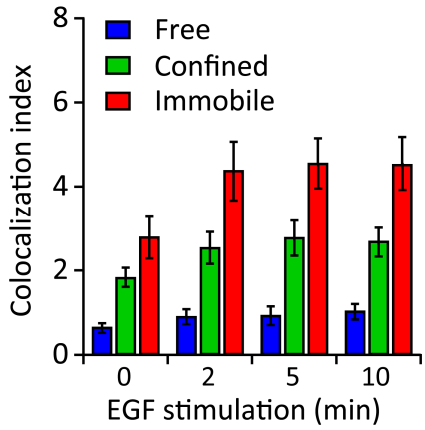

Figure 45: Colocalization index of immobile Cy3-SNAP-ErbB1 with EGFP-hLCA. A: Colocalization index of ErbB1 receptors with clathrin coated-pits in MCF-7 cells per state after stimulation with EGF. *n* = 16 cells per time point.

From the calculated colocalization indices could be established that receptors in the immobile and confined states localized significantly more to clathrin-coated pits compared to receptors in the free state (Figure 45). Upon stimulation with EGF the colocalization index for receptors in the confined and immobile states with clathrin increased, indicating that the active receptor aggregated in clathrin coated pits.

4.5.2. Inhibition of endocytosis with dynasore

The fission of clathrin-coated pits from the plasma membrane is mediated by dynamin. Dynamin can be inhibited by the non-competitive small-molecule inhibitor dynasore, which arrests clathrin-coated pits in intermediate stages of maturation[125].

When MCF-7 cells expressing EGFP-hLCA and SNAP-ErbB1, labeled with BG-Cy3, were preincubated for 30 minutes with 80 µM dynasore, the colocalization indices of immobile ErbB1 receptors in the confined and immobile states with clathrin were lower than without dynasore and increased only slowly upon EGF stimulation (Figure 46). Only after 10 minutes of EGF stimulation the colocalization indices for all states approached the values measured for cells without dynasore treatment (compare with Figure 45).

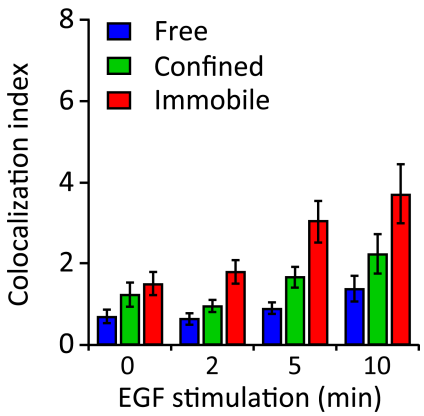

Figure 46: Colocalization index of immobile Cy3-SNAP-ErbB1 with EGFP-hLCA after incubation with the dynamin inhibitor dynasore. A: Colocalization index of ErbB1 receptors with clathrin coated-pits in MCF-7 cells per state after 30 minutes incubation with 80 µM dynasore followed by stimulation with 16 nM EGF. *n* = 16 cells per time point.

To further investigate the role of endocytosis via clathrin-coated pits on ErbB1 activity, cells coexpressing SNAP-ErbB1 and EGFP-PTB were preincubated for 30 min with 80 µM dynasore before tracking.

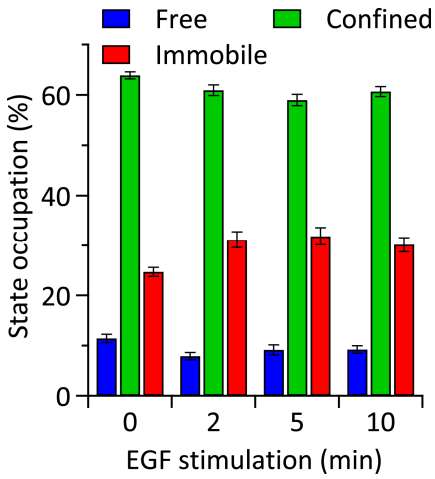

Figure 47: State occupations for ErbB1 after incubation with the dynamin inhibitor dynasore and stimulation with EGF. Occupations of mobility states for Cy3-SNAP-ErbB1 in MCF-7 cells preincubated for 30 minutes with 80 µM dynasore and stimulated with 16 nM EGF. *n* = 28 cells per time point.

The comparison of the state occupations of ErbB1 receptors with and without dynasore revealed no difference for the immobile population (Figure 47). But the basal level of receptors in the free state was considerably reduced when incubated with dynasore. At the same time, the population of receptors in the confined state was higher than without dynasore (Figure 47).

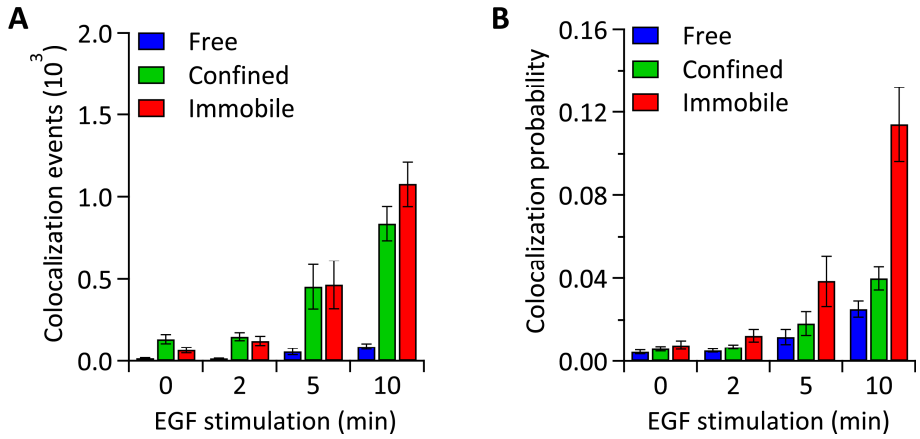

Figure 48: Colocalization analysis of EGFP-PTB domains with SNAP-ErbB1 after incubation with the dynamin inhibitor dynasore. MCF-7 cells were incubated for 30 min with 80 µM dynasore and stimulated with 16 nM EGF. **A**: Colocalization events of PTB domains with ErbB1 per state. **B:** Colocalization probability for PTB domains with ErbB1 per state. *n* = 28 cells per time point.

The analysis of PTB domain recruitment to ErbB1 receptors after incubation with dynasore and stimulation with EGF showed a delayed response to the stimulus (Figure 48).

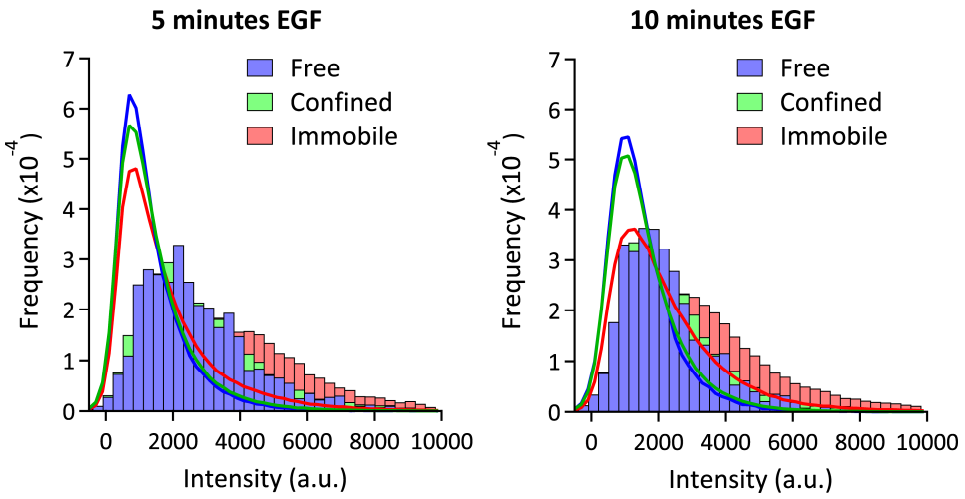

Figure 49: Intensity histograms of Cy3-labeled ErbB1 receptors after incubation with the dynamin inhibitor dynasore. Intensity histograms of the fluorescence of tracked Cy3-SNAP-ErbB1 particles after incubation for 30 min with 80 µM dynasore and stimulated with 16 nM EGF for 5 and 10 minutes, for all particles (lines) and for the particles that colocalized with EGFP-PTB domains (bars). *n* = 28 cells per time point.

Besides the delayed activation of the receptors after dynasore treatment, a delayed cluster formation was implied by the comparison of the intensity histograms after 5 and 10 minutes of EGF stimulation (Figure 49). After dynasore treatment, the difference between the intensities of all particles in the immobile state (red lines) and all particles in the free or confined states (blue and green lines) after 5 minutes of EGF stimulation was less than after 10 minutes (Figure 49). For untreated cells the difference after 5 minutes was already nearly as large as after 10 minutes (Figure 31), indicating that the clustering of receptors treated with dynasore was delayed. After 10 minutes both treated and untreated receptors reached the same level of aggregation.

By inhibition of dynamin with dynasore more of the free diffusing receptors were converted to a confined state but they were not activated. The signaling fraction was still mainly represented by immobile receptors which colocalized with clathrin-coated pits later than without dynasore. Along with the delayed colocalization of immobile receptors with clathrin-coated pits, a delayed phosphorylation and clustering of the receptors was observed, which indicates that receptors convert to the immobile state also when endocytosis is inhibited, but for a stable activation and cluster formation fully formed clathrin-coated pits are important.

4.6. ErbB1 mutants

4.6.1. Kinase-dead ErbB1 K721A mutant

The K721A point mutation in ErbB1 was found to lead to an inactive kinase domain of ErbB1 and is often used to investigate the influence of kinase activity on ErbB1 receptor behavior[74,75]. In confocal microscopy experiments no recruitment of EGFP-tagged PTB domains to the plasma membrane was observed after addition of EGF-Alexa647, which was instantly binding to the SNAP-tagged receptor mutant, labeled with BG-Cy3 (Figure 50). This indicated that the kinase of the K721A mutant was indeed inactive.

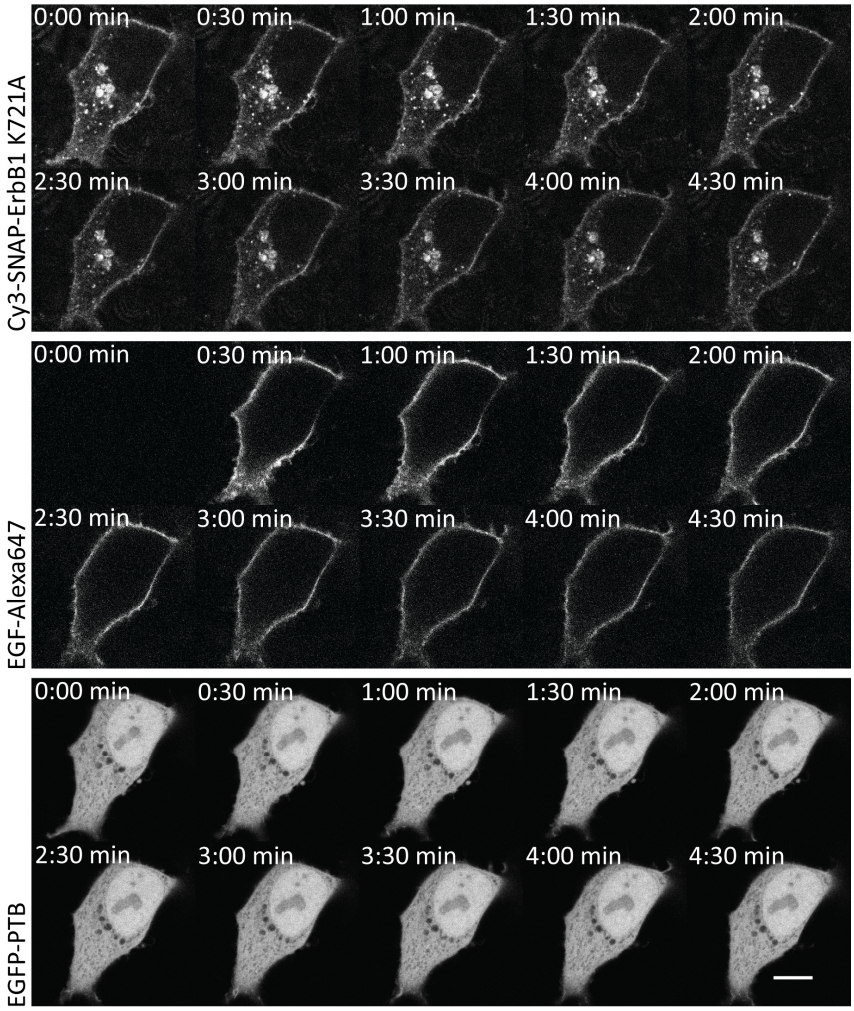

Figure 50: SNAP-ErbB1 K721A mutant coexpressed with EGFP-PTB stimulated with EGF-Alexa647. MCF-7 cell coexpressing SNAP-ErbB1 K721A, labeled with BG-Cy3, with EGFP-PTB stimulated with 16 nM EGF-Alexa647. Scale bar is 10 µm.

In accordance with the confocal data, western blots showed no phosphorylated fraction of the K721 mutant after EGF stimulation (Figure 51).

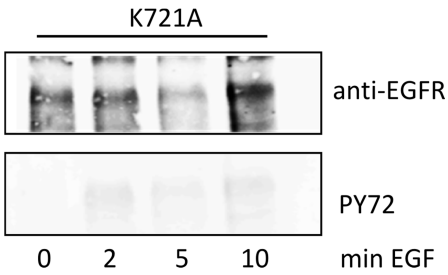

Figure 51: Western blots of MCF-7 lysates transfected with ErbB1 K721A stimulated with EGF. MCF-7 cells transfected with SNAP-ErbB1 K721A were stimulated for indicated times with 16 nM EGF. Western blots were stained against total EGFR (anti-EGFR) and phosphorylated tyrosines (pY72).

In order to evaluate the characteristics of the mobility states of the K721 mutant on a single molecule level, tracking experiments were performed and analyzed. The occupations of the mobility states of the K721A mutant without stimulation did not differ from the wild type (compare Figure 52 with Figure 23 B). Upon EGF stimulation the population of mutant receptors in the free state decreased slowly, while the population of confined receptors increased and the population of immobile receptors remained almost constant.

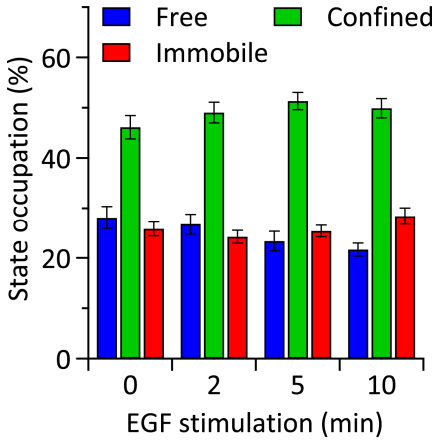

Figure 52: State occupations for ErbB1 receptor mutant K721A upon EGF stimulation. Occupations of mobility states for Cy3-SNAP-ErbB1 K721A mutant in MCF-7 cells stimulated with 16 nM EGF**.** *n* = 8 cells per time point.

PTB domain recruitment to the K721A mutant was very low compared to the wild type (compare Figure 53 C with Figure 29 B), which was expected as auto-phosphorylation by the kinases of the receptors should be inhibited by the mutation.

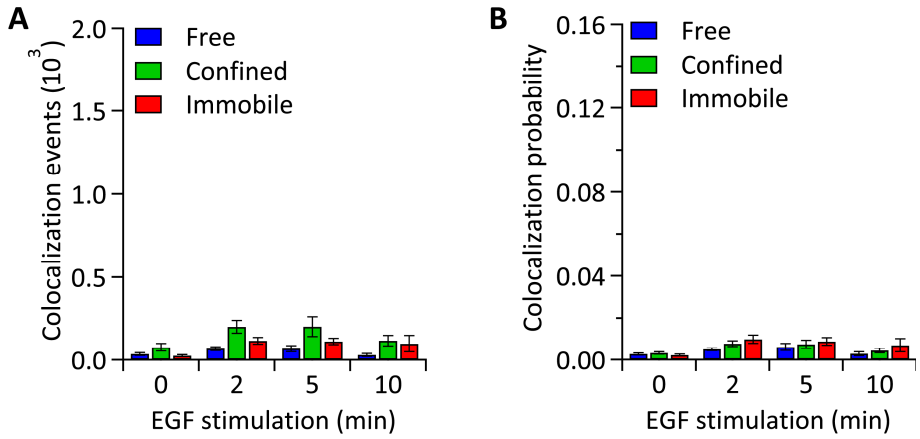

Figure 53: PTB domain localization with SNAP-ErbB1 K721A mutant in MCF-7. Coexpression and colocalization analysis of EGFP-PTB with SNAP-ErbB1 K721A. Colocalization events of PTB domains with ErbB1 K721A mutant per state. **B:** Colocalization probability for PTB domains with ErbB1 K721A mutant per state. *n* = 8 cells per time point.

From the single particle tracking experiments it can be concluded that although the K721A receptor mutants might form dimers upon EGF stimulation, indicated by the increase in confined receptors, they do not get activated or convert to the immobile state.

4.6.2. Dimerization-enhanced ErbB1 mutant L834R

The ErbB1 mutant L834R occurs in several cancer species with a phenotype of high activation levels without EGF stimulation[26,70,71]. It was reported that the phosphorylation levels of some tyrosine residues (Y845 and Y1068) are considerably increased for this receptor mutant[71]. These increased phosphorylation levels might result from an increased tendency to dimerize or oligomerize.

Confocal microscopy experiments in MCF-7 cells coexpressing EGFP-PTB together with the SNAP-tagged ErbB1 L834 mutant, which was labeled with BG-Cy3, showed that the basal level of PTB domains at the plasma membrane was significantly higher than in cells expressing SNAP-tagged wild type ErbB1 (Figure 54).

After stimulation with EGF-Alex647, less EGF binding to the mutant receptors than to the wild type receptors was observed (compare with Figure 15) and an increase in PTB domain recruitment to the plasma membrane was not visible or very low (Figure 54).

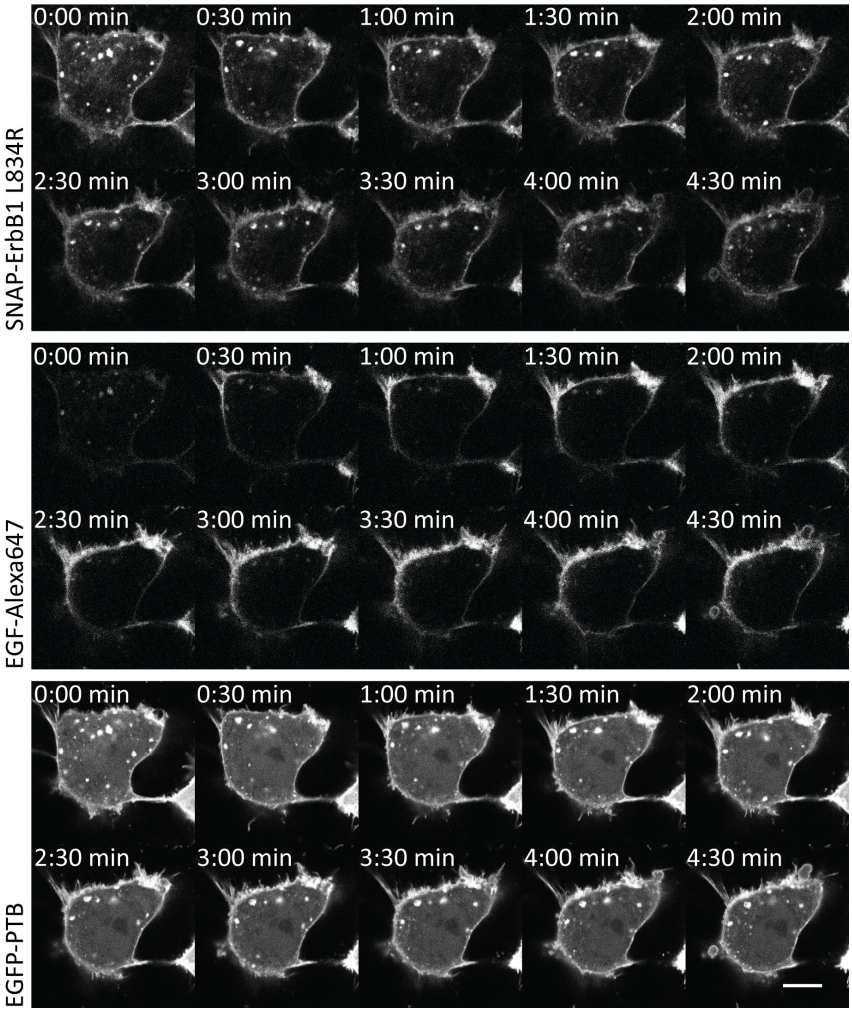

Figure 54: SNAP-ErbB1 L834R coexpressed with EGFP-PTB stimulated with EGF-Alexa647. MCF-7 coexpressing SNAP-ErbB1 L834R, labeled with BG-Cy3, and EGFP-PTB stimulated with 16 nM EGF-Alexa647. Scale bar is 10 µm.

In accordance with the confocal data a high probability for PTB domain colocalization with the ErbB1 receptor mutant was observed in single particle tracking experiments in the absence of a stimulus (Figure 55). In unstimulated cells the probability of PTB domains to colocalize with mutant ErbB1 receptors in the three states was already 5 times higher than with unstimulated wild type receptors (compare Figure 55 with Figure 29). Upon EGF stimulation the recruitment of PTB domains to mutant receptors increased to the values observed after 2 - 5 minutes of EGF stimulation with wild type receptors but did not reach the same level of activation after 10 minutes.

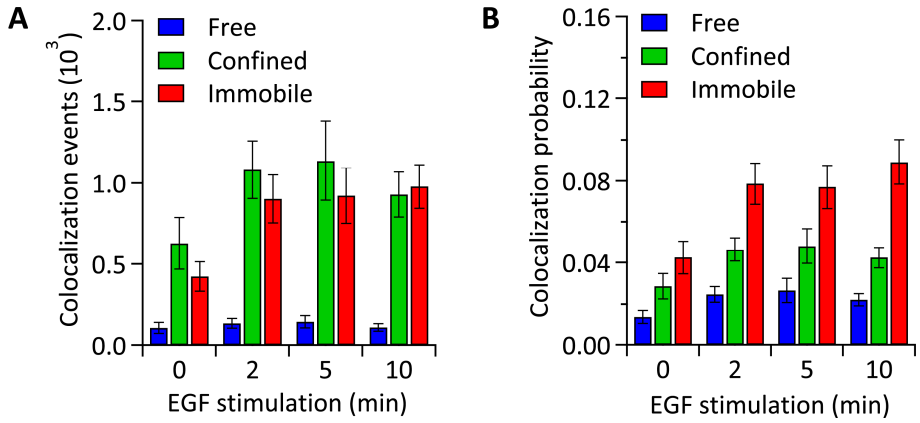

Figure 55: Colocalization probability of PTB domains with ErbB1 receptor mutant L834R upon EGF stimulation. A: Colocalization events of PTB domains with ErbB1 L834R mutant. **B**: Colocalization probability for PTB domains with ErbB1 L834R mutant per state. *n* = 24 cells per time point.

The intensity histograms for each state showed that cluster formation of mutant receptors in the immobile state after 10 minutes of EGF stimulation was slightly less than for the wild type (compare Figure 56 with Figure 31). In resting cells, the intensities of the receptors that colocalized with PTB domains (bars) showed high intensities, indicating that the mutant receptors already form clusters without EGF. However, for all receptors (plotted as lines) the intensity histograms did not differ between the states, which implied that the clustered population was small.

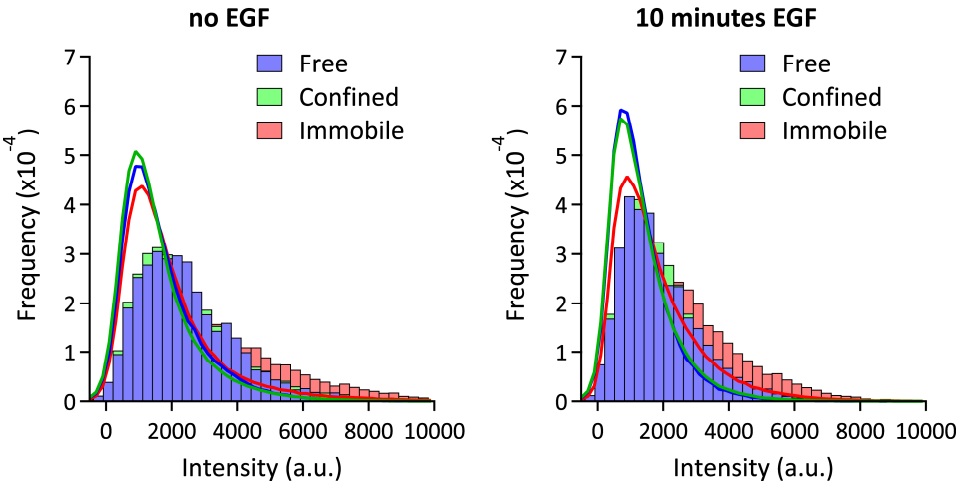

Figure 56: Intensity histograms of Cy3-labeled ErbB1 L834R mutants per mobility state. Intensity histograms of the fluorescence of tracked Cy3-SNAP-ErbB1 L834R particles before and after 10 minutes of EGF stimulation, for all particles (lines) and for the particles that colocalized with EGFP-PTB domains (bars). *n* = 24 cells per time point.

The state occupations of unstimulated ErbB1 L834R (Figure 57 A) were comparable to occupations of wild type ErbB1 after 2 - 5 minutes of EGF stimulation and did not change upon EGF stimulation (Figure 23 B). However, for the mutant more receptors were in the confined state and less in the free state. Since the free state mainly consists of monomers (chapter

4.4.1), the results indicate that the L834R mutant receptor exhibits a higher dimerization affinity, resulting in more confined and immobile receptors.

The state lifetimes for the immobile state did not increase upon EGF stimulation as was observed for the wild type. However, when comparing the lifetimes of receptors states for the L834R mutant with wild type, the longer lifetime of mutant receptors in the immobile and the confined states and the shorter lifetime of the free state before stimulation are visible (Figure 57 B).

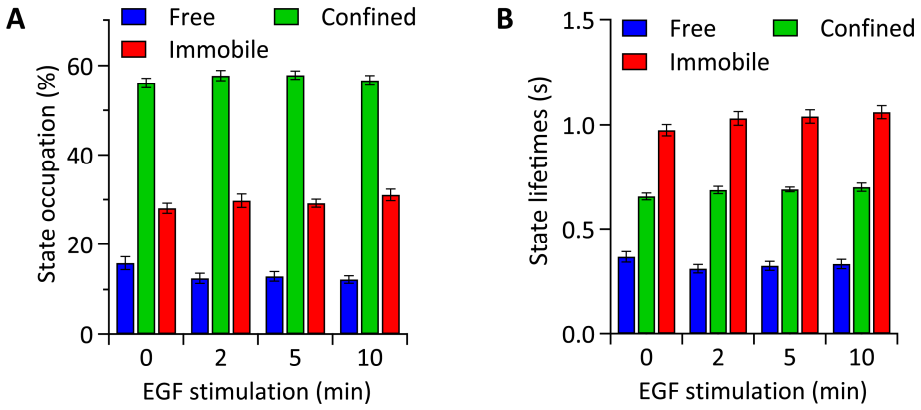

Figure 57: State occupations and lifetimes for ErbB1 receptor mutant L834R upon EGF stimulation. A: Occupations of mobility states for Cy3-SNAP-ErbB1 L834R mutant in MCF-7 cells stimulated with 16 nM EGF**.** **B**: Lifetimes of mobility states for Cy3-SNAP-ErbB1 L834R mutant in MCF-7 cells stimulated with 16 nM EGF**.** *n* = 24 cells per time point.

Taken together, the observations in single particle tracking measurements support the findings that the L834R mutation leads to an increased basal activation of the ErbB1 receptor caused by an increased dimerization affinity, while cluster formation is less than for the wild type.

5. DISCUSSION AND PERSPECTIVES

5.1. Benefits and challenges of single particle tracking

In this work, the analysis of single particle tracking data was shown to be a versatile tool to quantify the mobility of ErbB1 at the plasma membrane. It was possible to monitor even small changes in receptor dynamics in real time, changes that cannot be easily detected by ensemble fluorescence measurements, such as FLIM or FRAP. Furthermore, the dual-color setup allows monitoring additional characteristics such as activation status, self-association and colocalization with other proteins or cellular structures.

A general problem for single molecule tracking is the bleaching of the fluorophore, which restricts the acquisition time. Most published tracking experiments employed quantum dots[41,42,98,126,127], which allow long observation periods. Fluorescent proteins, which can be genetically encoded, are less frequently used because they bleach relatively fast. For example, Xiao *et al.* tracked GFP tagged ErbB2 receptors and reported bleaching after 2 - 4 seconds[128], which might be too short for proper analysis. For this reason, in this work a genetically encoded SNAP-tag was used to add a variable extracellular labeling position to the N-terminus of the ErbB1 receptor, which was shown to have no influence on the functionality of the receptor compared to previously published data with C-terminal EGFP (chapter 4.1). Several derivatives of O^6-Benzylguanine can be used as SNAP substrates to label the receptor with organic dyes, such as Alexa488 or Cy3, that are much more photo-stable than fluorescent proteins. For experiments performed in this work the acquisition time of 10 seconds was long enough to gain highly qualitative information about the diffusion of the ErbB1 receptor as the mean bleaching time of Cy3 was approximately 30 seconds.

Besides the opportunity to introduce several organic fluorophores, another advantage of the SNAP-tag is that it is much smaller than antibodies and quantum dots, which have been used in other studies to label ErbB1 for tracking. Because diffusion depends on the size of the particle, the use of quantum dots might bias the diffusion of ErbB1. Additionally a labeling ratio of 1:1 is usually not achieved with quantum dots. On the other hand the SNAP-tag has to be introduced genetically, while antibodies can be used to label endogenous receptors. Hence, for experiments with SNAP-tagged ErbB1 the endogenous expression level of receptors has to be taken into account. Because the endogenous receptors are not labeled, this could lead to a biased result, especially the level of aggregation could be underestimated when SNAP-tagged

receptors cluster with unlabeled endogenous receptors. For this reason, MCF-7 cells were used in this work as they have only low expression levels of ErbB1. But it has to be taken into account that MCF-7 cells express ErbB2 and ErbB3 in medium levels, so that hetero-dimerization can occur. As a control, the tracking experiments should be repeated in cells without endogenous ErbB1 and ErbB2 expression, such as the cell line CHO-K1 that originates from a parental CHO cell line initiated 1957 by T. T. Puck from a Chinese hamster ovary[129]. Of this cell line also a variant exists that stably expresses ErbB2[130], which could be used to determine the influence of hetero-dimerization with ErbB2 on ErbB1 diffusion. Another possibility to investigate the role of hetero-dimerization of ErbB1 would be to colocalize ErbB2 receptors with ErbB1 receptors in a dual-color experiment similar to those shown in chapter 4.4.2.

5.2. Dynamics of ErbB1 diffusion

The data presented in this work show that ErbB1 receptors alternate between three short-lived mobility states: a free, a confined and an immobile state (chapter 4.3). These states were clearly distinguishable by their diffusion coefficients that spanned two orders of magnitude. The lifetime of the immobile state was significantly longer compared to the other states, which further increased upon stimulation with EGF (Figure 25), while also the population of receptors in this state grew (Figure 23 B). At the same time the population of freely diffusing receptors decreased upon EGF stimulation. But receptors did not directly convert from the free to the immobile state, pointing to a role of the confined state as an intermediate state. This was underscored by the fact that the confined state represented the biggest population, which only marginally changed upon stimulation. Since EGF stimulation mainly increased the transition between free and confined states, it can be concluded that ligand binding drives freely diffusing ErbB1 receptors into the confined state, thereby shifting the balance towards the immobile population. Between 5 and 10 minutes of EGF stimulation, the population of immobile receptors decreased again, while the population of free receptors increased. This could be explained by the internalization of the immobile receptors that are recycled back to the membrane as monomers, which contributes to the population of receptors in the free state. The time frame in which this increase of the free receptor population was observed, 5 - 10 minutes after addition of EGF, matches the reported times for fast recycling of 5 – 7 minutes[52,131].

The recycling process of ErbB1 needs to be further investigated. By other studies it was already shown that the rate of recycling depends on the ligand that is bound to ErbB1[60,61]. TGF-α for example leads to significant increased recycling of the receptor. Single particle tracking experiments with TGF-α stimulation might reveal how an increased recycling rate influences the occupations of the mobility states of the receptor. This could possibly show which state is preferentially occupied by the recycled receptors.

5.3. Interplay of ErbB1 aggregation and activation

Together with the intensity histograms of dual-color tracking experiments (chapter 4.4.2, Figure 34) and the PTB colocalization experiments (chapter 4.4.1, Figure 31), the EGF colocalization experiments (chapter 4.4.3, Figure 35) indicate that immobile ErbB1 receptors form clusters upon EGF stimulation that represent the main signaling fraction. Receptors in the confined state also bind EGF and are activated but they mostly form dimers and do not cluster, while the free population mainly consists of monomeric receptors that do not bind EGF and are not active.

The comparison of the fluorescence intensities of receptors in the different states before and after stimulation (chapter 4.4.1, Figure 30) revealed that receptors in resting cells were mainly monomeric in all states, arguing against a relevance of pre-dimerization for ErbB1 activation. This was supported by the results of experiments with dual-color labeled ErbB1 receptors (chapter 4.4.2), where no self-association was observed without EGF (Figure 33). Other single molecule studies contradict each other regarding the role of pre-dimerization[41,42]. However, it was also reported that pre-dimerization only occurs in cells expressing the receptor at high levels[43]. Thus, dimerization rates observed in single molecule measurements depend on the expression level that varies strongly between cell lines, which could explain the contradictory observations.

5.3.1. Relevance of the expression level

In nearly all of the experiments in this work the dependency on the receptor density became clear. It was repeatedly shown that receptor overexpression leads to altered behavior (Figure 28, Figure 37), particularly to ligand-independent activation of the receptor (chapter 4.4.1), which was already reported by other studies[23,43–45]. TIRF image series of cells expressing the SNAP-tagged ErbB1 receptor at different levels, labeled with BG-Cy3, together with EGFP-

PTB, showed altered clustering behavior upon EGF stimulation (chapter 4.4.4, Figure 37). Phosphorylated ErbB1 receptors were found to be equally distributed over the cell, when the expression level was high. Whereas in cells with low expression levels, phosphorylated receptors were focused in small spots. This gives a hint that proper receptor localization on the plasma membrane cannot be maintained in overexpressing cells.

5.3.2. Conditions for cluster formation

An important finding is that the immobile population is not equal to the clustered population. It contains the clustered population that is formed upon EGF binding, but it already exists in unstimulated cells, where the receptors are mainly monomeric. Experiments with cells incubated with the kinase inhibitor erlotinib showed that the balance of mobility states was driven to more immobile states (chapter 4.4.5, Figure 40), but the receptors showed significantly less clustering (Figure 42). Erlotinib competitively binds to the ATP binding site of the kinase domain of the receptor, thereby trapping the receptor in its extended conformation[69,124]. In the extended conformation the dimerization arm of subdomain II is exposed (Figure 4) leading to a higher dimerization affinity of the receptor[13]. This was confirmed by the reduction of receptors in the free state and an increase in the confined and immobile receptor populations when treated with erlotinib (Figure 40). However, dimer formation alone is apparently not sufficient to induce cluster formation, indicating that kinase activity is required. Experiments with the phosphatase inhibitor pervanadate showed that ErbB1 forms clusters after ligand-independent activation (chapter 4.4.4, Figure 39), indicating that EGF binding is not required for cluster formation.

5.3.3. Amplification of signaling by clustering

A comparison of the amount of bound EGF with the activation status, which was detected by PTB recruitment, revealed that in the immobile state the amount of activated receptors increased stronger than the amount of bound EGF relative to the confined state (chapter 4.4.3, Figure 36). These results indicate that the signal is amplified in the immobile state, which could result from clustering[132]. Since the active clusters of immobile receptors were mainly colocalized with clathrin-coated pits (chapter 4.5.1, Figure 44), one reason could also be the strong curvature of the plasma membrane in the area of the clathrin-coated pits[133] or the presence or absence of regulating effectors leading to an enhanced signal processing. Either way, the signaling activity of ErbB1 receptors is localized and amplified in highly active clusters rather than being uniformly distributed over the cell.

5.4. Stabilization of ErbB1 signaling in clathrin-coated pits

It was shown that activation of the receptors increased the lifetime of the immobile state (Figure 30), indicating that the active receptors are maintained at the plasma membrane. The reason could be that clathrin-coated pits stabilize receptor activity and aggregation to enable signal amplification prior to termination of signaling by endocytosis.

Colocalization analysis of ErbB1 receptors with clathrin-coated pits revealed that receptors in the confined and immobile states colocalize strongly with clathrin coated pits after stimulation with EGF (chapter 4.5.1).

Inhibition of dynamin with dynasore leads to the arrest of clathrin mediated endocytosis at intermediate stages[125]. As a result, clathrin-coated pits accumulate at the plasma membrane after dynasore treatment, which drives the ErbB1 receptor into the confined state (chapter 4.5.2, Figure 47). However, the colocalization of receptors in the confined and immobile states with clathrin-coated pits is less than without dynasore (Figure 45 and Figure 46). The reason is likely that the receptors are not trapped in clathrin-coated pits, as they maintain their ability to switch between states and the diffusion of receptors out of immature clathrin-coated pits is facilitated. This is in agreement with a recent study that described the highly dynamic nature of the interaction of clathrin-coated pits with their cargo and that the probability for the cargo to escape decreases with the maturation of a clathrin-coated pit[134]. Upon stimulation with EGF the colocalization increased, together with an increase in clustering (Figure 49) and activation (Figure 48), but all three were delayed compared to untreated cells. The delayed response observed in cells treated with dynasore indicates that fully formed clathrin-coated pits support activation and clustering of the receptor, while intermediate states of clathrin-coated pits only lead to confinement of the receptors, which do not reach their maximal active state. The reason could be that in fully formed clathrin-coated pits the receptor density is locally increased, supporting cluster formation and propagation of the signal as has been reported for cells with high expression levels of the receptor[44].

Colocalization experiments with dynamin could potentially provide further information about which maturation stage of clathrin-coated pits is relevant for signal amplification. With dynamin clathrin-coated pits in the process of scission could be identified and correlated to cluster formation and signal amplification.

5.5. Characteristics of ErbB1 receptor mutants

The K721A mutation of the ErbB1 receptor leads to the inactivation of the tyrosine kinase. In this work, the behavior of the mutant upon EGF stimulation in comparison to the wild type receptor was investigated by single particle tracking experiments. The colocalization analysis of the mutant receptor with PTB domains revealed that the phosphorylation level upon EGF stimulation is very low (chapter 4.6.1, Figure 53), consistent with other studies, describing the mutant as "kinase-dead"[25,135]. The result from the single particle tracking experiments indicated that the kinase-dead mutant forms dimers upon stimulation with EGF but not higher order oligomers. To underline this result, dual-color experiments as performed for the wild type receptor should be done with the K721A mutant to demonstrate its self-aggregation level after EGF stimulation. Additionally, EGF-colocalization experiments should be done to evaluate the EGF binding affinity of the mutant receptor in comparison to the wild type.

The ErbB1 mutant L834R was shown to exhibit an increased basal activity in several cancer species[26,70,71]. Single particle tracking experiments indeed confirmed that the basal activity of the mutant receptor is high compared to the wild type (chapter 4.6.2, Figure 55). The population of mutant receptors in the free state was significantly reduced compared to the wild type (Figure 57 A), which points to an increased dimerization affinity of the mutant receptor. The analysis of the intensities of the receptors in each state indicated that the mutant is able to cluster without EGF stimulation, but since the population of clustered receptors was low, the mutant receptors are more likely to form dimers. To further investigate the aggregation state of the mutant receptors, dual-color tracking experiments with the receptor labeled with two colors should be performed. Upon stimulation the activation of the mutant receptors increased but did not reach the activation level of wild type receptors (Figure 55). Apparently the mutant receptor tends to dimerize strongly but does not cluster so effectively, at least with itself. This is consistent with a recently study, in which the L834R mutation was shown to destabilize the inactive conformation of the kinase rather than locking the kinase in its active conformation[136]. Thus, the mutant receptor still depends on asymmetric dimer formation to exhibit full activation. Brewer *et al.* described a 'superacceptor activity' of the mutant that leads to an increased affinity to form asymmetric dimers with the wild type receptors, in which the mutant adopts the acceptor kinase conformation[136]. Thus, coexpression of wild type receptors with the L834R mutant is possibly required to induce cluster formation.

Apart from the dimerization and clustering behavior of the L834R mutant, confocal measurements indicated that EGF binding to the mutant is lower that to wild type receptors (chapter 4.6.2, Figure 54). This should be further investigated on a single molecule level by colocalization experiments with labeled EGF. Furthermore, experiments with phosphatase inhibition by pervanadate could be of interest to compare the basal activity of the L834R mutant to wild type ErbB1.

5.6. Future directions

There are several more aspects of ErbB1 signaling that are worth investigating by the presented single particle tracking and colocalization methods.

So far only self-aggregation of ErbB1 was addressed in this work. But as hetero-dimerization is also known to play an important role for receptor signaling, the presented methods could be applied to investigate dimerization and cluster formation between other members of the ErbB receptor family. Furthermore, colocalization experiments with effector proteins, such as Grb2 or Ras, could provide information about the activation of different pathways. For example, the confinement of the ErbB1 receptor upon EGF stimulation could lead to spatial effects on proteins involved in downstream signaling, such as Ras, which has been reported to form clusters[137]. As already mentioned the stimulation of the receptor with other ligands, such as TGF-α, could reveal differences in its diffusion and clustering behavior. Moreover, colocalization experiments with cytoskeleton proteins, such as actin, could reveal if they play a role for receptor confinement.

Another significant point could be to determine the causality between EGF binding and the transition of ErbB1 to a slower mobility state by further analyzing the tracking data. The order of events could be determined by analyzing the number of EGF binding events before and after a state transition event.

To complete the picture of ErbB1 signaling besides the activation, also the termination and recycling process should be further explored by single particle methods. As this work gives some hints for the role of clathrin-mediated endocytosis and recycling, endocytosis and recycling process would need further investigation.

5.7. Concluding remarks

Pre-dimerization was shown to be irrelevant for activation of ErbB1 receptors, which are mainly monomeric in unstimulated cells and switch rapidly between a free, a confined and an immobile state. Upon EGF binding receptors in the immobile state form clusters, for which kinase activity and subsequent phosphorylation of the receptors are required. In the immobile clusters the signal is amplified, which is supported by recruitment of the receptors to fully formed clathrin-coated pits. As a result, the signaling activity of ErbB1 receptors is localized and amplified in highly active clusters rather than being uniformly distributed over the cell. In cells with low expression levels of the receptor, which is closer to the physiological situation than the case of overexpression, the spatial focusing of the receptor's activity enables robust signaling.

In this work, the activity of ErbB1 receptors was for the first time measured on single molecule level by using EGFP-PTB as a probe for receptor phosphorylation. The connection of activity measurements with mobility states in living cells in a single measurement provides a general tool to investigate receptor activation on a single molecule level.

6. REFERENCES

1. Blume-Jensen, P. & Hunter, T. Oncogenic kinase signalling. *Nature* **411,** 355–65 (2001).

2. Ullrich, A. & Schlessinger, J. Signal transduction by receptors with tyrosine kinase activity. *Cell* **61,** 203–212 (1990).

3. Lemmon, M. A. & Schlessinger, J. Cell signaling by receptor tyrosine kinases. *Cell* **141,** 1117–34 (2010).

4. Carpenter, G. Receptors for epidermal growth factor and other polypeptide mitogens. *Annu. Rev. Biochem.* **56,** 881–914 (1987).

5. Yarden, Y. & Sliwkowski, M. X. Untangling the ErbB signalling network. *Nat. Rev. Mol. Cell Biol.* **2,** 127–37 (2001).

6. Klapper, L. N., Glathe, S., Vaisman, N., Hynes, N. E., Andrews, G. C., Sela, M. & Yarden, Y. The ErbB-2/HER2 oncoprotein of human carcinomas may function solely as a shared coreceptor for multiple stroma-derived growth factors. *Proc. Natl. Acad. Sci.* **96,** 4995–5000 (1999).

7. Cho, H.-S., Mason, K., Ramyar, K. X., Stanley, A. M., Gabelli, S. B., Denney, D. W. & Leahy, D. J. Structure of the extracellular region of HER2 alone and in complex with the Herceptin Fab. *Nature* **421,** 756–60 (2003).

8. Garrett, T. P. J., McKern, N. M., Lou, M., Elleman, T. C., Adams, T. E., Lovrecz, G. O., Kofler, M., Jorissen, R. N., Nice, E. C., Burgess, A. W. & Ward, C. W. The Crystal Structure of a Truncated ErbB2 Ectodomain Reveals an Active Conformation, Poised to Interact with Other ErbB Receptors. *Mol. Cell* **11,** 495–505 (2003).

9. Guy, P. M., Platko, J. V, Cantley, L. C., Cerione, R. A. & Carraway, K. L. Insect cell-expressed p180erbB3 possesses an impaired tyrosine kinase activity. *Proc. Natl. Acad. Sci. U. S. A.* **91,** 8132–6 (1994).

10. Jones, J. T., Akita, R. W. & Sliwkowski, M. X. Binding specificities and affinities of egf domains for ErbB receptors. *FEBS Lett.* **447,** 227–231 (1999).

11. Falls, D. Neuregulins: functions, forms, and signaling strategies. *Exp. Cell Res.* **284,** 14–30 (2003).

12. Rowinsky, E. K. The erbB family: targets for therapeutic development against cancer and therapeutic strategies using monoclonal antibodies and tyrosine kinase inhibitors. *Annu. Rev. Med.* **55,** 433–57 (2004).

13. Ferguson, K. M., Berger, M. B., Mendrola, J. M., Cho, H.-S., Leahy, D. J. & Lemmon, M. A. EGF Activates Its Receptor by Removing Interactions that Autoinhibit Ectodomain Dimerization. *Mol. Cell* **11,** 507–517 (2003).

14. Garrett, T. P. J., McKern, N. M., Lou, M., Elleman, T. C., Adams, T. E., Lovrecz, G. O., Zhu, H.-J., Walker, F., Frenkel, M. J., Hoyne, P. A., Jorissen, R. N., Nice, E. C., Burgess, A. W. &

Ward, C. W. Crystal Structure of a Truncated Epidermal Growth Factor Receptor Extracellular Domain Bound to Transforming Growth Factor α. *Cell* **110,** 763–773 (2002).

15. Ogiso, H., Ishitani, R., Nureki, O., Fukai, S., Yamanaka, M., Kim, J.-H., Saito, K., Sakamoto, A., Inoue, M., Shirouzu, M. & Yokoyama, S. Crystal Structure of the Complex of Human Epidermal Growth Factor and Receptor Extracellular Domains. *Cell* **110,** 775–787 (2002).

16. Egan, S. E., Giddings, B. W., Brooks, M. W., Buday, L., Sizeland, A. M. & Weinberg, R. A. Association of Sos Ras exchange protein with Grb2 is implicated in tyrosine kinase signal transduction and transformation. *Nature* **363,** 45–51 (1993).

17. Li, N., Batzer, A., Daly, R., Yajnik, V., Skolnik, E., Chardin, P., Bar-Sagi, D., Margolis, B. & Schlessinger, J. Guanine-nucleotide-releasing factor hSos1 binds to Grb2 and links receptor tyrosine kinases to Ras signalling. *Nature* **363,** 85–8 (1993).

18. Rozakis-Adcock, M., Fernley, R., Wade, J., Pawson, T. & Bowtell, D. The SH2 and SH3 domains of mammalian Grb2 couple the EGF receptor to the Ras activator mSos1. *Nature* **363,** 83–5 (1993).

19. Schlessinger, J. Cell Signaling by Receptor Tyrosine Kinases. *Cell* **103,** 211–225 (2000).

20. Cantley, L. C. The phosphoinositide 3-kinase pathway. *Science* **296,** 1655–7 (2002).

21. Roepstorff, K., Grøvdal, L., Grandal, M., Lerdrup, M. & van Deurs, B. Endocytic downregulation of ErbB receptors: mechanisms and relevance in cancer. *Histochem. Cell Biol.* **129,** 563–78 (2008).

22. Arkhipov, A., Shan, Y., Das, R., Endres, N. F., Eastwood, M. P., Wemmer, D. E., Kuriyan, J. & Shaw, D. E. Architecture and Membrane Interactions of the EGF Receptor. *Cell* **152,** 557–569 (2013).

23. Endres, N. F., Das, R., Smith, A. W., Arkhipov, A., Kovacs, E., Huang, Y., Pelton, J. G., Shan, Y., Shaw, D. E., Wemmer, D. E., Groves, J. T. & Kuriyan, J. Conformational Coupling across the Plasma Membrane in Activation of the EGF Receptor. *Cell* **152,** 543–556 (2013).

24. Jura, N., Endres, N. F., Engel, K., Deindl, S., Das, R., Lamers, M. H., Wemmer, D. E., Zhang, X. & Kuriyan, J. Mechanism for activation of the EGF receptor catalytic domain by the juxtamembrane segment. *Cell* **137,** 1293–307 (2009).

25. Zhang, X., Gureasko, J., Shen, K., Cole, P. A. & Kuriyan, J. An allosteric mechanism for activation of the kinase domain of epidermal growth factor receptor. *Cell* **125,** 1137–49 (2006).

26. Shan, Y., Eastwood, M. P., Zhang, X., Kim, E. T., Arkhipov, A., Dror, R. O., Jumper, J., Kuriyan, J. & Shaw, D. E. Oncogenic mutations counteract intrinsic disorder in the EGFR kinase and promote receptor dimerization. *Cell* **149,** 860–70 (2012).

27. Bae, J. H. & Schlessinger, J. Asymmetric tyrosine kinase arrangements in activation or autophosphorylation of receptor tyrosine kinases. *Mol. Cells* **29,** 443–8 (2010).

28. Endres, N. F., Engel, K., Das, R., Kovacs, E. & Kuriyan, J. Regulation of the catalytic activity of the EGF receptor. *Curr. Opin. Struct. Biol.* **21,** 777–84 (2011).

29. Lemmon, M. A., Bu, Z., Ladbury, J. E., Zhou, M., Pinchasi, D., Lax, I., Engelman, D. M. & Schlessinger, J. Two EGF molecules contribute additively to stabilization of the EGFR dimer. *EMBO J.* **16,** 281–94 (1997).

30. Martin-Fernandez, M., Clarke, D. T., Tobin, M. J., Jones, S. V & Jones, G. R. Preformed oligomeric epidermal growth factor receptors undergo an ectodomain structure change during signaling. *Biophys. J.* **82,** 2415–27 (2002).

31. Sako, Y., Minoghchi, S. & Yanagida, T. Single-molecule imaging of EGFR signalling on the surface of living cells. *Nat. Cell Biol.* **2,** 168–72 (2000).

32. Lidke, D., Nagy, P., Barisas, B., Heintzmann, R., Post, J., Lidke, K., Clayton, A., Arndt-Jovin, D. & Jovin, T. Imaging molecular interactions in cells by dynamic and static fluorescence anisotropy (rFLIM and emFRET). *Biochem. Scociety Trans.* **31,** 1020–1027 (2003).

33. Liu, P., Sudhaharan, T., Koh, R. M. L., Hwang, L. C., Ahmed, S., Maruyama, I. N. & Wohland, T. Investigation of the dimerization of proteins from the epidermal growth factor receptor family by single wavelength fluorescence cross-correlation spectroscopy. *Biophys. J.* **93,** 684–98 (2007).

34. Yu, X., Sharma, K. D., Takahashi, T., Iwamoto, R. & Mekada, E. Ligand-independent dimer formation of epidermal growth factor receptor (EGFR) is a step separable from ligand-induced EGFR signaling. *Mol. Biol. Cell* **13,** 2547–57 (2002).

35. Moriki, T., Maruyama, H. & Maruyama, I. N. Activation of preformed EGF receptor dimers by ligand-induced rotation of the transmembrane domain11Edited by B. Holland. *J. Mol. Biol.* **311,** 1011–1026 (2001).

36. Teramura, Y., Ichinose, J., Takagi, H., Nishida, K., Yanagida, T. & Sako, Y. Single-molecule analysis of epidermal growth factor binding on the surface of living cells. *EMBO J.* **25,** 4215–22 (2006).

37. Clayton, A. H. A., Walker, F., Orchard, S. G., Henderson, C., Fuchs, D., Rothacker, J., Nice, E. C. & Burgess, A. W. Ligand-induced dimer-tetramer transition during the activation of the cell surface epidermal growth factor receptor-A multidimensional microscopy analysis. *J. Biol. Chem.* **280,** 30392–9 (2005).

38. Lidke, D. S., Lidke, K. A., Rieger, B., Jovin, T. M. & Arndt-Jovin, D. J. Reaching out for signals: filopodia sense EGF and respond by directed retrograde transport of activated receptors. *J. Cell Biol.* **170,** 619–26 (2005).

39. Hofman, E. G., Bader, A. N., Voortman, J., van den Heuvel, D. J., Sigismund, S., Verkleij, A. J., Gerritsen, H. C. & van Bergen en Henegouwen, P. M. P. Ligand-induced EGF receptor oligomerization is kinase-dependent and enhances internalization. *J. Biol. Chem.* **285,** 39481–9 (2010).

40. Macdonald, J. L. & Pike, L. J. Heterogeneity in EGF-binding affinities arises from negative cooperativity in an aggregating system. *Proc. Natl. Acad. Sci. U. S. A.* **105,** 112–7 (2008).

41. Chung, I., Akita, R., Vandlen, R., Toomre, D., Schlessinger, J. & Mellman, I. Spatial control of EGF receptor activation by reversible dimerization on living cells. *Nature* **464,** 783–7 (2010).

42. Low-Nam, S. T., Lidke, K. a, Cutler, P. J., Roovers, R. C., Bergen, P. M. P. Van, Wilson, B. S., Lidke, D. S. & van Bergen en Henegouwen, P. M. P. ErbB1 dimerization is promoted by domain co-confinement and stabilized by ligand binding. *Nat. Struct. Mol. Biol.* **18,** 1244–9 (2011).

43. Nagy, P., Claus, J., Jovin, T. M. & Arndt-Jovin, D. J. Distribution of resting and ligand-bound ErbB1 and ErbB2 receptor tyrosine kinases in living cells using number and brightness analysis. *Proc. Natl. Acad. Sci.* **107,** 16524–16529 (2010).

44. Verveer, P. J., Wouters, F. S., Reynolds, A. R. & Bastiaens, P. I. H. Quantitative Imaging of Lateral ErbB1 Receptor Signal Propagation in the Plasma Membrane. *Science (80-.).* **290,** 1567–1570 (2000).

45. Reynolds, A. R., Tischer, C., Verveer, P. J., Rocks, O. & Bastiaens, P. I. H. EGFR activation coupled to inhibition of tyrosine phosphatases causes lateral signal propagation. *Nat. Cell Biol.* **5,** 447–53 (2003).

46. Clayton, A. H. a, Tavarnesi, M. L. & Johns, T. G. Unligated epidermal growth factor receptor forms higher order oligomers within microclusters on A431 cells that are sensitive to tyrosine kinase inhibitor binding. *Biochemistry* **46,** 4589–97 (2007).

47. Webb, S. E. D., Roberts, S. K., Needham, S. R., Tynan, C. J., Rolfe, D. J., Winn, M. D., Clarke, D. T., Barraclough, R. & Martin-Fernandez, M. L. Single-Molecule Imaging and Fluorescence Lifetime Imaging Microscopy Show Different Structures for High- and Low-Affinity Epidermal Growth Factor Receptors in A431 Cells. *Biophys. J.* **94,** 803–819 (2008).

48. Szabó, Á., Horváth, G., Szöllősi, J. & Nagy, P. Quantitative Characterization of the Large-Scale Association of ErbB1 and ErbB2 by Flow Cytometric Homo-FRET Measurements. *Biophys. J.* **95,** 2086–2096 (2008).

49. Wang, J., Yu, X., Boriskina, S. V & Reinhard, B. M. Quantification of differential ErbB1 and ErbB2 cell surface expression and spatial nanoclustering through plasmon coupling. *Nano Lett.* **12,** 3231–7 (2012).

50. Abulrob, A., Lu, Z., Baumann, E., Vobornik, D., Taylor, R., Stanimirovic, D. & Johnston, L. J. Nanoscale imaging of epidermal growth factor receptor clustering: effects of inhibitors. *J. Biol. Chem.* **285,** 3145–56 (2010).

51. Carpenter, G. 125I-labeled human epidermal growth factor. Binding, internalization, and degradation in human fibroblasts. *J. Cell Biol.* **71,** 159–171 (1976).

52. Sorkin, A. Recycling of epidermal growth factor-receptor complexes in A431 cells: identification of dual pathways. *J. Cell Biol.* **112,** 55–63 (1991).

53. Jiang, X., Huang, F., Marusyk, A. & Sorkin, A. Grb2 regulates internalization of EGF receptors through clathrin-coated pits. *Mol. Biol. Cell* **14,** 858–70 (2003).

54. Haigler, H. T., McKanna, J. A. & Cohen, S. Direct visualization of the binding and internalization of a ferritin conjugate of epidermal growth factor in human carcinoma cells A-431. *J. Cell Biol.* **81,** 382–95 (1979).

55. Chinkers, M., McKanna, J. A. & Cohen, S. Rapid induction of morphological changes in human carcinoma cells A-431 by epidermal growth factors. *J. Cell Biol.* **83,** 260–5 (1979).

56. Yamazaki, T., Zaal, K., Hailey, D., Presley, J., Lippincott-Schwartz, J. & Samelson, L. E. Role of Grb2 in EGF-stimulated EGFR internalization. *J. Cell Sci.* **115,** 1791–1802 (2002).

57. Orth, J. D., Krueger, E. W., Weller, S. G. & McNiven, M. A. A novel endocytic mechanism of epidermal growth factor receptor sequestration and internalization. *Cancer Res.* **66,** 3603–10 (2006).

58. Wiley, H., Herbst, J., Walsh, B., Lauffenburger, D., Rosenfeld, M. & Gill, G. The role of tyrosine kinase activity in endocytosis, compartmentation, and down-regulation of the epidermal growth factor receptor. *J. Biol. Chem.* **266,** 11083–11094 (1991).

59. Sorkin, A. & Goh, L. K. Endocytosis and intracellular trafficking of ErbBs. *Exp. Cell Res.* **315,** 683–696 (2009).

60. Ebner, R. & Derynck, R. Epidermal growth factor and transforming growth factor-alpha: differential intracellular routing and processing of ligand-receptor complexes. *Cell Regul.* **2,** 599–612 (1991).

61. Decker, S. J. Epidermal growth factor and transforming growth factor-alpha induce differential processing of the epidermal growth factor receptor. *Biochem. Biophys. Res. Commun.* **166,** 615–621 (1990).

62. Maxfield, F. R. & McGraw, T. E. Endocytic recycling. *Nat. Rev. Mol. Cell Biol.* **5,** 121–32 (2004).

63. Shigematsu, H. & Gazdar, A. F. Somatic mutations of epidermal growth factor receptor signaling pathway in lung cancers. *Int. J. Cancer* **118,** 257–62 (2006).

64. Chan, S. K., Gullick, W. J. & Hill, M. E. Mutations of the epidermal growth factor receptor in non-small cell lung cancer -- search and destroy. *Eur. J. Cancer* **42,** 17–23 (2006).

65. Pollack, V. A., Savage, D. M., Baker, D. A., Tsaparikos, K. E., Sloan, D. E., Moyer, J. D., Barbacci, E. G., Pustilnik, L. R., Smolarek, T. A., Davis, J. A., Vaidya, M. P., Arnold, L. D., Doty, J. L., Iwata, K. K. & Morin, M. J. Inhibition of Epidermal Growth Factor Receptor-Associated Tyrosine Phosphorylation in Human Carcinomas with CP-358,774: Dynamics of Receptor Inhibition In Situ and Antitumor Effects in Athymic Mice. *J. Pharmacol. Exp. Ther.* **291,** 739–748 (1999).

66. Herbst, R. S., Fukuoka, M. & Baselga, J. Gefitinib — a novel targeted approach to treating cancer. *Nat. Rev.* **4,** 956–965 (2004).

67. Lynch, T. J., Bell, D. W., Sordella, R., Gurubhagavatula, S., Okimoto, R. A., Brannigan, B. W., Harris, P. L., Haserlat, S. M., Supko, J. G., Haluska, F. G., Louis, D. N., Christiani, D. C., Settleman, J. & Haber, D. A. Activating mutations in the epidermal growth factor receptor underlying responsiveness of non-small-cell lung cancer to gefitinib. *N. Engl. J. Med.* **350,** 2129–39 (2004).

68. Paez, J. G., Jänne, P. A., Lee, J. C., Tracy, S., Greulich, H., Gabriel, S., Herman, P., Kaye, F. J., Lindeman, N., Boggon, T. J., Naoki, K., Sasaki, H., Fujii, Y., Eck, M. J., Sellers, W. R., Johnson, B. E. & Meyerson, M. EGFR mutations in lung cancer: correlation with clinical response to gefitinib therapy. *Science* **304,** 1497–500 (2004).

69. Yun, C.-H., Boggon, T. J., Li, Y., Woo, M. S., Greulich, H., Meyerson, M. & Eck, M. J. Structures of lung cancer-derived EGFR mutants and inhibitor complexes: mechanism of activation and insights into differential inhibitor sensitivity. *Cancer Cell* **11,** 217–27 (2007).

70. Sordella, R., Bell, D. W., Haber, D. A. & Settleman, J. Gefitinib-sensitizing EGFR mutations in lung cancer activate anti-apoptotic pathways. *Science* **305,** 1163–7 (2004).

71. Choi, S. H., Mendrola, J. M. & Lemmon, M. A. EGF-independent activation of cell-surface EGF receptors harboring mutations found in gefitinib-sensitive lung cancer. *Oncogene* **26,** 1567–76 (2007).

72. Kim, Y., Li, Z., Apetri, M., Luo, B., Settleman, J. E. & Anderson, K. S. Temporal resolution of autophosphorylation for normal and oncogenic forms of EGFR and differential effects of gefitinib. *Biochemistry* **51,** 5212–22 (2012).

73. Ichinose, J., Murata, M., Yanagida, T. & Sako, Y. EGF signalling amplification induced by dynamic clustering of EGFR. *Biochem. Biophys. Res. Commun.* **324,** 1143–9 (2004).

74. Honegger, A. M., Szapary, D., Schmidt, A., Lyall, R., Van Obberghen, E., Dull, T. J., Ullrich, A. & Schlessinger, J. A mutant epidermal growth factor receptor with defective protein tyrosine kinase is unable to stimulate proto-oncogene expression and DNA synthesis. *Mol. Cell. Biol.* **7,** 4568–4571 (1987).

75. Honegger, A. M., Dull, T. J., Felder, S., Van Obberghen, E., Bellot, F., Szapary, D., Schmidt, A., Ullrich, A. & Schlessinger, J. Point mutation at the ATP binding site of EGF receptor abolishes protein-tyrosine kinase activity and alters cellular routing. *Cell* **51,** 199–209 (1987).

76. Axelrod, D., Hellen, E. & Fulbright, R. in *Top. Fluoresc. Spectrosc.* (Lakowicz, J. R.) **3,** pp 289–343 (Springer US, 2002).

77. Abbe, E. Beiträge zur Theorie des Mikroskops und der mikroskopischen Wahrnehmung. *Arch. für Mikroskopische Anat.* **9,** 413–418 (1873).

78. Moerner, W. & Kador, L. Optical detection and spectroscopy of single molecules in a solid. *Phys. Rev. Lett.* **62,** 2535–2538 (1989).

79. Brooks Shera, E., Seitzinger, N. K., Davis, L. M., Keller, R. A. & Soper, S. A. Detection of single fluorescent molecules. *Chem. Phys. Lett.* **174,** 553–557 (1990).

80. Orrit, M. & Bernard, J. Single pentacene molecules detected by fluorescence excitation in a p-terphenyl crystal. *Phys. Rev. Lett.* **65,** 2716–2719 (1990).

81. Funatsu, T., Harada, Y., Tokunaga, M., Saito, K. & Yanagida, T. Imaging of single fluorescent molecules and individual ATP turnovers by single myosin molecules in aqueous solution. *Nature* **374,** 555–9 (1995).

82. Lord, S. J., Lee, H. D. & Moerner, W. E. Single-molecule spectroscopy and imaging of biomolecules in living cells. *Anal. Chem.* **82,** 2192–203 (2010).

83. Huang, B., Babcock, H. & Zhuang, X. Breaking the diffraction barrier: super-resolution imaging of cells. *Cell* **143,** 1047–58 (2010).

84. Hohlbein, J., Gryte, K., Heilemann, M. & Kapanidis, A. N. Surfing on a new wave of single-molecule fluorescence methods. *Phys. Biol.* **7,** 031001 (2010).

85. Axelrod, D., Koppel, D. E., Schlessinger, J., Elson, E. & Webb, W. W. Mobility measurement by analysis of fluorescence photobleaching recovery kinetics. *Biophys. J.* **16,** 1055–69 (1976).

86. Magde, D., Elson, E. & Webb, W. Thermodynamic Fluctuations in a Reacting System—Measurement by Fluorescence Correlation Spectroscopy. *Phys. Rev. Lett.* **29,** 705–708 (1972).

87. Wiseman, P. W., Squier, J. A., Ellisman, M. H. & Wilson, K. R. Two-photon image correlation spectroscopy and image cross-correlation spectroscopy. *J. Microsc.* **200,** 14–25 (2000).

88. Zhang, B., Zerubia, J. & Olivo-Marin, J.-C. Gaussian approximations of fluorescence microscope point-spread function models. *Appl. Opt.* **46,** 1819 (2007).

89. Miaczynska, M. & Kalaidzidis, Y. Intracellular objects tracking. *Eur. J. Cell Biol.* **86,** 569–578 (2007).

90. Jaqaman, K., Loerke, D., Mettlen, M., Kuwata, H., Grinstein, S., Schmid, S. L. & Danuser, G. Robust single-particle tracking in live-cell time-lapse sequences. *Nat. Methods* **5,** 695–702 (2008).

91. Jonker, R. & Volgenant, A. A shortest augmenting path algorithm for dense and sparse linear assignment problems. *Computing* **38,** 325–340 (1987).

92. Ehrlich, M., Boll, W., Van Oijen, A., Hariharan, R., Chandran, K., Nibert, M. L. & Kirchhausen, T. Endocytosis by random initiation and stabilization of clathrin-coated pits. *Cell* **118,** 591–605 (2004).

93. Barak, L. S. & Webb, W. W. Diffusion of low density lipoprotein-receptor complex on human fibroblasts. *J. Cell Biol.* **95,** 846–52 (1982).

94. Schütz, G. J., Kada, G., Pastushenko, V. P. & Schindler, H. Properties of lipid microdomains in a muscle cell membrane visualized by single molecule microscopy. *EMBO J.* **19,** 892–901 (2000).

95. Fujiwara, T., Ritchie, K., Murakoshi, H., Jacobson, K. & Kusumi, A. Phospholipids undergo hop diffusion in compartmentalized cell membrane. *J. Cell Biol.* **157,** 1071–81 (2002).

96. Murase, K., Fujiwara, T., Umemura, Y., Suzuki, K., Iino, R., Yamashita, H., Saito, M., Murakoshi, H., Ritchie, K. & Kusumi, A. Ultrafine membrane compartments for molecular diffusion as revealed by single molecule techniques. *Biophys. J.* **86,** 4075–93 (2004).

97. Lommerse, P. H. M., Snaar-Jagalska, B. E., Spaink, H. P. & Schmidt, T. Single-molecule diffusion measurements of H-Ras at the plasma membrane of live cells reveal microdomain localization upon activation. *J. Cell Sci.* **118,** 1799–809 (2005).

98. Lidke, D. S., Nagy, P., Heintzmann, R., Arndt-Jovin, D. J., Post, J. N., Grecco, H. E., Jares-Erijman, E. a & Jovin, T. M. Quantum dot ligands provide new insights into erbB/HER receptor-mediated signal transduction. *Nat. Biotechnol.* **22,** 198–203 (2004).

99. Shimomura, O., Johnson, F. H. & Saiga, Y. Extraction, Purification and Properties of Aequorin, a Bioluminescent Protein from the Luminous Hydromedusan,Aequorea. *J. Cell. Comp. Physiol.* **59,** 223–239 (1962).

100. Prasher, D. C., Eckenrode, V. K., Ward, W. W., Prendergast, F. G. & Cormier, M. J. Primary structure of the Aequorea victoria green-fluorescent protein. *Gene* **111,** 229–233 (1992).

101. Chalfie, M., Tu, Y., Euskirchen, G., Ward, W. W. & Prasher, D. C. Green fluorescent protein as a marker for gene expression. *Science* **263,** 802–5 (1994).

102. Shaner, N. C., Campbell, R. E., Steinbach, P. A., Giepmans, B. N. G., Palmer, A. E. & Tsien, R. Y. Improved monomeric red, orange and yellow fluorescent proteins derived from Discosoma sp. red fluorescent protein. *Nat. Biotechnol.* **22,** 1567–72 (2004).

103. Hamers-Casterman, C., Atarhouch, T., Muyldermans, S., Robinson, G., Hamers, C., Bajyana Songa, E., Bendahman, N. & Hamers, R. Naturally occurring antibodies devoid of light chains. *Nature* **363,** 446–448 (1993).

104. Yano, Y. & Matsuzaki, K. Tag-probe labeling methods for live-cell imaging of membrane proteins. *Biochim. Biophys. Acta* **1788,** 2124–31 (2009).

105. Keppler, A., Gendreizig, S., Gronemeyer, T., Pick, H., Vogel, H. & Johnsson, K. A general method for the covalent labeling of fusion proteins with small molecules in vivo. *Nat. Biotechnol.* **21,** 86–9 (2003).

106. Griffin, B. R., Adams, S. R. & Tsien, R. Y. Specific Covalent Labeling of Recombinant Protein Molecules Inside Live Cells. *Science (80-.).* **281,** 269–272 (1998).

107. Los, G. V, Encell, L. P., McDougall, M. G., Hartzell, D. D., Karassina, N., Zimprich, C., Wood, M. G., Learish, R., Ohana, R. F., Urh, M., Simpson, D., Mendez, J., Zimmerman, K., Otto, P., Vidugiris, G., Zhu, J., Darzins, A., Klaubert, D. H., Bulleit, R. F. & Wood, K. V. HaloTag: a novel protein labeling technology for cell imaging and protein analysis. *ACS Chem. Biol.* **3,** 373–82 (2008).

108. Cochet, C., Kashles, O., Chambaz, E., Borrello, I., King, C. & Schlessinger, J. Demonstration of epidermal growth factor-induced receptor dimerization in living cells using a chemical covalent cross-linking agent. *J. Biol. Chem.* **263,** 3290–3295 (1988).

109. Gadella, T. W. & Jovin, T. M. Oligomerization of epidermal growth factor receptors on A431 cells studied by time-resolved fluorescence imaging microscopy. A stereochemical model for tyrosine kinase receptor activation. *J. Cell Biol.* **129,** 1543–58 (1995).

110. Clayton, A. H. A., Orchard, S. G., Nice, E. C., Posner, R. G. & Burgess, A. W. Predominance of activated EGFR higher-order oligomers on the cell surface. *Growth Factors* **26,** 316–24 (2008).

111. Ariotti, N., Liang, H., Xu, Y., Zhang, Y., Yonekubo, Y., Inder, K., Du, G., Parton, R. G., Hancock, J. F. & Plowman, S. J. Epidermal growth factor receptor activation remodels the plasma membrane lipid environment to induce nanocluster formation. *Mol. Cell. Biol.* **30,** 3795–804 (2010).

112. Schindelin, J., Arganda-Carreras, I., Frise, E., Kaynig, V., Longair, M., Pietzsch, T., Preibisch, S., Rueden, C., Saalfeld, S., Schmid, B., Tinevez, J.-Y., White, D. J., Hartenstein, V., Eliceiri, K., Tomancak, P. & Cardona, A. Fiji: an open-source platform for biological-image analysis. *Nat. Methods* **9,** 676–82 (2012).

113. Persson, F., Lindén, M., Unoson, C. & Elf, J. Extracting intracellular diffusive states and transition rates from single-molecule tracking data. *Nat. Methods* **10,** 265–9 (2013).

114. Wouters, F. S. & Bastiaens, P. I. Fluorescence lifetime imaging of receptor tyrosine kinase activity in cells. *Curr. Biol.* **9,** 1127–30 (1999).

115. Sanger, F. DNA Sequencing with Chain-Terminating Inhibitors. *Proc. Natl. Acad. Sci.* **74,** 5463–5467 (1977).

116. Bradford, M. M. A rapid and sensitive method for the quantitation of microgram quantities of protein utilizing the principle of protein-dye binding. *Anal. Biochem.* **72,** 248–254 (1976).

117. Laemmli, U. K. Cleavage of Structural Proteins during the Assembly of the Head of Bacteriophage T4. *Nature* **227,** 680–685 (1970).

118. Stoll, S. W., Kansra, S., Peshick, S., Fry, D. W., Leopold, W. R., Wiesen, J. F., Sibilia, M., Zhang, T., Werb, Z., Derynck, R., Wagner, E. F. & Elder, J. T. Differential utilization and localization of ErbB receptor tyrosine kinases in skin compared to normal and malignant keratinocytes. *Neoplasia* **3,** 339–50

119. Michalet, X. Mean square displacement analysis of single-particle trajectories with localization error: Brownian motion in an isotropic medium. *Phys. Rev. E. Stat. Nonlin. Soft Matter Phys.* **82,** 041914 (2010).

120. Gelléri, M. TIRF-anisotropy microscopy: homo-FRET and single molecule measurements. *Dissertation* TU Dortmund (2013).

121. Manders, E. M. M., Verbeek, F. J. & Aten, J. A. Measurement of co-localization of objects in dual-colour confocal images. *J. Microsc.* **169,** 375–382 (1993).

122. Offterdinger, M., Georget, V., Girod, A. & Bastiaens, P. I. H. Imaging phosphorylation dynamics of the epidermal growth factor receptor. *J. Biol. Chem.* **279,** 36972–81 (2004).

123. Keese, M., Magdeburg, R. J., Herzog, T., Hasenberg, T., Offterdinger, M., Pepperkok, R., Sturm, J. W. & Bastiaens, P. I. H. Imaging epidermal growth factor receptor phosphorylation in human colorectal cancer cells and human tissues. *J. Biol. Chem.* **280,** 27826–31 (2005).

124. Stamos, J., Sliwkowski, M. X. & Eigenbrot, C. Structure of the epidermal growth factor receptor kinase domain alone and in complex with a 4-anilinoquinazoline inhibitor. *J. Biol. Chem.* **277,** 46265–72 (2002).

125. Macia, E., Ehrlich, M., Massol, R., Boucrot, E., Brunner, C. & Kirchhausen, T. Dynasore, a cell-permeable inhibitor of dynamin. *Dev. Cell* **10,** 839–50 (2006).

126. Serge, A., Bertaux, N. & Marguet, D. Dynamic multiple-target tracing to probe spatiotemporal cartography of cell membranes. *Nat. Methods* **5,** 687–694 (2008).

127. Danglot, L., Chaineau, M., Dahan, M., Gendron, M.-C., Boggetto, N., Perez, F. & Galli, T. Role of TI-VAMP and CD82 in EGFR cell-surface dynamics and signaling. *J. Cell Sci.* **123,** 723–35 (2010).

128. Xiao, Z., Ma, X., Jiang, Y., Zhao, Z., Lai, B., Liao, J., Yue, J. & Fang, X. Single-molecule study of lateral mobility of epidermal growth factor receptor 2/HER2 on activation. *J. Phys. Chem. B* **112,** 4140–5 (2008).

129. Puck, T. T. Genetics of somatic mammalian cells: III. Long-term cultivation of euploid cells from human and animal subjects. *J. Exp. Med.* **108,** 945–956 (1958).

130. Tzahar, E., Waterman, H., Chen, X., Levkowitz, G., Karunagaran, D., Lavi, S., Ratzkin, B. J. & Yarden, Y. A hierarchical network of interreceptor interactions determines signal transduction by Neu differentiation factor/neuregulin and epidermal growth factor. *Mol. Cell. Biol.* **16,** 5276–87 (1996).

131. Hopkins, C. R. & Trowbridge, I. S. Internalization and processing of transferrin and the transferrin receptor in human carcinoma A431 cells. *J. Cell Biol.* **97,** 508–21 (1983).

132. Cebecauer, M., Spitaler, M., Sergé, A. & Magee, A. I. Signalling complexes and clusters: functional advantages and methodological hurdles. *J. Cell Sci.* **123,** 309–20 (2010).

133. Rangamani, P., Lipshtat, A., Azeloglu, E. U. U., Calizo, R. C. C., Hu, M., Ghassemi, S., Hone, J., Scarlata, S., Neves, S. R. R. & Iyengar, R. Decoding Information in Cell Shape. *Cell* **154,** 1356–69 (2013).

134. Weigel, A. V., Tamkun, M. M. & Krapf, D. Quantifying the dynamic interactions between a clathrin-coated pit and cargo molecules. *Proc. Natl. Acad. Sci.* E4591–E4600 (2013).

135. Wang, Q., Villeneuve, G. & Wang, Z. Control of epidermal growth factor receptor endocytosis by receptor dimerization, rather than receptor kinase activation. *EMBO Rep.* **6,** 942–8 (2005).

136. Red Brewer, M., Yun, C.-H., Lai, D., Lemmon, M. A., Eck, M. J. & Pao, W. Mechanism for activation of mutated epidermal growth factor receptors in lung cancer. *Proc. Natl. Acad. Sci. U. S. A.* **110,** E3595–604 (2013).

137. Henis, Y. I., Hancock, J. F. & Prior, I. A. Ras acylation, compartmentalization and signaling nanoclusters (Review). *Mol. Membr. Biol.* **26,** 80–92 (2009).

ABBREVIATIONS

A	Adenine
aa	Amino acid
Amp	Ampicillin
bp	Base pair
BSA	Bovine serum albumine
ddH_2O	Double distilled water
DMEM	Dulbecco's modified Eagle's medium
C	Cytosine
CCP	Clathrin-coated pit
DNA	Deoxy ribonucleic acid
EDTA	Ethylene diamine tetraacetic acid
EE	Early endosomes
EGF	Epidermal growth factor
EGFP	Enhanced green fluorescent protein
ER	Endoplasmic reticulum
FLIM	Fluorescence Lifetime Imaging Microscopy
G	Guanine
h	Hour
hLCA	Human clathrin light chain A
kDa	Kilo Dalton
LE	Late endosomes
MAPK	Mitogen Activated Protein Kinase
min	Minute/s
MVB	Multi vesicular bodies
MW	Molecular weight
nt	Nucleotide
PALM	Photoactivated Localization Microscopy
PCR	Polymerase chain reaction
PTB	Phosphotyrosine-binding domain
PTP	Protein tyrosine phosphatase
PVDF	Polyvinylidene Difluoride
RTK	Receptor Tyrosine Kinase
rpm	Revolutions per minute

RT	Room temperature
S	Second/s
SDS	Sodium dodecyl sulfate
SPT	Single Particle Tracking
T	Thymine
TBS-T	Tris-buffered saline Tween-20
TIRF	Total Internal Reflection Fluorescence
UV	Ultraviolet
wt	Wild type

ACKNOWLEDGEMENTS

I would like to thank Prof. Dr. Philippe Bastiaens for the opportunity to work in his laboratory.

I thank Peter Verveer for the supervision of my thesis and the help with the data analysis.

For being the second examiner of my thesis I thank Prof. Dr. Roger S. Goody.

I thank Michael Sonntag for providing me with labeled and unlabeled EGF, Piotr Liguzinski and Marc Dittmann for BG-labeling and Peter Bosch for discussions on single particle tracking.

I thank Jutta Luig for help and advice in the lab, Kirsten Michel and Hendrike Schütz, for western blotting, Manuela Grygier for plasmid preparations, as well as Anette Langerak, Petra Glitz and Michael Reichl for their support and company in the cell culture, especially in the many early morning hours.

For the organizational part I thank Astrid Krämer and Tanja Forck.

For all the good times, the help and discussions in the lab, at lunch and in between, I would like to thank Katrin Prost, Björn Papke, Amit Mhamane, Marija Kovacevic, Martin Baumdick, Sven Müller, Michael Schulz, Klaus Schürmann, Jens Christmann, Lale Azer, Ola Sabet, Sina Koch, Zeta Xouri, Lisaweta Roßmannek, Thomas Klein, Sven Fengler, Dina Truxius, Kirsten Walther, Christian Klein, Katia van Eickels, Kaatje Heinelt and all the other people from department 2. Not to forget former members of the department that became friends: Ruth Stricker and Romy Marx.

Special thanks go to Yvonne Radon for helping me out many times with my experiments. And very special thanks go to Justine Mondry und Márton Gelléri for the support and company during my time at the institute, for all the funny and also more serious moments.

Finally, I would like to thank my family and especially Jens Binschik for the help and support in many ways.